# INFORMATION TO USERS

This manuscript has been reproduced from the microfilm master. UMI films the text directly from the original or copy submitted. Thus, some thesis and dissertation copies are in typewriter face, while others may be from any type of computer printer.

**The quality of this reproduction is dependent upon the quality of the copy submitted.** Broken or indistinct print, colored or poor quality illustrations and photographs, print bleedthrough, substandard margins, and improper alignment can adversely affect reproduction.

In the unlikely event that the author did not send UMI a complete manuscript and there are missing pages, these will be noted. Also, if unauthorized copyright material had to be removed, a note will indicate the deletion.

Oversize materials (e.g., maps, drawings, charts) are reproduced by sectioning the original, beginning at the upper left-hand corner and continuing from left to right in equal sections with small overlaps.

Photographs included in the original manuscript have been reproduced xerographically in this copy. Higher quality 6" x 9" black and white photographic prints are available for any photographs or illustrations appearing in this copy for an additional charge. Contact UMI directly to order.

Bell & Howell Information and Learning
300 North Zeeb Road, Ann Arbor, MI 48106-1346 USA

UMI®
800-521-0600

# Numerical Studies of Ising Models defined on a Random Lattice as Applied to the Phase Behaviour of Lipid Bilayer Systems

Morten Nielsen
Centre for the Physics of Materials
Department of Physics, McGill University
Montréal, Québec

A Thesis submitted to the
Faculty of Graduate Studies and Research
in partial fulfillment of the requirements for the degree of
Doctor of Philosophy

# ACKNOWLEDGMENTS

I would like to thank several people for helping me in the preparation of this thesis. First and foremost I would like to thank my thesis supervisor Martin J. Zuckermann. I would not have been able to carry through the work of this thesis without his constant encouragement and support. His constant flow of inspiration and ideas has been an enormous stimulus for my research.

During my PhD I have collaborated with the people from the MemPhys (Membrane and Statistical Physics) group at the Technical University of Copenhagen, Denmark. Professor Ole G. Mouritsen has been an important help as co-supervisor on this thesis and I am grateful for our discussions that helped me focus on the essential parts of my research. I am also thankful to Dr. Ling Miao. I had the chance of working together with Ling both when she was at McGill and when she moved to the Memphys group in Copenhagen. Her constructive criticism of my work has been an indispensable source of motivation and has taught me always to search for a deeper comprehension of a problem. Her precise understanding of the statistical mechanical problems addressed in my research has been essential for the work presented in this thesis. I highly appreciate her patience in our discussions of concepts of statistical mechanics, which very often helped clear my thoughts.

I also wish to thank John H. Ipsen (Memphys, Denmark) for introducing me to his work on dynamic-triangulated networks and for his advise and comments during the course of my PhD. Furthermore I am grateful to Jens Risbo for sharing with me his expertise on implementing simulation techniques involving modified Hamiltonians.

Dealing with computer systems is not an easy task and I would like to thank both the system administrators at McGill, Juan Gallego and at Memphys, Bernd Dammann for their infinite patience in helping me to cope with the computer systems at McGill and Memphys.

In writing up the manuscript for this thesis Proffesor Martin J. Zuckermann, Proffesor Ole G. Mouritsen and Dr. Ling Miao have been very helpful in correcting and improving my English.

Finally, I would like to thank my colleagues and friends on the 4th floor in the McGill Physics Department for sharing immense quantities of horrible coffee with me in the Physics lounge, and the people in MemPhys for sharing lunch breaks with equally horrible food in the canteen at DTU.

Til sidst, men ikke mindst, vil jeg sige tak til Silvia for den hjælp og støtte hun har givet mig, specielt igennem de sidste måneder af min PhD. Sos la mejor.

The financial support from Proffesor Martin J. Zuckermann, the Danish Research Academy, the Dow-Hickson and Alexander McFee Fellowship and the Dr. James Marchall's Dissertation Fellowship as well as the financial support from Proffesor Ole G. Mouritsen during my visits in Denmark are greatly acknowledged.

Morten Nielsen
Copenhagen, December 1998

# ABSTRACT

We examine complex fluid systems where both translational and conformational degrees of freedom are present and focus on systems in which the interplay between the two sets of degrees of freedom is manifested in the macroscopic phase behaviour. We develop an efficient random lattice algorithm describing the translational degrees of freedom and analyze a series of microscopic models defined on a two dimensional fluid surface. Different degrees of complexity in the description of the microscopic coupling between the translational and conformational degrees of freedom allow us to study a variety of models related to pure lipid membrane and lipid-sterol membrane systems.

The phase equilibrium described by the models is calculated by use of Monte Carlo simulation techniques. The different models are shown to exhibit a rich phase behaviour. Depending on the specific model parameters, the phase transition associated with the conformational degrees of freedom is found to be either coupled to, or uncoupled from, that associated with the translational degrees of freedom.

Specifically, the order-disorder transition of an Ising model defined on a fluid surface is shown to be of first order, when the two sets of degrees of freedom are strongly coupled. In contrast, the transition falls in the universality class of the two-dimensional Ising model when the two sets of degrees of freedom are weakly coupled.

We next analyze a model for pure lipid bilayers which is shown to exhibit a phase behaviour with different types of macroscopic coupling between the two sets of degrees of freedom. Depending on the strength of the microscopic interactions the lipid chain melting transition and the lattice melting transition may be either macroscopically coupled or uncoupled.

A related model for lipid-sterol mixtures is shown to provide a consistent interpretation of the various phases of lipid-cholesterol and lipid-lanosterol binary mixtures based on the microscopic dual action of the sterol molecule on the lipid-chain degrees of freedom. We discuss the results for the systems in the context of membrane evolution and suggest that evolution has tended to optimize the lipid-sterol interaction so as to stabilize optimally the mechanical properties of the membrane. Furthermore, a specific small-scale structure is identified and characterized in the liquid-ordered phase in lipid-cholesterol mixtures. This structure is found to be absent in lipid-lanosterol mixtures.

Finally, a model for membrane lysis gives evidence for the high mechanical stabilizing effect of cholesterol on the membrane. The inclusion of cholesterol is shown to inhibit lysis whereas lanosterol only has little stabilizing effect.

# RÉSUMÉ

Dans cette thèse on analyse des systèmes fluides complexes où les degrés de liberté translationels et conformationels sont tous les deux présents. On met l'emphase sur les systèmes dans lesquels le couplage entre les deux types de degrés de liberté se manifeste dans le comportement de la phase macroscopique. On développe une description réseau aléatoire efficace des degrés de liberté translationels, et on analyse une série de modèles microscopiques définis sur une surface fluide en deux dimensions. Les degrés de liberté conformationels sont traités en essence comme les variables de spin du modèle Ising. Des différents degrés de complexité dans la description du couplage entre les degrés de liberté translationels et conformationels nous permettent d'étudier une variété de modèles liés aux systèmes de membranes purement lipidiques et lipide-stérol.

On calcule les équilibres de phase décrits par les modèles en utilisant des techniques de simulation Monte Carlo. Les différents modèles présentent un comportement de phase riche. Dépendant des paramètres spécifiques du modèle, la transition de phase associée aux degrés de liberté conformationels peut être couplée à, ou découplée de, la transition de phase associée aux degrés de liberté translationels.

Spécifiquement, on démontre que la transition d'ordre-désordre d'un modèle Ising défini sur la surface fluide est de premier ordre, résultant de la transition de fusion du réseau quand les deux types de degrés de liberté sont fortement couplés. Par contre, la transition Ising tombe dans la classe universelle des modèles Ising en deux dimensions quand les deux types de degrés de liberté sont faiblement couplés.

Un modèle des bi-couches purement lipidiques présente aussi un comportement de phase avec différentes sortes de couplage macroscopique entre les deux degrés de liberté. Dépendant de la grandeur des intéractions microscopiques, la transition de fusion des chaînes lipidiques et celle du réseau peuvent être macroscopiquement couplées ou découplées.

Un modèle des mélanges lipide-stérol apporte une interprétation consistante des différents phases des mélanges binaires de lipide-cholestérol et de lipide-lanostérol, basée sur l'action duale microscopique de la molécule de stérol sur les degrés de liberté des chaînes lipidiques. On discute les résultats des deux systèmes lipid-stérol dans le contexte de l'évolution des membranes et on suppose que l'évolution a eu la tendance d'optimiser l'intéraction lipide-stérol de facon à stabiliser optimalement les propriétés

mécaniques de la membrane. De plus, une structure à courte portée de la phase liquide ordonnée est identifiée et caracterisée dans les mélanges lipide-cholestérol. On démontre que cette structure est absente dans les mélanges lipide-lanostérol.

Finalement, un modèle de la lyse des membranes met en évidence le grand effet stabilisant du cholestérol sur les propriétés mécaniques de la membrane. On démontre que l'inclusion du cholestérol dans la membrane empêche la lyse, tandis que l'inclusion du lanostérol a peu d'effet stabilisant.

# CONTENTS

# LIST OF FIGURES

# List of Tables

# Numerical Studies of Ising Models defined on a Random Lattice as Applied to the Phase Behaviour of Lipid Bilayer Systems

# 1

# INTRODUCTION

Simple fluids such as argon exhibit three phase lines in their phase diagrams, representing solid-liquid, liquid-gas and solid-gas phase transitions, respectively. Such fluids are composed of atoms or molecules which have no conformational (internal) degrees of freedom, but the fluids themselves clearly have configurational (translational) degrees of freedom and the various phases can be characterized structurally in terms of the translational variables. Complex fluids, however, are composed of molecules which also have internal degrees of freedom due to their structure. Examples are polymers, surfactant molecules, liquid crystalline molecules and lipid molecules (Prost and de Gennes [93]; Bloom, Evans and Mouritsen [91]; Safran [94]; Gelbart, Ben-Shaul and Roux [94]). The possible internal degrees of freedom include orientational variables and thermally induced isomeric changes of structure. The purpose of this thesis is to examine complex fluid systems for which the interplay between fluctuations in the two sets of degrees of freedom is manifested in the macroscopic phase behaviour. Specifically, we analyze a series of microscopic models of molecular species described by both conformational and translational degrees of freedom defined on a two dimensional fluid surface in terms of their phase behaviour and physical properties. The models are defined in a statistical mechanical framework and the equilibrium thermodynamic properties are determined by using different numerical simulation techniques.

A central part of the simulation method developed in this thesis is an efficient algorithm which implements the translational degrees of freedom of the different microscopic models. The algorithm essentially employs a random lattice description to provide an efficient representation of the translational degrees of freedom. This simulation approach offers an accurate description of the translational degrees of freedom

for dense fluid systems and an efficient framework within which several of the aspects that stem from the complex phase behaviour of the systems described below can be addressed. The simulation method and the associate algorithm are general and can be applied to any dense two dimensional system described by a set of translational degrees of freedom. In this thesis we have mainly concentrated on the application of the random lattice algorithm to calculate the phase behaviour of a series of models related to biophysical systems. It is however important to emphasize that the method is general and can be applied to any statistical mechanical model for a dense two dimensional fluid system. Furthermore, all the models investigated are essentially variations of the two dimensional Ising models defined on a fluid surface and the models are thus of general statistical mechanical interest. The connection to biological systems nevertheless offers an interesting frame of reference with the dual purpose of being both a source of inspiration for the questions we investigate in this thesis and a reference that casts the results obtained from the analysis of the statistical mechanical models into a broader perspective.

A large variety of phenomena observed in nature arise from a subtle coupling between the molecular conformational degrees of freedom (rotational orientation, conformational state etc.) and the translational degrees of freedom (shape fluctuations, surface diffusion, density fluctuations etc.) of the specific system. Common to these systems is that an understanding of the details underlying the interplay between the conformational degrees of freedom and the degrees of freedom associated with the translational motion of the related particles is required in order to gain insight into the nature of the thermodynamic properties as manifested in the phase behaviour. The list of systems which exhibit such an interesting interplay between the two types of degrees of freedom is large. Liquid crystals and biological membranes are just two of the more prominent systems in which the interplay plays a key role in defining the phase behaviour.

In liquid crystals, the phase behaviour is controlled by an interplay between the lateral organization and the orientation of the molecules (Prost and de Gennes [93]). Liquid crystals are materials that exhibit a phase behaviour with aspects of both the low symmetry of the ordered crystalline solid phase and the high symmetry of the

isotropic liquid phase. The molecules of a liquid crystal material are highly anisotropic and can to a good approximation be described as rigid rods or ellipsoids with length $l$ greater than the width $d$. At high temperatures, the anisotropic molecules are randomly oriented and their center of mass positions randomly distributed. The high temperature phase is thus an isotropic liquid. As the liquid is cooled, the system undergoes a series of transitions. The first phase to condense is the *nematic phase.* This phase is characterized by a rotational order of the anisotropic molecules. The molecules align so that they are on the average parallel to a particular direction, $\hat{n}$, called the director. The position of the center of mass of the molecules remains random. The nematic phase thus breaks the orientational symmetry of the isotropic liquid phase but leaves the translational symmetry intact. When the system is cooled further, a sequence of distinct phases *(smectic A, smectic C)* condense before the system enters the low temperature crystalline ordered solid phase characterized by both long range rotational and translational order. In some systems an *hexatic* phase exists at temperatures just above the solid phase. In the hexatic phase the rod-like molecules are organized into two-dimensional layers each with a thickness close to the rod length $l$. Each layer is characterized by a mixed order in that it exhibits long-range hexagonal orientational order as manifested in the six-fold symmetry of the diffuse ring in the structure factor and the long range positional order is absent. It is clear from the above discussion that the complex phase behaviour of the liquid crystal system is a direct consequence of a subtle coupling between the conformational (rotational) order of the asymmetric molecules and their translational motion.

*Lyotropic* liquid crystals form a specific class of liquid crystals. Here, liquid crystalline phases are formed in response to variations in solvent concentration and/or solvent type. As the name suggests, these liquid crystals are stabilized by mixing certain types of molecules with a solvent. In fact, lyotropic liquid phases are in general formed by amphiphilic molecules consisting of two parts that repel each other and/or have different solubility in the solvent. A large class of lyotropic liquid crystals are the hydrated lipid systems. A lipid is an amphiphilic molecule with a hydrophilic (water "liking") polar head-group and a hydrophobic (water "hating") tail. The hydrophobic tail consists of two hydrocarbon chains, also called acyl chains (see Fig. 1.1(a)).

Different lipid species differ with respect to the length of their hydrocarbon chains and the degree of saturation as well as in the nature of the polar head group.

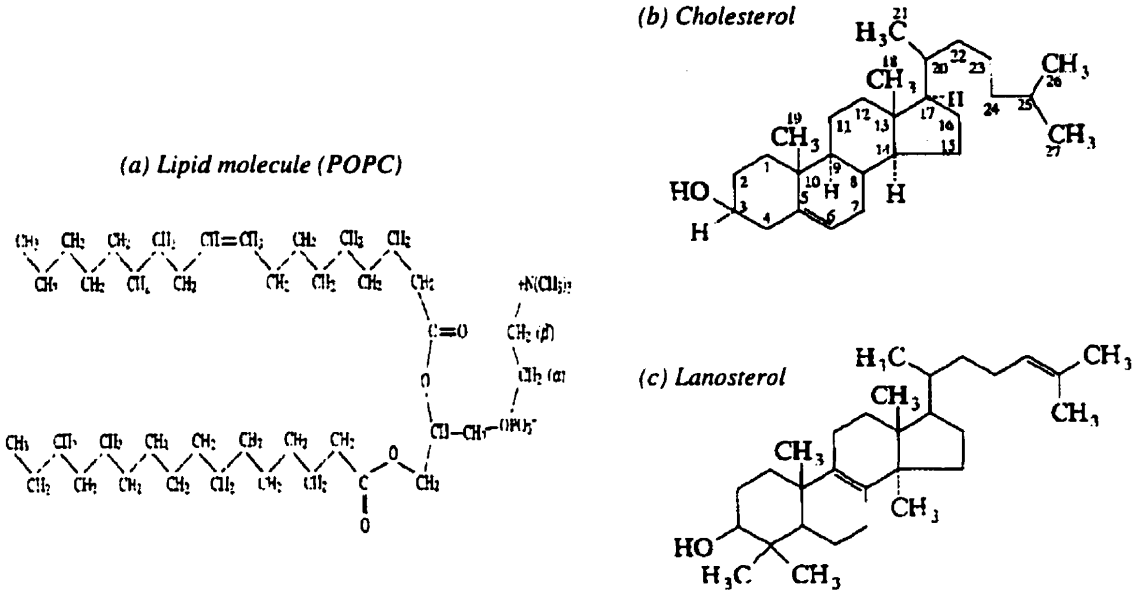


Figure 1.1: The chemical structure of (a) a POPC lipid molecule, (b) a cholesterol molecule, and (c) a lanosterol molecule.

When mixed with water, the amphiphilic lipid molecules self-organize to form aggregates where the hydrophobic hydrocarbon chains are shielded from contact with water. The force driving the formation of aggregates is known as the *hydrophobic effect* and it is predominantly of entropic origin. Since water molecules cannot form hydrogen bonds with the non-polar hydrocarbon chains, a free hydrocarbon chain dissolved in water will lower the free volume available for the water molecules and hence cause the water molecules to be more ordered locally. By shielding the hydrocarbon chains from contact with water, the free volume of the water can be maximized and the entropy loss of the water minimized. It is this balance between the loss of entropy of the hydrocarbon chains associated with the formation of aggregates and a maximization of the free volume of the water that is the origin of the hydrophobic effect.

The hydrocarbon chains achieve this shielding by forming a variety of geometrical conformations. Common aggregate structures are micelles, inverted micelles, hexago-

nal (cylindrical micelles), bilayer sheets, vesicles and bicontinuous cubic phases (Chaikin and Lubensky [95]). The relative stability of the various types of aggregates of different morphology is determined by a subtle balance between the hydrophobic energy, the surface free energy of the aggregate, the electrostatic free energy and the loss in entropy associated with the formation of the specific aggregate. The stability of these different aggregate phases can, to some extent, be understood in terms of packing constraints on lipids with different geometrical shapes (See Fig. 1.2). Phase transitions can also take place between the different equilibrium aggregate phases by varying the temperature, degree of hydration, pH, etc.

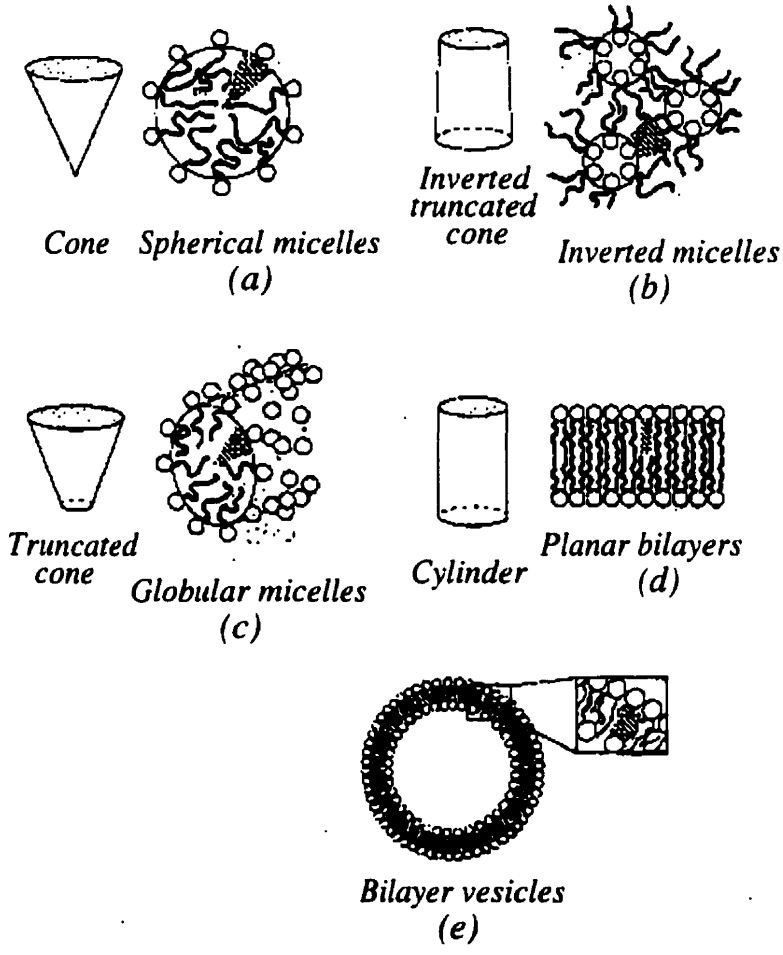


Figure 1.2: Different aggregate structures formed by hydrated lipids: (a) micelle, (b) inverted micelle, (c) cylindrical micelle, (d) flat bilayer, and (e) closed vesicle. Planar bilayer aggregates close into vesicle structures due to the hydrophobic energy of the edges exposed to water of planar bilayers. Along with the different aggregate structures is shown the different average shapes of the lipid molecules. Adapted from P. M. Chaikin and T. C. Lubensky [95], p. 73.

It should be noted that the different equilibrium phases are not stabilized by covalent bondings between the molecules as they owe their existence solely to the hydrophobic effect. Turning to bilayer aggregates, once the bilayer structure is formed the internal structure and dynamics is predominantly determined by intermolecular interactions *within* the aggregate. The in-plane motion of the lipid molecules is hence controlled by a series of in-plane forces among which the van der Waals force acting between the acyl chains and the electro-static force acting between charged polar head groups are predominant. It turns out that these forces often give raise to very low values of, for instance, the bending rigidity on the scale of the thermal energy (Evans [74]; Helfrich [75]). In giant SOPC vesicles, the bending rigidity is thus of the order of $1.5k_BT$ at room temperature (Evans and Rawicz [90]). This means that lipid bilayer aggregate phases are soft matter systems characterized by a high degree of deformability and thermally renormalized properties.

The plasma membrane of a biological cell can in many respects be described as a pseudo two dimensional fluid-mosaic aggregate of a lipid bilayer where the membrane bound proteins are anchored or embedded (Singer and Nicolsen [72]). The properties of the lipid bilayer thus play a very important role in determining the functional properties of the cell membrane. The membrane of a biological cell is an extremely complex system. Lipid molecules constitute about 50 % of the mass of most animal cell membranes, nearly all the remaining part being proteins. The number of lipids molecules in a small animal cell membrane is typically of the order $10^9$ (Alberts et al. [89]). Natural cell membranes typically contain a large number of different lipid species, a phenomenon referred to a lipid diversity. The three major types of lipids in the eucaryotic cell membrane are *phospholipids* (the most abundant), *cholesterol* and *glycolipids*, all three of which are amphiphilic molecules. The plasma cell membrane of most eucaryotic cells contains a large amount of cholesterol (about 25 %) (Alberts et al. [89]). It is believed that the high concentration of cholesterol in the eucaryotic cell membrane plays an important role as a stabilizer against mechanical stress (Needham and Hochmuth [89]; Zhelev and Needham [93]). The eucaryotic cell membrane also contains a variety of different phospholipids. The membrane of many mammalian cells, for example, contains four major phospholipids - *phosphatidylcholine*,

*sphingomyelin*, *phosphatidylserine* and *phosphatidylethanolamine* (Alberts et al. [89]).

## 1.1 Lipid Bilayers

Due to the similarity in structure, lipid bilayers are commonly used as simplified model systems for biological cell membranes. Depending on the type of lipid head-group and lipid chain length, the bilayer thickness lies in the range from 50 Å to 100 Å. The linear extension of the lipid bilayer can vary between 200 Å and 300 $\mu$m . When mixed in water many lipid molecules spontaneously form heterogeneous mixtures of vesicular structures which contain multiple bilayers organized in an "onion-like" structure of concentric shells. Through different experimental preparative techniques, these multi-lamellar vesicles (MLV) can be transformed into different types of liposomes. For example, small unilamellar vesicles (SUV) are single bilayer vesicles with diameters in the range from 200 Å to 500 Å, whereas large unilamellar vesicles (LUV) are unilamellar vesicles with diameters up to 5,000 Å. Finally, giant unilamellar vesicles can be prepared with diameters as large as 300 $\mu$m (Gennis [89]).

Pure lipid bilayers display phase transitions and a very rich phase behaviour. The existence of two principal thermodynamic phases has been well established for such bilayers. These are characterized by different types of macroscopic behaviour of both the translational and the chain conformational degrees of freedom: a low-temperature (*gel*) phase, which is a 2D solid phase with (quasi[1]) long-range translational order and which also has a high degree of collective ordering in the chain conformations of the lipid molecules in the system and a high-temperature (*liquid-crystalline*) phase, which displays macroscopic disorder in both the translational (as does a liquid) and the chain conformational degrees of freedom. Although the common terminology in biophysical literature describes the two phases as the *gel* phase and the *liquid-crystalline* phase, we for our purposes in this work shall label the two phases with **so** (solid, chain ordered) and **ld** (liquid, chain disordered), respectively.

The transition known as the *main-transition* takes the membrane from the high

[1]The terminology *quasi* long-range order refers to the fact that two dimensional system cannot exhibit true long-range translational order and the low-temperature phase of the lipid-bilayer is hence only quasi long-range ordered.

temperature liquid crystalline disordered phase to the low temperature gel ordered phase. This transition is a very sharp and co-operative transition characterized by a well defined transition temperature and transitional enthalpy (G. Cevc [93]). One significant experimental observation is that, although the main transition is accompanied by a large area expansion of around 20%, it hardly involves any change in the bilayer volume. Lipid bilayer are thus, to a good approximation, incompressible systems and there is an almost constant reciprocal relationship between the lipid bilayer thickness and the cross-sectional area per lipid molecule.

The entropy of transition associated with the main transition is large ($\sim 15\ k_{\mathrm{B}}T$ per molecule (G. Cevc [93])) and much larger than the entropy change associated with a traditional two dimensional melting transition ($\sim 1\ k_{\mathrm{B}}T$ per molecule (Doniach [78])). The main source of this large change in entropy is the change in conformational order of the lipid chains at the main transition. The main transition has thus often been described as a *chain melting* transition, and many of the aspects of the main transition have been successfully described solely in terms of the chain conformational degrees of freedom. It can be concluded from experimental data that, thermally driven, the translational order and the chain conformational order that are characteristic of the so phase appear *simultaneously* on cooling through the temperature of the "main transition", for almost all of the systems of one-component lipid bilayers studied (Mouritsen [91]). In other words, the translational and the conformational degrees of freedom appear *macroscopically* coupled.

However, there are no fundamental physical principles dictating that this macroscopic coupling be a necessary generic feature of the thermodynamic behaviour of either two-dimensional systems with both translational and internal degrees of freedom in general, or lipid-bilayers in particular. Indeed, a previous study of minimal models for 2D random lattice Ising systems and one-component lipid bilayers has shown that it is only a matter of engineering the microscopic interactions in order to macroscopically uncouple the two types of degrees of freedom (Nielsen et al. [96b]). An intermediate phase does exist as part of the generic phase behaviour of systems (such as lipid bilayers) with both translational and internal degrees of freedom. In this phase the (quasi) long-range translational order is broken, but the internal (chain

conformational) degrees of freedom remain macroscopically ordered. We refer to this intermediate phase as the **lo** (for liquid, chain ordered) phase. We note, however, that concrete experimental evidence has yet to be found for the existence of such a phase in one-component lipid bilayers, although some evidence has been found for lipid monolayers (Mouritsen and Zuckermann [87a]). The **lo** phase has been discovered, however, in bilayer systems of some lipid-cholesterol binary mixtures and the lipid-cholesterol mixture system thus provides a prominent example of a system where the coupling between the chain conformational and the translational degrees of freedom is manifested macroscopically in the phase behaviour.

The question of the biological relevance of cholesterol has intrigued many researchers, as evidenced by a large body of both theoretical and experimental work on lipid-cholesterol bilayers and monolayers (Ipsen et al. [87]; Lemmich et al. [97]; Mitchell and Litman [98]; Halstenberg et al. [98]; Needham, McIntosh and Evans [88]; Vist and Davis [90]), among which we briefly review those that are most relevant to the purpose of our study. Evidence for the existence of a liquid **lo** phase in bilayers of dimyristoyl phosphatidylcholine (DMPC)-cholesterol mixtures was first provided by Needham and Evans on the basis of their micromechanical measurements (Needham, McIntosh and Evans [88]). A full phase diagram in terms of cholesterol concentration and temperature was firmly established for bilayers of dipalmitoyl phosphatidylcholine (DPPC)-cholesterol mixtures by M. Vist and J. H. Davis by combining data from deuterium-NMR, Differential-Scanning-Calorimetry (DSC) and ESR studies (Vist and Davis [90]) (see Fig. 1.3). This phase diagram displays a modest depression of the main-transition (**so-ld**) temperature for low concentrations of cholesterol; and remarkably, it demonstrates a macroscopic uncoupling of the translational and the chain conformational degrees of freedom, as manifested by a high-temperature **ld-lo** coexistence and a low-temperature **so-lo** coexistence at intermediate concentrations of cholesterol as well as a single **lo** phase region at high cholesterol concentrations.

As stated earlier, the plasma membrane of eucaryotic cells contains considerable concentrations of cholesterol. These high cholesterol concentrations have a profound influence on the thermodynamic and mechanical properties of the cell membrane (Al-

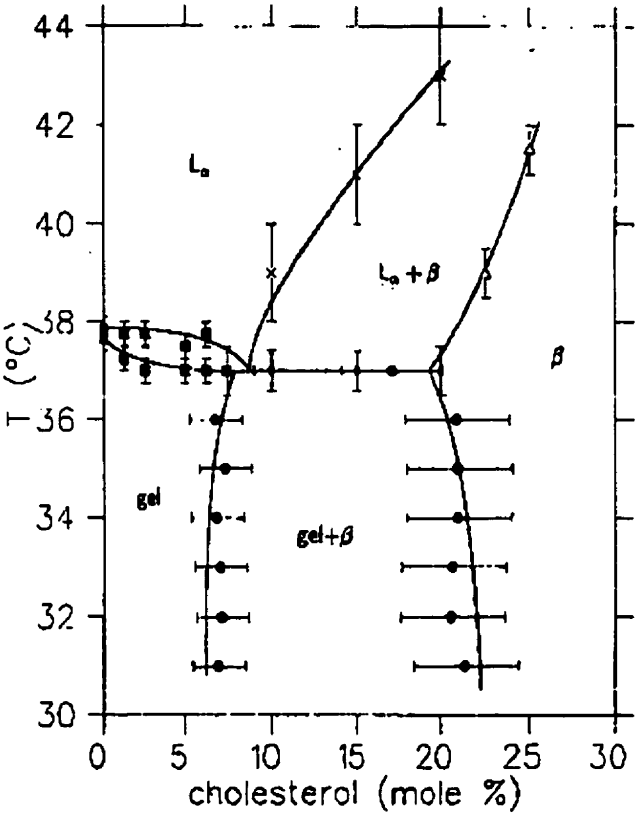


Figure 1.3: The Vist-Davis phase diagram for the DPPC-cholesterol system as determined by NMR spectroscopy, differential scanning calorimetry and micromechanics. The phases are labeled as follows: $L_\alpha$ is the fluid or liquid crystalline phase; gel is the gel phase; and $\beta$ is the high-cholesterol-content phase characteristic of biological membranes. Solid (□) and (•) are determined by difference $^2$H NMR spectroscopy; solid (◇) show the three-phase line determined from DSC; (×) are from the upper limit of the broad component of the DSC traces and (△) are from the abrupt sharpening of the resonance at high cholesterol concentrations. Adapted from M. Vist and J. H. Davis [90].

berts et al. [89]). One of the important structural properties of the cholesterol molecule is the conformationally almost inflexible planar steroid ring (see Fig. 1.1(b)). This chemical structure governs most of the interactions between cholesterol and the lipid bilayer. When a cholesterol molecule is adjacent to a lipid acyl chain, the flat steroid ring restricts the conformational flexibility of the acyl chain and the cholesterol molecule thus induces a local increase in the order of the lipid chains (Stockton and Smith [76]). Cholesterol also acts as an impurity in that it prevents the formation of the low temperature gel phase of a lipid bilayer by inhibiting close packing of the lipid acyl chains (Estep et al. [78]). This dual molecular effect of cholesterol stabilizes the thermal and mechanical properties of the lipid membrane and inhibits possible

phase transitions (Alberts et al. [89]). No other component of biological membranes affects the membrane in the same manner (Yeagle [92]).

Sterols are synthesized according to long, complicated and energetically expensive biosynthetic pathways. Along the biosynthetic pathway of cholesterol, a large number of sterols are synthesized as intermediates. Starting with lanosterol, which is the first intermediate sterol synthesized along the pathway, 19 different sterols are formed on the way to cholesterol. Extensive cellular energy as well as molecular oxygen is utilized in the synthesizing process. The structural differences between lanosterol and cholesterol are not very great (see Fig. 1.1(b) and Fig. 1.1(c)) and the question naturally arises as to why the cell spends so much energy in producing specifically cholesterol. It has been suggested by Bloom and Mouritsen ([88]) that cholesterol played a crucial role in the evolution of eucaryotic cells. These authors also hypothesized that the manner in which cholesterol modifies the thermodynamic and mechanical properties of the lipid membrane may have been essential for the development of a mechanically stable plasma membrane of the eucaryotic cell. Bloom and Mouritsen pointed out that it is the specific differences between the molecular structure of lanosterol and cholesterol that allow for the specific phase behaviour of cholesterol in lipid bilayers. In order to shed some light on the role of cholesterol in the optimization process specifically developed by nature to achieve optimal mechanical and biophysical properties for the cell membrane, a detailed analysis comparing the effects of different sterol on the lipid bilayer properties is needed. At the present, the amount of experimental work published on lipid-sterol mixture systems other than cholesterol is however rather limited and so far no consensus has been reached as to the specific properties of cholesterol that makes its effect on lipid bilayers different from for example lanosterol.

Cholesterol has been shown to have important stabilizing effects on the membrane against rupture (Needham and Hochmuth [89]; Zhelev and Needham [93]). The mechanical stability of a lipid membrane can be modified in many ways (Needham and Hochmuth [89]; Wilhelm et al. [93]; Winterhalter [96]). The absorption of peptides induces defect formation and lysis of the lipid membrane as the concentration of peptides is increased (Dimitrova and Matsumura [97]; Heller et al. [97]; Ludtke et al.

[96]; Matsuzaki et al. [97]). The inclusion of cholesterol, on the other hand, increases the mechanical stability of the lipid membrane and thus its stability against lysis (Needham and Hochmuth [89]; Zhelev and Needham [93]; Benachir et al. [97]). Little theoretical work has been done in the field of membrane lysis. A simple model was recently proposed for the description of the thermal stability of the membrane in the presence of pores (Shillcock and Boal [96]; Shillcock and Seifert [98]). This model, however, does not include a description of the conformational degrees of freedom in the membrane and it thus gives no insight into the function of cholesterol as a mechanical stabilizer of the membrane.

From the above discussion, it is clear that many aspects of the phase behaviour of the lipid bilayer are due to the coupling between the chain conformational and the translational degrees of freedom of the lipid bilayer. A description of many of the important properties of the lipid bilayer, therefore has to include a detailed description of the translational motion of the lipid molecules. It is a key objective of this thesis to develop descriptions of the lipid bilayer based on minimal models that include a full representation of the translational degrees of freedom. These models permit an investigation, using simulation techniques, of what importance the coupling between the two types of degrees of freedom has on the phase behaviour of the lipid bilayer system.

The phase behaviour of lipid bilayer systems has been determined from several different experimental techniques. Among the most important are deuterium NMR and differential scanning calorimetry (DSC). The technique of $^2$H NMR is an useful tool for studies of the orientation and dynamics of the lipids in the membrane. The $^2$H NMR spectrum provides information on changes in lipid chain structure as function of, for example, variations in temperature or membrane composition (Davis [79]). The $^2$H NMR spectrum changes dramatically at the gel-to-liquid crystalline phase transition, hence demonstrating the large change in lipid chain order associated with the chain melting involved in the main transition. Since there is a large heat of transition associated with the first order transitions in lipid bilayers, DSC is a key method for identifying temperatures where bilayer systems undergo phase transitions. The method provides information on the location of phase boundaries

and the corresponding latent heats of transition. For pure DPPC water mixture systems, a DSC experiment thus gives evidence for a series of phase transitions, the most prominent being the main transition occurring at about 41 °C with a corresponding latent heat of $\sim 16 k_B T$ per molecule (G. Cevc [93]).

As described earlier, the phase diagram of the DPPC-cholesterol mixture system by M. Vist and J. H. Davis was derived by combining data from $^2$H NMR and DSC studies (Vist and Davis [90]).

## 1.2 Models for Lipid Bilayers

During the last decades, many theoretical models have been developed in order to elucidate different aspects of the phase behaviour of lipid bilayer membrane systems. The majority of these models can be classified as either statistical mechanical models studied by the use of Monte Carlo algorithms (Dammann et al. [95]; Mouritsen et al. [95]), microscopic molecular models examined using molecular dynamics algorithms (Tieleman, Marrink and Berendsen [97]), or force field models investigated by minimization of a free energy potential function (Schlenkrich et al. [96]).

All the theoretical approaches invoke different kinds of approximations when describing the lipid bilayer system. It is practically impossible (and in general undesirable) to examine the physics of lipid bilayers by using a full description of all of the variables in the system. First, such a treatment involves a large number of degrees of freedom and hence makes computer simulations very costly, and second (and perhaps more important) it leads to a description with a wealth of details which would make it very difficult to grasp the essential and relevant physics of the phenomenon investigated. As stated earlier, the lipid molecules can, from a physical point of view, be described by two distinct fundamental sets of degrees of freedom corresponding to internal and translational motion. A model for the lipid bilayer is hence most usefully described in terms of these two sets of variables which are coupled by some kind of interaction. The variables may each represent a large set of coarse-grained microscopic details and the effective interactions are not necessarily directly related to the basic molecular interactions. For the statistical mechanical models for the lipid layer, the general approach has been to model the bilayer as composed of two non-interacting

monolayers. In each monolayer, the degrees of freedom of the lipid head groups is disregarded and the two acyl chains of the lipid molecule are treated as independent systems. Finally, the degrees of freedom associated with the translational mobility of the lipid chains on the surface are omitted by adopting a lattice description for the lateral degrees of freedom, where the lipid chains are positioned on a regular triangular two-dimensional lattice. In this lattice description, the conformational degrees of freedom of the lipid chains are commonly approximated by a small finite number of conformational states corresponding to a mapping of the three-dimensional acyl chain conformations onto a small discrete set of projected coarse-grained variables.

A model for the cooperative behaviour of a lipid bilayer system of this kind was first proposed by Doniach ([78]) and later extended by Pink *et. al* ([80]). In the Pink Model the conformational degrees of freedom of the lipid chains are described in terms of ten discrete states, each characterized by an internal conformational energy, $\epsilon_i$, a cross-section area, $A_i$ and a degeneracy, $D_i$, denoting the number of different conformational chain states with energy $\epsilon_i$ and area $A_i$. The lowest energy state is the all-*trans* state where the number of *gauche* rotations is zero. This state has zero degeneracy. The 10th state, which has the characteristics of the fluid phase, has a high conformational energy and large degeneracy corresponding to the many different conformational states of the fluid chain. The eight gel-like intermediate states are the lowest-lying excitations of the all-*trans* state subject to conditions of low conformational energy and optimal packing. The interaction potential between the lipid chains is approximated as a van der Waals interaction between long rigid cylindrical rods with a radius defined by the cross section area, $A_i$. Finally, the stabilizing force against lateral expansion is modelled by a lateral pressure, $\pi$.

The Pink model has been quite successful in describing several essential thermodynamic properties of the main transition that are mainly related to the chain conformational degrees of freedom (Mouritsen et al. [95]). However, it does not take into consideration the interplay between the conformational (or internal) and translational degrees of freedom, an important issue in understanding the structural properties and thermodynamic behaviour of lipid systems. For example, both the surface density of the bilayer and the lateral mobility of individual lipid molecules strongly depend on

the chain conformational states as revealed by considerable experimental data.

The molecular mechanisms underlying the ability of cholesterol to uncouple the macroscopic processes of lateral ordering and chain ordering in a lipid bilayer have been investigated in a theoretical study based on a *lattice* model (Ipsen et al. [87]). In this model, each lattice site was assigned a multi-valued variable corresponding to chain conformational states. The physics governing this set of degrees of freedom was described by the Pink model (Pink, Green and Chapman [80]). In addition, a multi-state Potts model was employed to give, in a very approximate way, a phenomenological description of the lateral crystallization process, describing the process only in terms of thermal energetics of the grain boundaries (Sahni, Grest and Anderson [83]). The final essential ingredient of the model was a hypothesis of a dual molecular effect for cholesterol. On the one hand, a cholesterol molecule acts as an "ice breaker", i.e., as a substitutional impurity that weakens the inter-lipid interactions responsible for crystallization. On the other hand, cholesterol also acts as a "chain rigidifier", tending to induce its neighbouring lipid chains into conformationally ordered states. Calculations based on a mean-field theory of the model predicted a phase diagram of DPPC-cholesterol bilayers that agreed qualitatively with the experimental phase diagram (see Fig. 1.3). This model study provided concrete theoretical support for the hypothesis and strongly suggested that the lattice model could capture the essence of the microscopic physics governing the thermodynamic phase behaviour of lipid-cholesterol bilayers. This model, however, suffers a fundamental shortcoming inherent in the lattice description: the description of the translational degrees of freedom and the microscopic physics underlying the associated ordering process is only little realistic.

It is one of the themes of the work in the present thesis to eliminate this shortcoming of the lattice models and explore the interplay between conformational and transformational degrees of freedom of two dimensional systems by developing microscopic models that contain a full description of the transformational degrees of freedom as well as microscopic interactions that couple the transformational degrees of freedom explicitly to the conformational degrees of freedom.

## 1.3 2D Melting, Two Dimensional Hard Disk Models

The nature of 2D melting transitions has been a focal point of numerous statistical mechanical studies of two-dimensional systems for the past two decades (Strandburg [89]; Joós [96]). In the work presented in this thesis, where we consider the effects of coupling the translational degrees of freedom to internal degrees of freedom of the particles, we are inevitably confronted with this issue. Two scenarios for this transition have been presented and discussed in the literature. Halperin and Nelson, and Young (Nelson and Halperin [79]; Young [79]) developed the basic idea of Kosterlitz and Thouless, and Berenzinskii (Kosterlitz and Thouless [73]; Berenzinski [71]) and proposed that the 2D solid-liquid transition can proceed via two continuous (second-order) transitions corresponding, respectively, to dissociation of dislocations (the solid-hexatic transition) and dissociation of disclinations (the hexatic-liquid transition). A single conventional first-order transition is the other possible scenario. Despite the significant amount of effort devoted to resolve the issue, no consensus has been reached. A prominent model developed for the study of two dimensional systems with translational degrees of freedom is the *hard disk* model (Alder and Wainwright [62]). In this model, each particle is described as a hard disk with a diameter $d$. The disks interact through steric interactions in that each point in space cannot be occupied by more than one hard disk. The hard disk system exhibits a phase transition between a triangular ordered solid phase and a fluid disordered phase as a function of the lateral pressure. The models presented in the present thesis are all variations of the hard disk model in that all model particles are described as hard disks decorated with conformational degrees of freedom and in that the excluded volume interaction between particles is modelled through the hard disk repulsion. While most Monte Carlo simulations on hard disk systems suggest a first-order 2D melting (Lee and Strandburg [92]), others suggest a one-stage continuous transition (Fernández, Alonso and Stankiewicz [95]). In the work presented in this thesis we are not concerned with the details of the type of transition involved in the 2D melting process, since we cannot, in principle, provide any new information on the true nature of the transition when studying more complex models. However, for all practical purposes we can consider that the melting is a first-order transition. In fact, for the

models examined in this thesis all the simulation data obtained for the solid-liquid transition are consistent with a first-order transition.

The work presented in this thesis is based on results that either have already been published as original research articles or have been prepared for submission for publication;

- **Model of the sub-main transition in long-chain phosphatidylcholine lipid bilayers.** M. Nielsen, L. Miao, J. H. Ipsen, K. Jørgensen, M. J. Zuckermann, and O. G. Mouritsen. *Biochim. Biophys. Acta.* **1283** 170-176 (1996).

- **Random Lattice Models and Simulation Algorithms for the Phase Equilibria in Two-dimensional Condensed Systems of Molecules with Coupled Internal and Translational Degrees of Freedom.** M. Nielsen L. Miao, J. H. Ipsen, O. G. Mouritsen and M. J. Zuckermann. *Phys. Rev. E.* **54**, 6889 (1996).

- **Lipid–Cholesterol Phase Diagrams**, M. Nielsen, L. Miao, J. H. Ipsen, O. G. Mouritsen and M. J. Zuckermann. *Biophys. J.* A132 (1997).

- **An off-lattice model for the phase behaviour of lipid-cholesterol bilayers.** M. Nielsen, L. Miao, J. H. Ipsen, M. J. Zuckermann and O. G. Mouritsen. Accepted for publication in *Phys. Rev. E.* (Feb. 1999).

- **A Model for the phase behaviour of lipid-sterol mixtures.** M. Nielsen, L. Miao, J. H. Ipsen, M. J. Zuckermann and O. G. Mouritsen. In preparation. (1998)

- **A model for thermally induced lysis in lipid membranes containing sterols.** M. Nielsen, L. Miao, J. H. Ipsen, M. J. Zuckermann and O. G. Mouritsen. In preparation. (1998)

The plan for the presentation of the thesis is as follows. In Chapter 2, we present the various models investigated in this work. The models are minimal models in that they contain an approximate description of the molecular structure and internal degrees of freedom of the related model particles and in that the microscopic interaction

potentials are all designed to contain only features that are essential for describing systems where the complex interplay between the internal and lateral degrees of freedom can manifest itself in a simple manner in the phase behaviour.

In Chapter 3, we discuss the series of numerical methods we have applied to calculate the equilibrium phase behaviour of the microscopic models. In particular, we describe the general use of the Monte Carlo simulation algorithm as a tool for determining the nature and loci of phase transitions in a microscopic model, the use of finite-size scaling analysis in the context of first and second order phase transitions, the application of thermodynamic reweighting techniques to calculate equilibrium distribution functions at a set of different temperatures based on data from one single simulation, and finally the use of the Umbrella Sampling Method to optimize the sampling of the equilibrium phase space in situations where two coexisting phases are separated by a free energy barrier. Chapter 3 also contains a description of the random-lattice algorithm developed to provide an accurate and highly efficient description of the translational degrees of freedom of fluid two dimensional systems.

In Chapter 4, Chapter 5 and Chapter 6, we give the results which describe the equilibrium phase behaviour of the different microscopic models. The results include a series of phase diagrams calculated for these models as well as equilibrium thermal averages for specific quantities characterizing their phase behaviour. Each chapter is concluded with a short discussion of the simulation results that underlines the generic phenomenology of, and the physical mechanisms underlying, the macroscopic coupling and uncoupling between the translational and conformational degrees of freedom in the different models.

Finally, Chapter 7 concludes the thesis with a brief summary of the work reported here and remarks on future applications of the random lattice model approach.

# 2

# Models. Microscopic Hamiltonians

In this chapter, we present the different microscopic models investigated in this thesis. All the models studied are minimal models in the sense that they give a very limited description of the molecular structure or internal degrees of freedom of the related model particles. The microscopic interaction potentials are all designed to contain only features that are necessary for describing systems where the complex interplay between the internal and translational degrees of freedom can manifest itself in a simple manner in the phase behaviour. Our studies of the interplay between internal and translational degrees of freedom of many-particle systems is largely motivated by the collective phenomena found in lipid-bilayer systems, and we naturally see the purpose of developing microscopic models as being two-fold: 1) to study the generic thermodynamic behaviour of two-dimensional systems where the two types of degrees of freedom are present and coupled, and 2) to model this coupling in a way that is relevant to lipid-bilayer systems. To this end, we have chosen to study a series of statistical mechanical models, which have different emphasis and levels of complexity in describing the microscopic interactions that govern the interplay between the two types of degrees of freedom.

The various models are introduced by starting with the simplest case and then gradually increasing the complexity. Five models are described in total and are numbered I to V. Model I is a regular Ising model on a random lattice, Model II is an Ising model with a distant dependent Ising interaction, Model III is specific for pure lipid bilayer systems, Model IV extends Model III to include sterols, and finally Model V is a model for membrane lysis. All models are basically variants of the nearest neighbour Ising model defined on a two-dimensional fluid surface.

In the models, the particles are free to move on the 2D surface and the particles

are hence described by two distinct sets of degrees of freedom, the translational and the internal degrees of freedom, respectively. The details of the implementation of the random lattice algorithm describing the translational degrees of freedom is given in Section 3.2 and we will here just describe the essential ingredients of the algorithm. The algorithm employs a tethered random lattice representation of the spatial configurations of a dense 2D system of many particles and generates the phase space of the spatial configurations. Each particle is considered as a hard disk of diameter $d$, and every site on the random lattice is occupied by such a hard-disk particle. The algorithm contains a compact "link" data structure that allows for efficient access to the nearest-neighbour structure of a microconfiguration.

In all of the models, the short-range repulsion between particles is modelled through the hard-disk repulsion and the particles interact via nearest-neighbour interactions defined by the "link structure".

Although we often refer to the particles in our models as "lipid molecules" and "sterol molecules" and to the systems as "lipid bilayers", we are fully aware that the descriptions of the microscopic properties of the "model molecules" are considerably simplified pictures of those of real lipid and sterol molecules, as our emphasis is on revealing generic physics rather than on providing quantitative interpretations for the experiments. Furthermore, the generic physics with which we are concerned should be viewed in a broader context: it should also be relevant to certain two-dimensional non-lipid systems where both translational and internal molecular degrees of freedom are thermodynamically relevant.

## 2.1 *Ising Models on a Random Lattice (Model I and Model II)*

The 2D spin-1/2 Ising model defined on a regular triangular lattice has a continuous phase transition from a high-temperature paramagnetic (spin disordered) phase to a low-temperature ferromagnetic (spin ordered) phase at a critical temperature $\frac{k_B T_C}{J_0} = 3.641$, where $J_0$ is the exchange interaction between nearest-neighbour spins.

Ising models defined on different types of 2D random lattices have received considerable attention over the last years, in particular as model systems involving 2D gravity. Considerable progress was made by the finding of the exact solution for an

Ising model on an unconstrained random triangular lattice (Boulatov and Kazakov [87]). It was shown that the critical behaviour of this model is characterized by the critical exponents, $\alpha = -1$ and $\beta = \frac{1}{2}$ (Boulatov and Kazakov [87]), which are very different from those of the universality class of the standard two-dimensional Ising model ($\alpha = 0$ and $\beta = \frac{1}{8}$). The same results were also obtained numerically by Monte Carlo simulations (Ben-av, Kinar and Solomon [92]). A different approach was taken in a recent study of an Ising model on a dynamically-generated lattice based on the spatial proximity of the particles in the plane (Vekić, Liu and Hamber [94]). In this study, spins were assigned to hard disks that were allowed to move in the plane, and in contrast to the random lattice considered here, the local lattice topology was not fixed. It was shown that, for systems where the hard disk radius is very small compared to the range of the Ising interaction, the spins tend to form tight ordered clusters at low temperatures. In the clusters, each spin interacts with a large number of neighbours. This clustering transition is found to be sudden and strongly first order. For condensed systems, where the hard disk radius is comparable to the range of the Ising interaction, the standard 2D Ising-model behaviour is recovered, irrespective of the presence of full translational invariance (Vekić, Liu and Hamber [94]). As the hard-disk radius decreases with respect to the interaction range, the line of Ising critical (temperature) points is found to terminate at a tricritical-like point and beyond the tricritical-like point, the spin order-disorder transition becomes first order. It was argued that the special critical behaviour displayed by the Ising model on the unconstrained random triangular lattice (Boulatov and Kazakov [87]) was again observed at the tricritical point. In comparison with the later work, our studies always correspond to the condensed regime.

In the present thesis, we have extended the standard Ising model in two ways. Our first extension, which will be referred to as Model I, is to associate a spin with each hard-disk particle on the random lattice. Nearest-neighbour particles are connected by tethers and interact through the usual Ising spin-spin exchange interaction. This leads to a *random* Ising model in which the number of nearest neighbours is a fluctuating quantity. In this model, the characteristic interaction range is set by the particle density of the system, which in turn is controlled by the external pressure, $P$,

and the translational and spin degrees of freedom are only coupled by the *fluctuating* local connectivity (or the number of nearest neighbours) of the random lattice. For later reference, we write down the microscopic interaction Hamiltonian used in our simulation,

$$H_{\mathrm{I}} = -J_0 \sum_{\langle i<j \rangle} S_i S_j \ , \tag{2.1}$$

where $\langle i < j \rangle$ denotes a sum over nearest neighbours connected by tethers, and $S_i = \pm 1$.

In the second extension of the standard Ising model, which will be referred to as Model II, we have modified the above model in Eq. (2.1) by introducing a spin-spin interaction that is *distance dependent*: the tethered spins only interact if they are within a certain distance, $R_0$, of each other. The random-lattice Hamiltonian is then given by

$$H_{\mathrm{II}} = -J_0 \sum_{\substack{\langle i<j \rangle, \\ R_{ij} < R_0}} S_i S_j \ , \tag{2.2}$$

where $\langle i < j \rangle$ again denotes a sum over all possible nearest neighbours, and $R_{ij}$ is the distance between spins $S_i$ and $S_j$. Hence, in this case, $R_0$ sets the range of interaction. The fact that the density of the system sets another length scale leads to a different type of coupling between the spins and the translational degrees of freedom.

Using these two models, we can address the basic issue of how and to what extent different types of microscopic coupling between the internal and translational degrees of freedom manifest themselves in the macroscopic thermodynamic behaviour of the systems, and understand and underline the generic physics associated with such coupling. Ising spin transitions in these models will be of particular interest, as the classical understanding of the critical transition in the Ising model defined on a regular lattice provides an essential framework of reference, with respect to which effects arising from the interplay between the two types of degrees of freedom can be mapped out.

## 2.2 The Doniach Model on a random lattice – a Model for Pure Lipid Bilayers (Model III)

Model III is in fact an Ising model similar to those introduced above, but with the basic difference that one of the spin states is assigned an internal degeneracy larger than one. This model is inspired by a *regular-lattice* model proposed by Doniach ([78]) to describe the essential thermodynamic properties of lipid bilayers, in particular the main transition, that are primarily associated with the conformational degrees of freedom of lipid chains in a planar array. Doniach and Nagle([73]) were the first researchers to give a statistical mechanical description of the lipid bilayer melting transition in terms of a cooperative change in the lipid conformational distribution. In particular, Doniach's minimal model of the lipid bilayer was used to estimate the lowering of the free energy barrier for transbilayer ion permeability due to enhanced lateral compressibility near the main transition.

Doniach's model is based on two states to represent the lipid-chain conformations. One state, the "ordered" state (denoted $S_i = 1$), has zero internal (conformational) energy ($E_o = 0$) and is non-degenerate ($D_o = 1$), characteristic of the chain conformational state of lipid molecules in the gel phase. The other state, the "disordered" state (denoted $S_i = -1$), has a high internal energy, $E_d$, corresponding to the excitation energy associated with a conformational change, and a large degeneracy, $D_d \gg 1$, representing the large number of possible chain conformations which have the same value of $E_d$, which is characteristic of the chain conformation of lipid molecules in the liquid-crystalline (fluid) phase. Each chain occupies a site on a regular triangular lattice and each state is assigned a cross-sectional area, $A_o$ or $A_d$, corresponding to the average area occupied by chains in the ordered and the disordered state, respectively. The model is formally described by the following Hamiltonian

$$H_D = H_0 + V_{int}^{(1)} + P\sum_i \left\{ A_d \left(\frac{1-S_i}{2}\right) + A_o \left(\frac{1+S_i}{2}\right) \right\} \quad , \tag{2.3}$$

where

$$H_0 = \sum_i E_d \left(\frac{1-S_i}{2}\right) \quad , \tag{2.4}$$

and

$$V_{\rm int}^{(1)} = -\frac{J_0}{4} \sum_{\langle i<j \rangle} (1+S_i)(1+S_j) \ , \tag{2.5}$$

with $\langle i < j \rangle$ denoting a sum over nearest neighbours on the lattice. In this case, $P$ plays the role of an internal interfacial pressure which provides the lateral stabilizing force controlled mainly by the hydrophobic effect at the lipid-water interface. $H_0$ describes the chain internal energy. $V_{\rm int}^{(1)}$ models the chain-chain interaction, which (somewhat arbitrarily) is taken to be nonzero only if a chain and its neighbour are both in the ordered state. This is an extreme approximation to the hypothesis, that the interaction forces are expected to decrease when either or both of the neighbouring chains are in the disordered state, but it is formally equivalent to setting the relative energy scales of the Hamiltonian. The third term in Eq. (2.3) represents the energy cost of stabilizing the lipid system against lateral expansion.

It is straightforward to determine the thermodynamic behaviour of this model (Doniach [78]), which is isomorphic to an Ising model in a temperature-dependent effective field, i.e.

$$H_{\rm D} = E_0 - \frac{J_0}{4} \sum_{\langle i<j \rangle} S_i S_j + \sum_i h_{\rm eff}(T) S_i \ , \tag{2.6}$$

where $E_0$ is a constant, $h_{\rm eff}(T) = -\frac{1}{2}(E_{\rm d} + \frac{z}{2}J_0 + P\Delta A - {\rm k_B}T \ln D_{\rm d})$, $\Delta A = A_{\rm d} - A_{\rm o}$, and $z$ is the coordination number of the lattice ($z = 6$ for a triangular lattice). At low temperatures the effective field prefers the chains to be in the ordered state. As $T$ increases, the system crosses over from the ordered state to the disordered state at a temperature $T_{\rm m}$ determined by

$$h_{\rm eff}(T_{\rm m}) = 0 \ , \tag{2.7}$$

provided that $T_{\rm m}$ is less than the critical temperature, $T_{\rm C}$, of the standard Ising model. This transition is effectively a field-induced transition below the critical temperature of the standard Ising model and is therefore a first-order transition usually referred to as the "chain-melting" transition.

While the Doniach lattice model includes the most essential physics associated with the lipid-chain conformational degrees of freedom, it ignores the translational

degrees of freedom. We therefore here propose an extension of the Doniach model to account for the interplay between the conformational and the translational degrees of freedom in the simplest way: the translational degrees of freedom of lipid chains are governed by interchain interactions that depend on the conformational states of the interacting chains. This extended model, which we refer to as Model III, is described by the following *random-lattice* Hamiltonian,

$$H_{\rm III} = H_0 + V_{\rm int}^{(1)} + V_{\rm int}^{(2)} + P \cdot A \ , \tag{2.8}$$

where

$$V_{\rm int}^{(2)} = \frac{1}{4} \sum_{(i<j)} V(|R_i - R_j|)(1 + S_i)(1 + S_j) \ , \tag{2.9}$$

and $A$ is the total area of the system. $V(R)$ in Eq. (2.9) is an attractive square-well potential of depth $V_0$ and range $R_0$. $V_{\rm int}^{(1)}$ and $V_{\rm int}^{(2)}$ together provide an approximation to the attractive intermolecular interaction between any two chains in the conformationally ordered state. The sum of the hard-disk potential and the two square-well potentials, $V_{\rm int}^{(1)}$ and $V_{\rm int}^{(2)}$, constitutes an approximation to a standard intermolecular potential of the Lennard-Jones type, as schematically illustrated in Fig. 2.1. By analogy with the Doniach lattice model, the effective interaction between any two chains in Model III is taken to be zero if either one or both of the chains are in the conformationally disordered state. The square-well potential described by $R_0$ and $V_0$ controls the minimum of the potential and hence the lattice parameter of the crystalline (solid) phase. The tail of the potential extending beyond $R_0$ permits a possible decoupling between the two melting (or order-disorder) processes associated with the translational and conformational degrees of freedom. This model is a minimal model in the sense that it contains only the most essential physics required to model the coupling between translational and internal degrees of freedom in lipid-bilayer systems.

The fundamental difference between Model III and the lattice model of Doniach is that each chain in Model III is allowed to have a varying number of nearest neighbours and varying distances from its neighbours. Furthermore, the chains are allowed to diffuse through the whole system, as the essential manifestation of translational invariance of the system. The two sets of degrees of freedom are coupled in a natural way through the intermolecular interactions. This model should display different

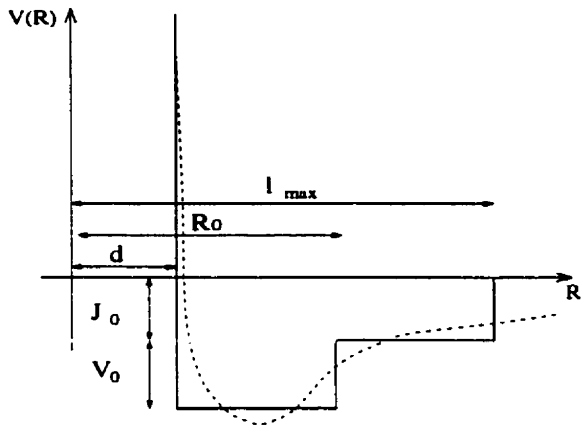


Figure 2.1: Schematic illustration of the interaction potential, $V(R)$, in Model III. It consists of a sum of a hard-disk potential and two square-well potentials. The hard-disk radius is $d$ and the range and strength of the square-well potentials are $(l_{max}, R_0)$ and $(J_0, V_0)$, respectively, described in the text. $l_{max}$ is the maximum tether length defined in Section 3.2. The dashed line illustrates a Lennard-Jones-like potential, to which the model potential is an approximation.

types of thermodynamic behaviour, depending on the strength of this coupling.

## 2.3 *A Model for Lipid-Cholesterol Mixtures (Model IV)*

The microscopic model discussed in this section is an extension of Model III proposed in the previous section to describe the generic phase behaviour of single-component lipid bilayers (Nielsen et al. [96a]).

The main result of the simulation studies of the model for the single-component system is given in Section 4.3 and summarized in Fig. 4.8, which shows a phase diagram given in terms of temperature and a parameter, $V_0/J_0$, measuring the relative strength of the two square-well attractions. The point of key importance in this phase diagram is the appearance of two distinct regimes, separated by a triple point, of different types of macroscopic interplay between the two types of degrees of freedom. A regime of macroscopic coupling between the two types of degrees of freedom, as observed experimentally in pure lipid bilayers, exists for values of $V_0/J_0$ greater than the triple-point value. However, a regime of macroscopic decoupling also exists as part of the generic thermodynamic behaviour of the model for values of $V_0/J_0$ smaller than the triple-point value, where two distinct ordering transitions take place successively, separated by an intermediate **lo** phase. The question then arises as to which part of the phase diagram of the single component system represents a pure lipid bilayer. In such a bilayer, the translational and conformational degrees of freedom are coupled. We therefore choose the phase behaviour of a pure lipid bilayer in the absence of

cholesterol to lie at a value of $V_0/J_0$ greater than the triple point value.

Based upon the model for the pure lipid bilayer system described in the previous section and the physics described above, a minimal model which describes a system containing both lipid chain particles and cholesterol molecules can be constructed by adding additional microscopic interaction terms to the Hamiltonian in Eq. (2.8):

$$H = H_0 + H_{o-c} + H_{d-c} + H_{c-c} + H_{o-d} \ . \tag{2.10}$$

Here $H_{o-c}$, $H_{d-c}$, $H_{c-c}$ and $H_{o-d}$, as indicated by the various subscripts, represent the pairwise interaction potentials between an ordered chain and a cholesterol molecule, a disordered chain and a cholesterol molecule, two cholesterol molecules, and an ordered chain and a disordered chain, respectively. They are defined as follows:

$$\begin{aligned} H_{o-c} &= \sum_{\langle i<j \rangle} V_{o-c}(R_{ij})\{\mathcal{L}_{io}\mathcal{L}_{jc} + \mathcal{L}_{jo}\mathcal{L}_{ic}\} \\ H_{d-c} &= \sum_{\langle i<j \rangle} V_{d-c}(R_{ij})\{\mathcal{L}_{id}\mathcal{L}_{jc} + \mathcal{L}_{jd}\mathcal{L}_{ic}\} \\ H_{c-c} &= \sum_{\langle i<j \rangle} V_{c-c}(R_{ij})\{\mathcal{L}_{ic}\mathcal{L}_{jc}\} \\ H_{o-d} &= \sum_{\langle i<j \rangle} V_{o-d}(R_{ij})\{\mathcal{L}_{io}\mathcal{L}_{jd} + \mathcal{L}_{jo}\mathcal{L}_{id}\} \ . \end{aligned} \tag{2.11}$$

Here $\langle i < j \rangle$ denotes a summation over nearest neighbours and $i$ is an index labeling the particles in the system. $\mathcal{L}_{id}$ and $\mathcal{L}_{io}$ are occupation variables which are unity when the $i$th particle is in the ordered and the disordered states, respectively and zero otherwise. $\mathcal{L}_{ic}$ is introduced so as to include the presence of the cholesterol molecules in the system and $\mathcal{L}_{ic}$ is unity if the $i$th particle is a cholesterol molecule and zero otherwise. The energy of interaction between two chains which are both in the disordered state is set to zero. For completeness, the model of Eq. (2.10) includes a term for the interaction between an ordered and a disordered lipid chain. This term was not included in the Hamiltonian in Eq. (2.8) since it has no importance for the generic phase behaviour of the model.

In terms of these occupation variables, the Hamiltonian for the pure lipid system Eq. (2.8) can be rewritten as

$$H_0 = \sum_i E_d \mathcal{L}_{id} + \sum_{\langle i<j \rangle} V_{o-o}(R)\mathcal{L}_{io}\mathcal{L}_{jo} + \Pi \cdot A \ . \tag{2.12}$$

Here $E_d$ is the excitation energy of the disordered conformational state and $V_{o-o}(R)$ is a distance-dependent interaction potential between two neighbouring particles that are both in the ordered state. $\Pi$ is, in effect, a lateral surface pressure stabilizing the system against lateral expansion and $A$ is the total area of the system.

Reflecting the strategy of minimal modelling, the additional microscopic interactions, $V_{o-c}(R)$, $V_{d-c}(R)$, $V_{c-c}(R)$ and $V_{o-d}(R)$, are each approximated in a similar manner to $V_{o-o}(R)$ in $H_0$, by a sum of a hard-disk repulsive potential of range $d$, a short-range square-well potential, $V^s(R)$, and a longer-range attractive square-well potential, $V^l(R)$. $V^s(R)$ and $V^l(R)$ are given by

$$V^s(R) = \begin{cases} -V^s & , \quad d < R \leq R_0 \\ 0 & , \quad \text{otherwise} , \end{cases} \tag{2.13}$$

$$V^l(R) = \begin{cases} -V^l & , \quad d < R \leq l_{\max} \\ 0 & , \quad \text{otherwise} . \end{cases} \tag{2.14}$$

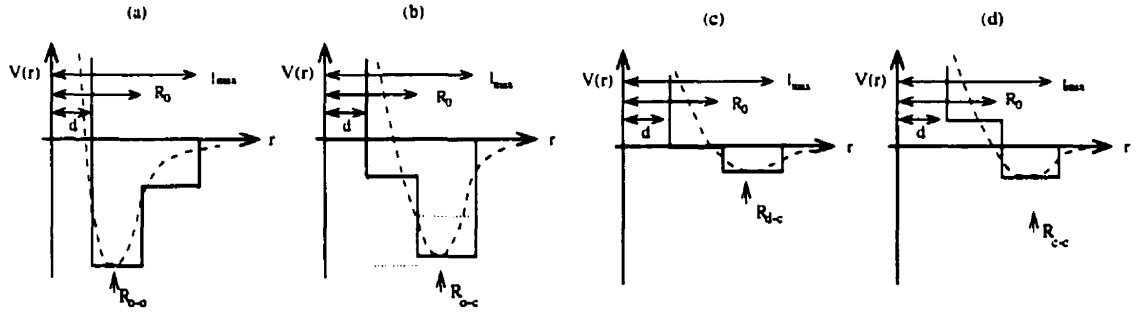


Figure 2.2: Model interaction potentials. (a) $V_{o-o}(R)$, (b) $V_{o-c}(R)$, (c) $V_{d-c}(R)$ and (d) $V_{c-c}(R)$. $d$ is the hard-disk radius, $R_0$ the radius of the short range square-well potential and $l_{max}$ the range of the longer range square-well potential. The ratio $\frac{R_0}{d}$ is chosen so that $\frac{R_{o-c}}{R_{o-o}} \approx 1.3$ giving an average surface area of the cholesterol molecules to be 30% larger than that of the lipid chains in the ordered state

Some of the microscopic interactions are sketched in Fig. 2.2 to illustrate our specific way of modelling the dual molecular mechanism of cholesterol molecules in lipid bilayers. A comparison between Fig. 2.2(a) and Fig. 2.2(b) illustrates the "ice-breaker" mechanism, as the interactions involved imply that a cholesterol molecule dissolved in an ordered-chain environment tends to have a larger surface area than that of a lipid chain, thus disrupting the lateral packing of the ordered chains. Similarly, a comparison between Fig. 2.2(b), Fig. 2.2(c) and Fig. 2.2(d) makes the "chain-rigidifier" mechanism clear, as the given interactions are such that a choles-

terol molecule prefers its neighbouring chains to be in the conformationally ordered state.

This simple model describes the dual effect of the cholesterol molecule on the lipid bilayer in a minimal manner. We can thus hope that the phase behaviour of the minimal model, as obtained from numerical simulations, gives the important phase characteristics of the lipid–cholesterol system and thus allows for an understanding of microscopic and macroscopic physical properties of lipid bilayers containing cholesterol.

## 2.4 A Model for Lipid-Sterol Mixtures

The model for lipid-cholesterol mixture systems given in the previous section was constructed without direct reference to the specific structure of the cholesterol molecules (Nielsen et al. [98]). Only the dual molecular mechanism of the sterol molecule being both a chain "rigidifier" and an "ice-breaker" made the model connect closely to the lipid-cholesterol system. It was hence expected that the model, given its various microscopic parameters, should be capable of describing more types of equilibrium phase behaviour than that of the lipid-cholesterol system. In other words, by systematically varying the values of certain parameters one should be able to establish a broader picture of the generic equilibrium phase behaviour of two-component systems. In particular, such a systematic variation could represent a change in the type of sterol dissolved in the lipid bilayer. This is particularly important in relation to the evolution of membranes. Bloom and Mouritsen ([88]) have proposed that cholesterol, which is the end-product along an evolutionary (biosynthetic) pathway for eucaryotic membranes, was specifically developed by nature to achieve optimal mechanical and biophysical properties for such eucaryotic membranes. It is therefore interesting to study the effect on the lipid bilayer of other sterols along the biosynthetic pathway so as to shed some light on this optimization process. In consequence, we have constructed a microscopic model designed with the aim of capturing the systematics of the equilibrium phase behaviour of a range of two-component systems modelling mixtures of lipids with different sterols. The model is identical to the one we proposed for the lipid-cholesterol mixture system, and the different sterol systems

are modelled via systematic variations in the model parameters.

Different sterol molecules should clearly have different effects on the lipid molecules when dissolved into the membrane bilayer. One way to distinguish the effect of the different sterol molecules on the lipid membrane system is to study their ability to rigidify the lipid acyl chains. Figure 2.3 shows the maximum chain order parameter as obtained by NMR measurements for the PPetPC bilayer as a function of concentration of two different sterol molecules, cholesterol and lanosterol (Thewalt [96]). At

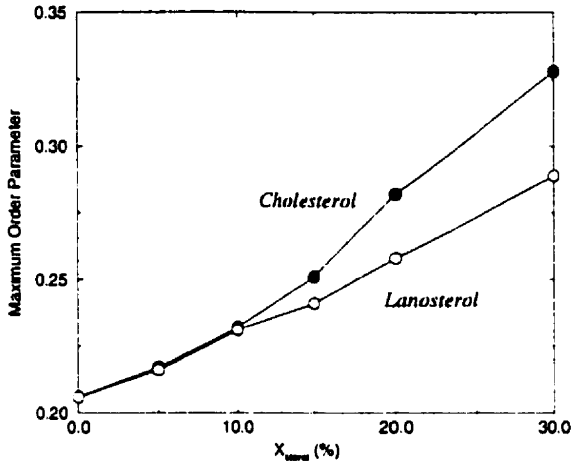


Figure 2.3: The maximum chain order parameter as a function of sterol concentration for the PPetPC-Cholesterol and the PPetPC-Lanosterol bilayer at T=40° C. (Adapted from J. Thewalt [96])

the temperature of $T = 40°$ C, the pure PPetPC lipid system is in the fluid phase characterized by a high degree of both lipid chain and lateral disorder. The chain rigidifying effect of both sterol types is clearly demonstrated in the figure. The figure also shows that lanosterol, which on an evolutionary time scale is the precursor of cholesterol, has a weaker rigidifying effect on the lipid chains in the membrane than cholesterol (Thewalt and Bloom [95]).

In the spirit of a minimal model, we assume that this ability to rigidify the lipid chains differently is the major difference between the various lipid sterol mixture systems. One way of modelling this effect is via a systematic variation in the strength of the lipid-sterol interaction potential $V_{o-c}$ in Eq. (2.10). In Fig. 2.4, we show a graph of the interaction potential suggested to describe a series of three different lipid-sterol

mixture systems along the biosynthetic pathway. It is clear from the figure that the dual molecular effect of being both a chain "rigidifier" and an "ice-breaker" is maintained in the form of the model interaction potential for all three sterol types. The only variation between the different sterol molecules is in the strength of the interaction with a lipid chain in the ordered state. This variation should lead to substantial differences between the different sterols in terms of both the effect of an "ice-breaker" and the effect of a chain "rigidifier".

The microscopic Hamiltonian for the different lipid-sterol systems is for all systems defined by Eq. (2.10) with the interaction potential $V_{o-sterol}$ defined as given in Fig. 2.4. All the other model parameters are taken to be identical for the different lipid-sterol mixtures. Since we invoke only one simple molecular mechanism in de-

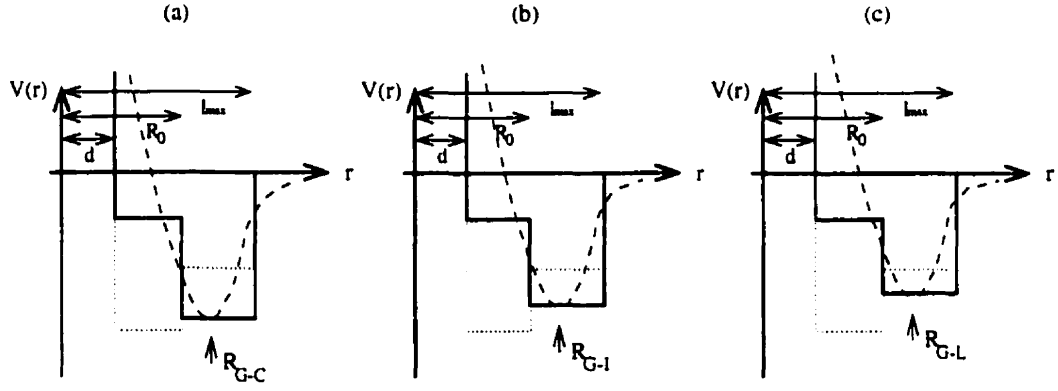


Figure 2.4: Model interaction potentials for a series of three lipid-sterol systems. (a) $V_{o-chol}(R)$, the cholesterol system, (b) $V_{o-int}(R)$, an intermediate sterol and (c) $V_{o-lan}(R)$, the lanosterol system.

scribing the different lipid-sterol mixture systems, we should be able to characterize the important molecular differences that distinguish the function of different sterols along the biosynthetic pathway in the lipid bilayer by comparing the phase behaviour of the model for different lipid-sterol mixture systems with that of the corresponding experimental ones.

## 2.5 Models for Thermally Induced Lysis of Fluid Lipid Membranes (Model V)

In the previous section, we constructed a model for the phase behaviour of lipid membranes containing sterols. This model can now serve as the basis for a description

of a large variety of problems related to lipid membrane systems. To illustrate the potential of the model, we shall in the following examine the lipid-sterol model in the context of membrane lysis and thermal stability of lipid membranes containing sterols.

A living cell depends crucially on its ability to maintain a mechanically stable plasma membrane that provides a tight chemical insulating layer with limited permeability to water, ions and other aqueous solutes. The fluid lipid bilayer encapsulating the living cell constitutes this insulating layer. The mechanical stability of the cell membrane can be modified in various ways. Electroporation experiments show that black lipid membranes (BLM's) rupture irreversibly when they experience an electric field of the order of 500 mV during a time period longer than several microseconds (Needham and Hochmuth [89]; Wilhelm et al. [93]; Winterhalter [96]). Absorption of foreign molecules also modifies the mechanical stability of the fluid membrane, e.g. absorption of peptides such as alamethicin, melittin and magainin induces defects and lysis of lipid membranes as the concentration of peptides is increased (Dimitrova and Matsumura [97]; Heller et al. [97]; Ludtke et al. [96]; Matsuzaki et al. [97]). The inclusion of sterols, such as cholesterol, in the lipid bilayer, on the other hand, increases resistance to pore formation and thus increases the mechanical stability against lysis of the lipid membrane (Needham and Hochmuth [89]; Zhelev and Needham [93]; Benachir et al. [97]).

A simple and commonly used model for membrane rupture is the zero temperature model of Litster ([75]). In this model, the appearance of a single hole with perimeter $\Gamma$ in the membrane under tension is associated with an edge energy cost, $\lambda\Gamma$, and an energy gain, $\sigma A$. The cost in edge energy is due to the hydrophobic properties of the lipid chains and the energy gain is due to the lateral tension. The two control parameters in the model are the line tension, $\lambda$, defined as the energy cost per unit length associated with the formation of a pore, and the lateral surface stress, $\sigma$, on the membrane. Note that $\sigma < 0$ corresponds to compression and $\sigma > 0$ corresponds to tension. The free energy controlling the stability of the membrane at zero temperature is then given as

$$\mathcal{F}_0 = -\sigma A + \lambda \Gamma \ , \tag{2.15}$$

where $A$ is the total area of the bulk membrane and hole, and $\Gamma$ is the length of the hole perimeter. At zero temperature, holes with a circular shape minimize the free energy. The creation of a circular hole with diameter $R$ is associated with a change in the free energy, $\Delta\mathcal{F}_0$, given by

$$\Delta\mathcal{F}_0 = -\sigma\pi R^2 + \lambda 2\pi R \ . \tag{2.16}$$

In Fig. 2.5 is shown a schematic plot of the function $\Delta\mathcal{F}_0(R)$. The figure shows that holes with a radius larger than a critical size $\lambda/\sigma$ are unstable and grow without bound. The membrane is thus metastable against formation of a large hole. In a situation where the critical free energy barrier $\Delta\mathcal{F}_0^* = \pi\lambda^2/\sigma$ is inaccessible to thermal fluctuations, the membrane will however remain intact in a finite time experiment since thermal fluctuations cannot take the system across the kinetic barrier $\Delta\mathcal{F}_0(R)$. The expression for the critical free energy barrier implies that the barrier vanishes only in the limits of $\lambda \to 0$ or $\sigma \to \infty$.

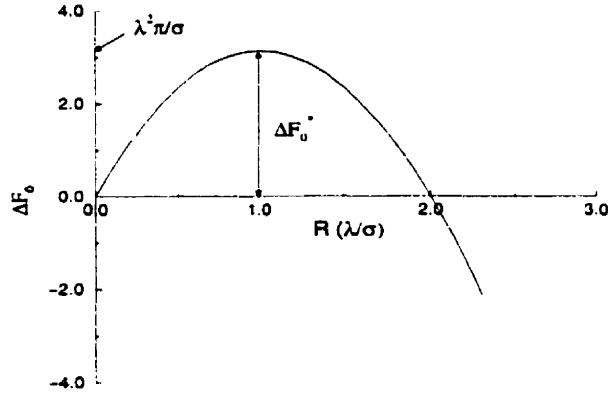


Figure 2.5: Schematic plot of the free energy cost, $\Delta\mathcal{F}_0(R)$, associated with the formation of a circular pore with diameter $R$. $\lambda/\sigma$ is the critical hole size. Holes with a radius larger than $\lambda/\sigma$ will grow without bound. The critical free energy barrier, $\Delta\mathcal{F}_0^*$, is $\pi\lambda^2/\sigma$.

### 2.5.1 Models for Thermal Stability of Lipid Membranes

The model presented here for the lysis of lipid membranes is an extension of a model first proposed by Shillcock and Boal ([96]) to describe the stability of fluid lipid membrane without internal degrees of freedom in the presence of a single hole. The

model was also extended by Shillcock and Seifert ([98]) to describe the stability of fluid lipid membranes in the presence of multiple holes. Before describing the model investigated in the present thesis, we give a short summary of the two earlier models.

*A Model for Thermal Stability of Membranes in the Presence of a Single Hole.*

The model of Shillcock and Boal ([96]) for the stability of lipid membranes in the presence of a single hole employs an algorithm similar to the random-lattice algorithm developed in this thesis. The fluid configurations of the membrane are defined in terms of the vertex positions and the connectivity of a random network (see Section 3.2). In the presence of a single hole, the number of vertices in the network is fixed but the number of tethers varies. Tethers can be inserted and removed at the boundary of the hole, thus allowing the hole size to fluctuate. Vertices defining the edge of the hole are called external as are tethers connecting two external vertices. All other vertices and tethers are internal. The Hamiltonian governing the thermal equilibrium properties of the single-hole membrane is the zero-temperature free energy defined in Eq. (2.15). The trial moves employed to sample phase space in the Monte Carlo simulation algorithm are the particle move, link flip and area change procedures described in Section 3.2.1 combined with an attempt to remove or add tethers along the edge of the hole. In the trial move that changes the area of the system, the side lengths $L_x$ and $L_y$ are attempted to be rescaled independently. This is in contrast to the procedure described in Section 3.2.1. The different types of trial moves are attempted with a fixed probability. In order to ensure detailed balance for the updating procedure of the length of the hole edge, we must insist that the probability for inserting a tether at a specific vertex equals the probability for removing a tether from a specific vertex. When removing a tether from a hole with $N_{edge}$ vertices along the edge, the probability for removing a tether from a specific vertex is $1/N_{edge}$. Note that the tether to be removed is always the tether connecting consecutive vertices in the anti-clockwise direction along the hole edge. If the trial move is accepted, the value of $N_{edge}$ is increased by one. When performing the reverse trial move, the probability for attempting an insertion of a tether at a specific vertex along the edge is then $1/(N_{edge}+1)$. In order for the two trial moves to be attempted with equal probability, the probability for removing a tether must hence be modified

according to $N_{edge}/(N_{edge}+1)$.

The central data structures in the algorithm implementing the single hole model of Shillcock and Boal ([96]) are link structures defining the configuration of the tethered network, a matrix defining the position of the vertices and a linked ordered list defining the edge of the single hole.

The central result in the work by Shillcock and Boal is a phase diagram for the stability of the lipid membrane as a function of the reduced line tension $\lambda^* = \beta\lambda d$ and applied reduced surface pressure $\sigma^* = \beta\sigma d^2$ ($\sigma < 0$). In situations where the membrane is under zero stress ($\sigma = 0$), they find that for $\lambda^* > 1.3$ only small holes are present in the membrane, whereas large holes are observed for $\lambda^* < 1.2$. The hole size is found to change rapidly around a value of $\lambda^*$ close to 1.24. They find that the value of $\lambda^* = 1.24$ separates the (meta)stable intact state from the ruptured state of the lipid membrane. When the membrane is under compression, they find that the membrane at values of the line tension larger than a specific (stress dependent) value is thermodynamically stable. The value of $\lambda^*$ that separates the stable and unstable state of the membrane is naturally smaller than 1.24 when the membrane is under compression.

*A Model for Thermal Stability of Membranes in the Presence of Multiple Holes.*

Shillcock and Seifert ([98]) extended the single-hole model of Shillcock and Boal so as to describe the stability of the lipid membrane in the presence of multiple holes.

In this model, both the number of holes and the length of the hole perimeter are fluctuating quantities. The free energy defining the equilibrium phase behaviour is given by Eq. (2.15). Holes are created in the internal part of the membrane, when a tether connecting two internal vertices is removed. The energy cost associated with the creation of such a hole is $Q$. This represents the barrier that thermal fluctuations must overcome in order to create a hole of minimal size in the lipid membrane. In the model, $Q$ is defined in terms of a chemical potential $\mu$ as follows; $Q = \lambda L_{min} - \mu$, where $L_{min}$ is the summed length of the tethers forming the edge of the new hole and $\lambda$ is the line tension. In the simulations, it is found that the minimum hole perimeter $L_{min}$ is always close to $5.33d$, and the barrier, $Q$, is thus related to the chemical potential, $\mu$, in a simple manner. The two dimensionless parameters controlling the

formation and stability of holes in the membrane are then

$$\lambda^* = \beta\lambda d \quad \text{and} \quad q^* = \beta Q \ , \tag{2.17}$$

where $d$ is the hard disk diameter and $\beta$ the inverse temperature.

The set of trial moves adapted to sample phase space for the multiple hole model is naturally larger than for the single hole model, since we now have to include moves that allow for a variation in the number of holes present in the membrane. In the model by Shillcock and Seifert ([98]), the number of holes is allowed to vary via two distinct processes. Holes are created and resealed in the membrane as described earlier. Furthermore, holes can coalesce and fragment. For the coalescence process, two holes come into contact and coalesce to form a larger hole. In a fragmentation process, a hole breaks up into two smaller ones. In order to ensure the correct implementation of the multiple hole model, the various trial moves for insertion and removal of tethers along the edge of the holes as well as the trial moves for creation, sealing, coalescence and fragmentation of holes must be attempted in a manner that obeys detailed balance. The details regarding how the multiple hole model is implemented in the simulations so as to ensure detailed balance is given in Appendix A.3.

The main result of the work of Shillcock and Boal is a phase diagram giving the stability of the lipid membrane under zero stress as a function of the reduced parameters $\lambda^*$ and $q^*$. This phase diagram is given in Fig. 2.6. The rupture line in the phase diagram separates two distinct regimes corresponding to an intact and a ruptured state of the lipid membrane, respectively. The rupture line can be described as a function of one of the two reduced parameters, $q^*$ or $\lambda^*$ as;

$$\lambda^* = \lambda_R(q^*) \quad \text{or} \quad q^* = q_R^*(\lambda^*) \ , \tag{2.18}$$

where the subscript $R$ refers to the rupture transition. In the asymptotic limit, the rupture transition occurs at

$$\lambda_R^*(q^* \to \infty) = 1.24 \pm 0.02 \quad \text{and} \quad q_R^*(\lambda^* \to \infty) = 3.3 \pm 0.2 \ . \tag{2.19}$$

In the limit of $q^* \to \infty$, corresponding to the limit of an infinitely high barrier against the formation of a single hole, the authors find that the membrane ruptures through the formation of a single hole that grows in size to pass the critical minimum hole

size for rupture (see Fig. 2.5). In this limit, the result of Shillcock and Boal ([96]) for the single hole model is thus recovered. For $\lambda^* \to \infty$, they find a rupture scenario where multiple small holes form and coalesce into a large hole with a size larger than the critical hole size for rupture. In the two limits, they thus find distinct scenarios for rupture.

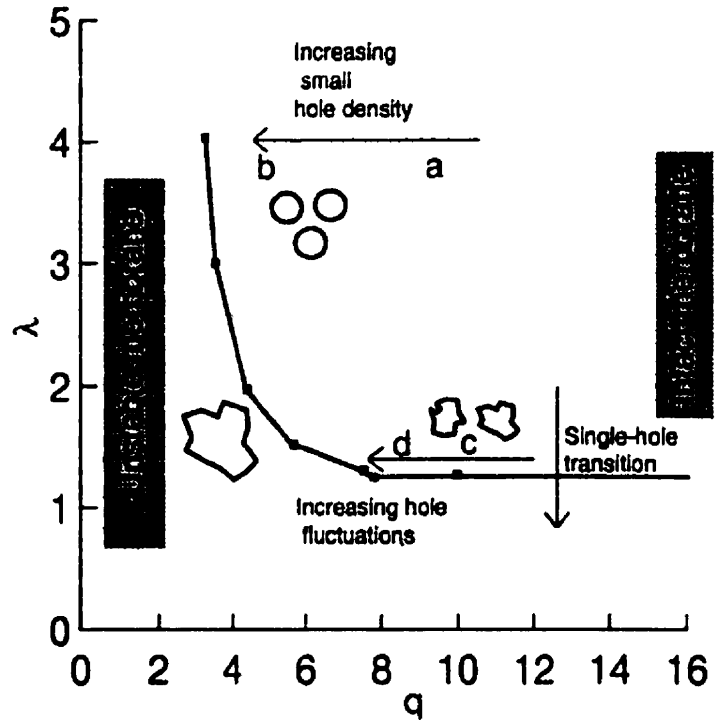


Figure 2.6: Phase diagram for the model fluid membrane in the reduced line tension, reduced barrier height plane at zero stretching tension. The bold line denotes the rupture transition separating an intact membrane form a disintegrated one, and the symbols mark the simulation data. At large line tension, multiple small holes are present in the membrane, and a single large hole fluctuates through the membrane close to $\lambda^* = 1.25$. The upper horizontal arrow represents a possible path for rupture at large $\lambda^*$ in which more small holes are created as $q^*$ is reduced. The lower horizontal arrow represents rupture at small $\lambda^*$. Rupture via the entropy-driven growth of a single fluctuating hole is indicated by the vertical arrow. Adapted from Shillcock and Seifert [98].

### 2.5.2 *A Model for Thermal Stability of Membranes Decorated with Lipid Chain Degrees of Freedom in the Presence of Holes*

We now present Model V, which is a model for the stability of lipid membranes decorated with lipid chain degrees of freedom in the presence of single holes. In this model, the configurational degrees of freedom of the lipid membrane are described

in the same way as in the models of Shillcock and Boal ([96]) and Shillcock and Seifert ([98]). We include the lipid chain degrees of freedom by decorating each vertex in the random-lattice description with a set of conformational states defined by the Model IV of Eq. (2.10). The edge free energy associated with a hole in the membrane is given by $\sum_\Gamma \lambda R_i + V(R_i)$. Here, the summation is over the perimeter of the hole, $R_i$ is the length of the tethers connecting consecutive vertices along the edge of the hole and $V(R_i)$ is the interaction potential between neighbouring particles at the vertices along the edge of the hole.

This minimal model for the thermal stability of the lipid membrane, allows us to address the question of how the stability of the lipid membrane is modified in the presence of sterols. The analysis of the phase behaviour of the lipid-sterol systems as described in Section 2.3 provides a detailed picture of the functional difference between cholesterol and lanosterol molecules when dissolved in lipid membranes. This knowledge combined with the results of a simulation study of the model (see Chapter 6) allows us to gain insight into the function of different sterols as mechanical stabilizers of lipid membranes in general and to obtain a specific understanding of the functional differences between different sterol types in the context of membrane lysis.

# 3

# NUMERICAL METHODS

In this chapter, we describe the different numerical methods that we have developed and employed in analyzing the equilibrium phase behaviour of the models proposed in Chapter 2. All the models were analyzed using the numerical method of Monte Carlo simulations. In the first part of this chapter, we describe in terms of the methodology and diagnostic tools how numerical methods can be applied to determine the phase behaviour of a microscopic thermodynamic model. Next we give a detailed description of the random-lattice algorithm developed to allow for an accurate and highly efficient description of the lateral degrees of freedom of the microscopic models.

## *3.1 Methodology and Diagnostic Tools*

A variety of diagnostic techniques were employed to determine the equilibrium phase behaviour of the different models described in the previous chapter. In the following, we will give a short summary of each of the different techniques.

- The Metropolis Monte Carlo algorithm and the calculation of thermodynamic averages.
- Finite size scaling.
- Histograms and Ferrenberg-Swendsen reweighting techniques.
- Spectral free energy functions and Lee-Kosterlitz finite size scaling.
- The Umbrella sampling or modified Hamiltonian technique.

### 3.1.1 The Metropolis Monte Carlo Algorithm

The thermodynamic behaviour of systems in equilibrium is described by thermal averages of appropriate physical quantities. In this section, we describe the Metropolis Monte Carlo method which is used in this thesis together with numerical simulations to calculate such averages. The relevant physical averages include the order parameter, internal energy, surface area, and corresponding thermodynamic response functions like susceptibility, specific heat and compressibility. It should be emphazised that one of the main forces of the Monte Carlo method is that it provides a solution for the equilibrium state of a model system where no analytic solution is available. Furthermore, this solution includes the effects of thermal fluctuations.

The thermal average of a quantity $\mathcal{O}$ is defined as

$$\begin{aligned} < \mathcal{O} > &= \frac{\sum_l e^{-\beta H(l)} \mathcal{O}(l)}{Z} \\ &= \sum_l \rho(l) \mathcal{O}(l) \ , \end{aligned} \tag{3.1}$$

where $\sum_l$ is a sum over the entire phase space. $Z$ is the partition function $Z \equiv \sum_l e^{-\beta H(l)}$, $\beta$ is the inverse temperature $1/k_B T$, $\rho(l)$ is the statistical weight and $H(l)$ is the internal energy of the microconfiguration $l$.

If the simulation algorithm is ergodic, then a single simulation is able to sample all of the equilibrium phase space. Suppose that the algorithm we are using will generate the different microconfigurations with a probability given by the probability distribution $\rho(l)$. Then we can approximate the thermal average in Eq. (3.1) by a "time" average

$$< \mathcal{O} >= \frac{1}{\tau} \sum_{t=1}^{\tau} \mathcal{O}(t) \ . \tag{3.2}$$

This relation between the thermal average and the "time" average is the key to all Monte Carlo simulations. It is important to note that relation (3.2) was derived using two criteria. First, the algorithm employed in the simulations must be able to explore the entire equilibrium phase space of the system (ergodic sampling). Second, the random sequence of microconfigurations (the underlying Markov chain) must generate the different microconfigurations with the probability $\rho(l)$. If either of these

two conditions fails the Monte Carlo algorithm will not give the correct equilibrium properties of the system.

How do we ensure that the algorithm generates the different microconfigurations with a probability given by $\rho(l)$? In the Metropolis Monte Carlo scheme (Metropolis et al. [53]), the probability for accepting a trial move from a microconfiguration $I$ to a microconfiguration $J$ is given by

$$acc(I \rightarrow J) = \min(1, e^{-\beta \Delta H}) \ , \tag{3.3}$$

where $\Delta H$ is the difference in energy between the microconfigurations $I$ and $J$. We now show that the Metropolis Monte Carlo scheme generates the correct distribution function, $\rho(l)$. One obvious criterion the Monte Carlo algorithm must satisfy is that it should not destroy a thermodynamic equilibrium state (Frenkel and Smit [97]). This is to say that, in equilibrium, the number of accepted trial moves that result in the system leaving state $I$ must be exactly counterbalanced by the number of accepted trial moves from all other states to state $I$. If, in equilibrium, the average number of accepted moves from a state $I$ to any other state $J$ is equal to the number of reverse moves from any state $J$ to state $I$, then detailed balance is said to be satisfied. It is clear that this criterion is stronger than the one given above, and that the criterion of detailed balance hence is a sufficient, but not necessary condition for the stability of the equilibrium state. The condition of detailed balance can be written as

$$\rho(I)\pi(I \rightarrow J) = \rho(J)\pi(J \rightarrow I) \ , \tag{3.4}$$

where $\rho(I)$ is the probability of the system being in the state $I$ and $\pi(I \rightarrow J)$ is the transition matrix defining the probability of performing the move from state $I$ to state $J$. Now $\pi$ can be decomposed in two parts, $\alpha(I \rightarrow J)$, the probability of attempting a trial move from $I$ to $J$ and $acc(I \rightarrow J)$, the probability of accepting this particular trial move,

$$\pi(I \rightarrow J) = \alpha(I \rightarrow J) acc(I \rightarrow J) \ . \tag{3.5}$$

If $\alpha$ is symmetric (i.e. $\alpha(I \rightarrow J) = \alpha(J \rightarrow I)$), we can then rewrite Eq. (3.4) as

$$\frac{acc(I \to J)}{acc(J \to I)} = e^{-\beta \Delta H} \quad . \tag{3.6}$$

The Metropolis Monte Carlo acceptance criteria (Eq. (3.3)) clearly satisfies this relation and we have hence shown that the Metropolis Monte Carlo scheme does indeed generate the correct equilibrium distribution function.

It is important to keep in mind that in deriving Eq. (3.6) we impose a strong constraint on the properties of the transition matrix, $\alpha$, since we assume it to be symmetric. This has important consequences for the manner in which the Monte Carlo algorithm must be constructed especially for complex systems with many degrees of freedom, as we shall see later.

Based on the Metropolis Monte Carlo scheme for accepting trial moves between different microconfigurations, we generate a series of random microconfigurations which we use to calculate the thermal averages using the Eq. (3.2).

Thermodynamic response functions are all related to thermal averages of first and second moments of thermodynamic quantities such as the internal energy, $E$, the order parameter, $M$, and the area, $A$, through the fluctuation-dissipation theorem. The specific heat at constant pressure, $C_P$, the order parameter susceptibility, $\chi$, and the area compressibility, $K$, are hence given by

$$\begin{aligned} C_{\mathrm{P}} &= \frac{\langle H^2 \rangle - \langle H \rangle^2}{N k_{\mathrm{B}} T^2} \quad , \\ \chi &= \frac{\langle M^2 \rangle - \langle M \rangle^2}{N k_{\mathrm{B}} T} \quad , \\ K &= \frac{\langle A^2 \rangle - \langle A \rangle^2}{k_{\mathrm{B}} T \langle A \rangle} \quad , \end{aligned} \tag{3.7}$$

where $H$ is the model Hamiltonian (for a system at constant pressure), $M$ is the total spin order parameter, $A$ is the total area of the system and $N$ the total number of particles. These response functions can thus be calculated via "time-averages" of first and second moments of $H$, $M$ and $A$, respectively. Signatures of phase transitions can then be identified from these measured equilibrium quantities without having to perform numerical differentiation.

### 3.1.2 Finite Size Scaling

In a computer simulation, one can only examine systems of finite size. When simulating a system close to a phase transition, this finite size alters the phase behaviour as compared to the infinitely large system. The nature of such finite-size effects depends on the type of transition.

In a second order (continuous) transition, the thermodynamic response functions diverge as the critical point is approached. This divergence is a direct consequence of the divergence of the correlation length $\xi$ at the critical point. Close to a critical point, the response functions $C_P$ and $\chi$ for a finite system can be expressed in the following scaling forms (Ferdinand and Fisher [69])

$$\begin{aligned} C_P(L,T) &= |t|^{-\alpha} g(L/\xi(t)) \ , \\ \chi(L,T) &= |t|^{-\gamma} f(L/\xi(t)) \ , \end{aligned} \tag{3.8}$$

where $t = (T - T_C)/T_C$, and $T_C$ is the critical temperature of the corresponding infinite system. $g$ and $f$ are non-singular scaling functions with the following limiting behaviour

$$g(x),\ f(x) \to \text{const} \ \text{ for } \ x \to \infty \ , \tag{3.9}$$

$$f(x) \to x^{\gamma/\nu} \ \text{ for } \ x \to 0 \ , \tag{3.10}$$

$$g(x) \to x^{\alpha/\nu} \ \text{ for } \ x \to 0 \ . \tag{3.11}$$

The first of these limits ensures the correct scaling relations $C_P \sim t^{-\alpha}$ and $\chi \sim |t|^{-\gamma}$ in the limit where $L \to \infty$. Since $\xi(t) \sim |t|^{-\nu}$ close to a critical point, the other two limits ensure that the response functions are temperature independent as the correlation length becomes much larger that $L$. Eq. (3.10) and Eq. (3.11) predict the following finite size scaling relations for the maximum of the specific heat, $C_{P,MAX}$, the maximum of the order parameter susceptibility, $\chi_{MAX}$, as well as for the half width of the susceptibility curve, $\delta\chi$ (Plischke and Bergensen [89])

$$\begin{aligned} C_{P,MAX} &\sim L^{\alpha/\nu} \ , \\ \chi_{MAX} &\sim L^{\gamma/\nu} \ , \\ \delta\chi &\sim L^{-1/\nu} \ . \end{aligned} \tag{3.12}$$

| $N$ | 125 | 1,000 | 64,000 | 1000,000 |
|---|---|---|---|---|
| $P_{int}$ | 78 % | 49 % | 14 % | 6 % |

Table 3.1: Percentage of particles ($P_{int}$) in the interface of a cubic domain containing $N$ particles. Only the outermost particles are assumed to belong to the interface. (Adapted from D. Frenkel and B. Smit [97] p. 184.)

For first order phase transitions, the nature of the finite-size effect on the phase behaviour is totally different. At a first order phase transition, two equilibrium phases coexist at a point where the temperature, pressure and chemical potential are identical for the two bulk phases. For an infinitely large system, the thermodynamic properties are hence determined by the properties of the bulk phases. This is because the number of particles on the interface between the two bulk phases is vanishing small compared to the number of bulk particles. In a finite size system, the situation is quite different. Here the number of particles on the interface plays an important role and even for rather large systems the fraction of particles on the interface is not negligible (see Table 3.1).

The phase behaviour close to a first order transition for a finite-size system hence depends strongly on system size simply because a large fraction of the particles is at the interface between the two coexisting phases. A direct simulation of phase coexistence is difficult under the best circumstances and often even impossible because of the large system sizes needed for the effects of the interface to be negligible. Many different methods have been developed to deal with the problems of simulating first order phase transitions and coexistence in a finite system. Two important methods are the finite size scaling theory of Lee and Kosterlitz ([90]) described in Section 3.1.4 and a series of techniques, commonly denoted Gibbs ensemble techniques, that simulate coexistence indirectly without having to deal explicitly with an interface (Panagiotopoulos [87]; Kofke [93]). In this work, we concentrate on the application of the finite size scaling method and we will not give here a detailed description of the different Gibbs ensemble methods but rather refer the reader to the book by D. Frenkel and B. Smit ([97]) and references in this book.

When analyzing the thermodynamic models defined in Chapter 2, we are dealing with systems undergoing solid–liquid phase transitions. It is in general a very difficult and time consuming task to perform direct Monte Carlo simulations of a solid-liquid

phase transition. The problems associated with a direct simulation of a solid–liquid phase coexistence are described in Section 3.1.5.

In the simulations of the phase equilibria of two component systems (Model IV), we perform the simulations within a semi-grand canonical ensemble. In the semi-grand canonical ensemble, the relative concentration of the two components is allowed to fluctuate. The equilibrium concentration is controlled by the difference in chemical potential between the two species. A simulation at coexistence within the semi-grand canonical ensemble thus samples the two pure equilibrium phases with equal probability and hence samples the thermodynamic equilibrium distribution function without generating an interface. The details of how this ensemble is implemented in the Monte Carlo algorithm is given in Section 4.1.1.

### 3.1.3 *Histograms and Ferrenberg-Swendsen Reweighting Techniques*

As described in the Section 3.1.1, the Monte Carlo algorithm generates a random sequence of points (microconfigurations) in such a way that the points are distributed in phase space according to the probability distribution function $\rho(l)$. Rather than just calculating the thermal averages as given by Eq. (3.2), we can thus extract the full information on the probability distribution function in a Monte Carlo simulation. Some of the related techniques are now described.

*Histograms*

The probability distribution function, $\mathcal{P}_\beta(E)$, at an inverse temperature $\beta = 1/k_B T$ is defined as

$$\begin{aligned} \mathcal{P}_\beta(E) &= \int \mathcal{D}\bar{r}\ \delta(E - E'(\bar{r}))\ \rho_\beta(\bar{r}, E'(\bar{r})) \\ &= < \delta(E - E') >_\beta \ , \end{aligned} \tag{3.13}$$

where $E'$ is the operator returning the energy of a microconfiguration $\bar{r}$ and $\int \mathcal{D}\bar{r}$ denotes integration over the entire phase space. In a Monte Carlo simulation, an energy histogram can be calculated by dividing the energy of the sampled microconfigurations into groups of bin-width $\Delta E$. The normalized energy histogram is then given by

$$\tilde{\mathcal{P}}_\beta(E_i) = \frac{N_\beta(E_i)}{\sum_j N_\beta(E_j)} \ , \tag{3.14}$$

where $N_\beta(E_i)$ is the number of microconfigurations with an energy $E$ in the interval $E_i - \Delta E/2 < E < E_i + \Delta E/2$. This energy histogram is then an approximation to the exact energy distribution function of Eq. (3.13) since

$$\tilde{\mathcal{P}}_\beta(E_i) = \mathcal{P}_\beta(E_i)\Delta E \ . \tag{3.15}$$

Once the histogram has been calculated for a thermodynamic quantity, $X$, it is straightforward to calculate the thermal average of any function of this quantity

$$\begin{aligned} < f(X) >_\beta &= \int dX f(X)\mathcal{P}_\beta(X) \\ &\simeq \sum_i f(X_i)\tilde{\mathcal{P}}_\beta(X_i) \ . \end{aligned} \tag{3.16}$$

*The Ferrenberg-Swensen Reweighting Technique*

Ferrenberg and Swensen ([88]) developed an important technique that greatly reduces the computational cost of analyzing the phase behaviour of microscopic models such as those described in Chapter 2. Ferrenberg and Swensen noted that a probability distribution function $\mathcal{P}_{\beta_0}$ calculated at an inverse temperature $\beta_0$ can be reweighted to another probability function at a new inverse temperature $\beta$ close to $\beta_0$. The method relies on the fact that the density of states, $\Omega(E)$, for a system is independent of temperature. The density of states is defined as

$$\Omega(E) = \sum_l \delta(E - E'(l)) \ , \tag{3.17}$$

where $\sum_l$ denotes a summation over the entire phase space. The energy distribution function is defined as

$$\begin{aligned} \mathcal{P}_{\beta_0}(E) &= < \delta(E - E') >_{\beta_0} \\ &= \sum_l \delta(E - E'(l))e^{-\beta_0 E'(l)}/Z_{\beta_0} \\ &= \frac{e^{-\beta_0 E}}{Z_{\beta_0}}\Omega_{\beta_0}(E) \ . \end{aligned} \tag{3.18}$$

Using the fact that $\Omega_{\beta_0}(E) = \Omega_\beta(E)$, the energy distribution function at $\beta$ can be written as

$$\mathcal{P}_\beta(E) = \frac{Z_{\beta_0}}{Z_\beta} e^{-(\beta-\beta_0)E} \mathcal{P}_{\beta_0}(E) \ . \tag{3.19}$$

Now the ratio $\frac{Z_\beta}{Z_{\beta_0}}$ can be expressed in terms of the distribution function $\mathcal{P}_{\beta_0}(E)$ as

$$\begin{aligned} \frac{Z_\beta}{Z_{\beta_0}} &= \frac{1}{Z_{\beta_0}} \sum_l e^{-\beta E(l)} \\ &= \frac{1}{Z_{\beta_0}} \sum_l e^{-(\beta-\beta_0)E(l)} \ e^{-\beta_0 E(l)} \\ &= \sum_i e^{-(\beta-\beta_0)E_i} \ \mathcal{P}_{\beta_0}(E_i) \ , \end{aligned} \tag{3.20}$$

where we in the last line have used the definition for $\mathcal{P}_{\beta_0}(E)$ of Eq. (3.18). Rewriting Eq. (3.19) in terms of the energy histogram and substituting the result of Eq. (3.20) we obtain a general expression for $\mathcal{P}_\beta(E_i)$

$$\mathcal{P}_\beta(E_i) = \frac{\mathcal{P}_{\beta_0}(E_i) e^{-(\beta-\beta_0)E_i}}{\sum_j \mathcal{P}_{\beta_0}(E_j) e^{-(\beta-\beta_0)E_j}} \ . \tag{3.21}$$

The reweighting technique can be generalized to any distribution function $\mathcal{P}(\mathcal{X}, \mathcal{Y}, \mathcal{Z}, \cdots)$ with respect to the corresponding conjugated fields $h_X, h_Y, h_Z, \cdots$. For our calculations, an important generalization is the reweighting of the two-dimensional distribution function $\mathcal{P}_{\beta,\mu_\Delta}(E, N_s)$, where $E$ is the total internal energy (enthalpy) of the system, $N_s$ the number of sterol particles, and $\mu_\Delta$ the conjugated field, i.e. the difference in chemical potential between the lipid and the sterol particles . If $\mathcal{P}_{\beta_0,\mu_{\Delta 0}}(E, N_s)$ is calculated at specific values $\beta_0$ and $\mu_{\Delta 0}$, the distribution function at a new set of values $\beta$ and $\mu_\Delta$ close to $\beta_0$ and $\mu_{\Delta 0}$ can be found from the following reweighting relation

$$\mathcal{P}_{\beta,\mu_\Delta}(E, N_s) = \frac{\mathcal{P}_{\beta_0,\mu_{\Delta 0}}(E, N_s) e^{-(\beta-\beta_0)E} \ e^{-(\mu_\Delta\beta - \mu_{\Delta 0}\beta_0)N_s}}{\sum_{E',N_s'} \mathcal{P}_{\beta_0,\mu_{\Delta 0}}(E', N_s') e^{-(\beta-\beta_0)E'} \ e^{-(\mu_\Delta\beta - \mu_{\Delta 0}\beta_0)N_s'}} \ . \tag{3.22}$$

Based on this two-dimensional distribution function, one can then calculate the two one-dimensional distribution functions as

$$\mathcal{P}_{\beta,\mu_\Delta}(N) = \sum_E \mathcal{P}_{\beta,\mu_\Delta}(E,N) \ , \tag{3.23}$$

$$\mathcal{P}_{\beta,\mu_\Delta}(E) = \sum_N \mathcal{P}_{\beta,\mu_\Delta}(E,N) \ . \tag{3.24}$$

It is important to note that reweighting will only be accurate if the "overlap" between the "old" and the "new" histogram is large so that the "old" histogram has an accurate statistical sampling where the "new" histogram has large values. Since the probability function becomes extremely sharply peaked as $N \to \infty$, the interval over which the probability function is accurately sampled becomes narrower as $N$ becomes larger. The parameter interval where the reweighting technique is accurate thus becomes very narrow as the system size is increased. An extension of the Ferrenberg–Swendsen reweighting method has been reported by Ferrenberg and Swendsen ([89]) and P.B. Bowen *et. al.* ([89]). This extension of the single histogram technique provides an optimized method for combining the data from an arbitrary number of simulations to obtain information over a wide range of parameters values in form of continuous functions. However, the method still requires a substantial overlap between the distribution function of the different simulations in order for the calculation of the combined histogram to be accurate. Close to a first order transition, the histogram must sample two coexisting phases and the corresponding free energy barrier. In these situations, the combination of multiple histograms will not give an improved statistical sampling of the free energy barrier and therefore will not provide a significant improvement as compared to the single histogram method. In this work, we have hence only applied the single histogram reweighting technique.

### *3.1.4 Spectral Free Energy Functions and Lee-Kosterlitz Scaling*

It was realized by Lee and Kosterlitz ([90]; [91]) that a free-energy-like function (the so-called spectral free energy function) can be constructed from the probability distribution function $\mathcal{P}_\beta(E)$ as follows

$$\beta\mathcal{F}_\beta(E) = -\ln \mathcal{P}_\beta(E) \ . \tag{3.25}$$

Using the definition of $\mathcal{P}_\beta(E)$ (Eq. (3.18)) and the definition of the microcanonical entropy function $S(E) \equiv k_B \ln \Omega(E)$, the distribution function $\mathcal{P}_\beta(E)$ can be written as

$$\mathcal{P}_\beta(E) = \frac{1}{Z_\beta} e^{-\beta(E-TS(E))} \ . \tag{3.26}$$

It can then be seen that the free energy function of Eq. (3.25) only differs from the Helmholtz free energy $F_\beta(E) \equiv E - ST$ of the system by an additive temperature and system size dependent constant

$$\beta \mathcal{F}_\beta(E) = \ln Z_\beta + \beta F_\beta(E) \ . \tag{3.27}$$

At fixed size and temperature, the shape of $\mathcal{F}_\beta(E)$ will be identical to that of $F_\beta(E)$ and more important $\Delta\mathcal{F}_\beta = \mathcal{F}_\beta(E) - \mathcal{F}_\beta(E')$ will be equal to $\Delta F_\beta = F_\beta(E) - F_\beta(E')$.

Based on this close connection between the spectral free energy function and the real free energy of the system, Lee and Kosterlitz proposed a powerful finite-size scaling method to determine the nature of a phase transition in a microscopic model.

Consider the spectral free energy function $\mathcal{F}_\beta(E, L)$ calculated for a finite system of size $L$ close to a first order transition. Then $\mathcal{F}_\beta(E, L)$ will have the general shape of a double well function with minima at $E = E_1$ and $E = E_2$ corresponding to the equilibrium energies of the two coexisting phases, respectively. The two minima will be separated by a barrier $\Delta\mathcal{F}_\beta(L)$ with a maximum at $E = E_{max}$. The height of this barrier is a measure of the interfacial free energy between the two coexisting phases and is given by

$$\begin{aligned} \Delta\mathcal{F}_\beta(L) &= \mathcal{F}_\beta(E_{max}, L) - \mathcal{F}_\beta(E_{1,2}, L) \\ &= \gamma_\beta L^{d-1} + \mathcal{O}(L^{d-2}) \ , \end{aligned} \tag{3.28}$$

where $d$ is the dimension of the system and $\gamma_\beta$ is the interfacial tension. This relation provides a clear and unambiguous (at least in principle) way to distinguish the types of transitions in play in a microscopic model. A first order phase transition is characterized in the thermodynamical limit by a non-zero interfacial tension between the two coexisting phases. Therefore, $\Delta\mathcal{F}_\beta(L)$ at a first order transition must increase

monotonically with $L$. On the other hand, the interfacial tension vanishes in the thermodynamical limit at a critical point and $\Delta\mathcal{F}_\beta(L)$ therefore in this case approaches a constant value. Finally, $\Delta\mathcal{F}_\beta(L)$ will tend to zero in the absence of a transition.

### 3.1.5 *The Umbrella Sampling or Modified Hamiltonian Technique*

One of the important criteria for the Metropolis Monte Carlo method is the ergodicity criterion stating that the Monte Carlo algorithm must be designed in such a way that the thermal average of a physical quantity is equal to the "time-average" of Eq. (3.2). This means that, close to a first order phase transition, the Monte Carlo algorithm must be able to sample microconfigurations corresponding to both of the coexisting phases. In doing so, the system must "travel" through the energy barrier separating the two coexisting phases several times during the simulations. At a first order transition, where the free energy barrier is an increasing function of system size (see Section 3.1.4), the use of the conventional Metropolis Monte Carlo scheme becomes difficult for large system sizes since the large value of the interfacial free energy causes the Monte Carlo trial moves to configurations with an interface to be energetically highly unfavorable and hence very improbable.

Risbo *et al.* ([97]) developed a method based on a modified Hamiltonian to overcome these difficulties. The method exploits the idea of constructing an "artificial" Hamiltonian that gives a considerably diminished energy barrier. The name *Umbrella sampling* refers to the bridging property of the Monte Carlo sampling of the "artificial" Hamiltonian, in that the distribution function of the "artificial" Hamiltonian bridges the minimum in the distribution function separating the two coexisting phases of the original Hamiltonian (Frenkel and Smit [97]).

The equilibrium distribution functions for the original Hamiltonian can then be established from simulations of the modified Hamiltonian through a simple reweighting relation. This method can be considered to be a generalization of other Monte Carlo sampling schemes such as the multicanonical-ensemble scheme (Berg and Neuhaus [92]). For a complete discussion of the method and related references, the reader is referred to Ref. (Risbo. [97]).

In our simulation study of the microscopic model of Eq. (2.10), this method was implemented in simulations performed within the semi-grand canonical ensem-

ble. One of the most important equilibrium distribution functions in this ensemble is $\mathcal{P}_{\beta,\mu_\Delta}(\varepsilon, x_c)$, where $\beta$ and $\mu_\Delta$ are the thermodynamic control parameters, and $\varepsilon \equiv \frac{E}{N}$ and $x_c$ are the energy per particle and the cholesterol concentration, respectively. A corresponding spectral free energy function can now be defined as $\mathcal{F}_{\beta,\mu_\Delta}(\varepsilon, x_c) = -k_B T \ln \mathcal{P}_{\beta,\mu_\Delta}(\varepsilon, x_c)$, which displays a barrier when coexistence conditions corresponding to special values of $T$ and $\mu_\Delta$ are approached. Given an original Hamiltonian, $H$, a natural candidate for a modified Hamiltonian can have the following functional form,

$$\bar{H} = H + f(\varepsilon) \ , \tag{3.29}$$

where $f(\varepsilon)$, known as the shape function, must be chosen in such a way that the spectral free-energy function corresponding to the modified Hamiltonian shows no significant barrier, as described below. Straightforward simulations of the modified Hamiltonian yield a modified probability distribution function, $\bar{\mathcal{P}}(\varepsilon, x_c)$,

$$\begin{aligned} \bar{\mathcal{P}}(\varepsilon, x_c) &= \frac{1}{\bar{Z}} \sum_l \delta(\varepsilon_l' - \varepsilon) e^{-\beta \bar{H}(l)} \\ &= \frac{Z}{\bar{Z}} \frac{1}{Z} \sum_l \delta(\varepsilon_l' - \varepsilon) e^{-\beta H(l)} \, e^{-\beta f(\varepsilon'(l))} \\ &= \frac{Z}{\bar{Z}} \mathcal{P}_\beta(\varepsilon, x_c) e^{-\beta f(\varepsilon)} \ , \end{aligned} \tag{3.30}$$

where $\mathcal{P}_\beta(\varepsilon)$ is the probability function of the original Hamiltonian. $\bar{Z}$ can be expressed in terms of $Z$ and the probability function $\mathcal{P}_\beta$ as

$$\begin{aligned} \bar{Z} &= \sum_l e^{-\beta \bar{H}(l)} \\ &= Z \frac{1}{Z} \sum_l e^{-\beta H(l)} e^{-\beta f(\varepsilon'(l))} \\ &= Z \sum_i \mathcal{P}_\beta(\varepsilon_i, x_{c\,i}) e^{-\beta f(\varepsilon_i)} \ . \end{aligned} \tag{3.31}$$

We then find the following relationship between the modified distribution function $\bar{\mathcal{P}}(\varepsilon, x_c)$ and the original distribution function $\mathcal{P}(\varepsilon, x_c)$,

$$\bar{\mathcal{P}}(\varepsilon, x_c) = \frac{\mathcal{P}(\varepsilon, x_c) e^{-\beta f(\varepsilon)}}{\sum_{\varepsilon', x_c'} \mathcal{P}(\varepsilon', x_c') e^{-\beta f(\varepsilon')}} \ . \tag{3.32}$$

An expression for $\mathcal{P}(\varepsilon, x_c)$ can then be obtained from $\bar{\mathcal{P}}(\varepsilon, x_c)$, based on the above

equation and the normalization of $\bar{\mathcal{P}}(\varepsilon, x_c)$:

$$\mathcal{P}(\varepsilon, x_c) = \frac{\bar{\mathcal{P}}(\varepsilon, x_c) e^{\beta f(\varepsilon)}}{\sum_{\varepsilon', x_c'} \bar{\mathcal{P}}(\varepsilon', x_c') e^{\beta f(\varepsilon')}} \quad , \tag{3.33}$$

which leads to the following definitions

$$\begin{aligned} \mathcal{P}(x_c) &= \sum_{\varepsilon} \mathcal{P}(\varepsilon, x_c) \quad , \\ \mathcal{P}(\varepsilon) &= \sum_{x_c} \mathcal{P}(\varepsilon, x_c) \quad . \end{aligned} \tag{3.34}$$

A judicious choice for $f(\varepsilon)$ requires some prior knowledge of the original spectral function $\mathcal{F}(\varepsilon) = -k_B T \ln \mathcal{P}(\varepsilon)$; such knowledge can be obtained from simulations of systems of very small sizes. Establishing the phase diagram, especially the loci of phase coexistence, requires sufficient data from systematic simulations of systems of larger sizes. Iteration of a five-step procedure accomplishes the task:

1. At values of $T$ and $\mu_\Delta$ estimated to be close to true coexistence conditions, an initial estimate of $\mathcal{F}(\varepsilon)$ is obtained from a simulation of a system of a relatively small size $L$ governed by the original Hamiltonian $H$.

2. An extrapolation based on the size dependence of the energy barrier is used to approximate the barrier of a system of larger size, $L'$, and in turn, the shape function:

$$f(\varepsilon) = -\mathcal{F}_{L'}(\varepsilon) = -\frac{L'}{L} \mathcal{F}_L(\varepsilon) \quad , \tag{3.35}$$

   when $\varepsilon$ lies in the barrier region. $f(\varepsilon)$ then defines the modified Hamiltonian of Eq.(3.29) which is used in a second simulation of a system of size $L'$. From this simulation, the modified probability distribution function, $\bar{\mathcal{P}}_{L'}(\varepsilon, x_c)$, is obtained.

3. $\mathcal{P}_{L'}(\varepsilon, x_c)$ is reconstructed from $\bar{\mathcal{P}}_{L'}(\varepsilon, x_c)$ by use of Eq. (3.33).

4. Based on $\mathcal{P}_{L'}(\varepsilon, x_c)$, the Ferrenberg-Swendsen reweighting technique (Ferrenberg and Swendsen [88]) is applied in order to obtain a better estimate of the coexistence values of $T$ and $\mu_\Delta$ and an improved approximation of $\mathcal{F}(\varepsilon)$ at the coexistence by $\mathcal{F}_{L'}(\varepsilon)$.

5. If desired, another iteration is started from step (2) with $\mathcal{F}_{L'}(\varepsilon)$, either to obtain an improved statistical sampling of $\mathcal{F}_{L'}(\varepsilon, x_c)$ for the same system size or to simulate a larger system.

*The Use of the Umbrella Sampling Technique*

In order to demonstrate the strength of the Umbrella sampling method, we now give a description of the general use of the method and the details of its application to the specific problem of sampling the free energy barrier between a liquid and a solid phase for the microscopic model of Eq. (2.10).

The Umbrella sampling technique is in the most cases applied to systems where the interfacial free energy between two coexisting phases is large. In these cases, the use of the modified Hamiltonian will allow for an efficient sampling of both of the two coexisting phases as well as the free energy barrier separating the equilibrium phases. This is because the ensemble described by the modified Hamiltonian samples all the corresponding microconfigurations with equal probability (Risbo. [97]). The use of the Umbrella sampling technique will hence enable an accurate and effective sampling of the free energy barrier of magnitude larger than $k_B T$. This can be illustrated by a simple example. A simulated process during which the system passes through a region of the barrier between two coexisting equilibrium phases corresponds to a sequence of correlated simulation steps. Each simulation step in the barrier-crossing sequence can only be tried with a probability $\alpha_0$ and realized with a smaller probability $\alpha_0 e^{-\beta \Delta E_1}$, where $\Delta E_1$ represents the energy increase in a single simulation step. Crossing a high or even modest energy barrier, $\Delta E$, therefore implies a long sequence of simulation steps and is dictated by a total probability of roughly $(\alpha_0)^M e^{-\beta \Delta E}$, where $M$ is the number of steps in the sequence. For a conventional Monte Carlo algorithm used in the simulation of a lattice model such as the Doniach model described in Section 2.2, the value of $M$ will generally be of the order of unity since the algorithm can in a few Monte Carlo steps generate variations in the microconfigurations corresponding to a change from one coexisting phase to the other. The average simulation time needed to cross the barrier will thus be of the order $e^{\beta \Delta E}$. If, for instance, $\beta \Delta E \simeq 15$, then the time to cross the barrier will be of the order $10^7$ MCS, making an accurate sampling of the free energy barrier a very time-consuming and inefficient process. On the other

hand, the use of a modified Hamiltonian will effectively remove the free energy barrier and thus allow for an accurate and efficient sampling of the equilibrium distribution function.

In the case of a random lattice model, the situation is more complicated. In these models, the phase space associated with each single molecule is very large. Each simulation step involves only a small variation in microscopic configurations, or microscopic energy, of the system. In the random lattice algorithm (as in conventional off lattice algorithms), the Monte Carlo move of a particle is thus confined to be within a small box of size $\delta r_{MAX} \times \delta r_{MAX}$ (see Section 3.2). Crossing an even modest energy barrier, $\Delta E$, therefore implies a very long sequence of correlated simulation steps. The total probability of realizing the sequence of simulation steps is still roughly $(\alpha_0)^M e^{-\beta\Delta E}$, but now this probability is made very small by the large number of steps in the sequence, $M$. For a modest height of an energy barrier of $4k_BT$, one barrier crossing from a solid to a liquid phase requires typically $10^7$ MCS for a system of linear size $L = 12$. This difficulty makes it practically impossible to reliably identify solid-liquid phase transitions.

The problem of accurate sampling of the free energy barrier separating the two phases with different lateral structures is thus not only related to the height of the free energy barrier alone but also (and more importantly) to the low probability for generating the long correlated sequence of Monte Carlo steps that will take the system from one free energy minimum to the top of the free energy barrier. It is clear that the value of $M$ will increase with the system size $L$, and the probability of generating the sequence of Monte Carlo steps will thus decrease with system size, making it difficult to sample accurately solid-liquid transitions for large system sizes.

The part of the problem of accurate sampling which is due to an extremely small value of $(\alpha_0)^M$ is inherent in the random lattice algorithm and, therefore, cannot be removed unless special algorithms are designed and implemented. However, the part of the difficulty that arises from the energy barrier can be overcome by employing the Umbrella technique. This method greatly reduces the computational cost associated with an accurate sampling of the free energy barrier. A removal of a moderate free energy barrier of height $\beta\Delta\mathcal{F} \simeq 4$ will thus reduce the time cost of the simulations

by a factor $e^{\beta\Delta\mathcal{F}} \simeq 50$.

In Fig. 3.1, we demonstrate the use of the Umbrella sampling technique. The figure shows the results of a simulation of the model defined in Eq. (2.10) for a system size of $L = 16$ at a temperature of $T = 0.969T_{\mathrm{M}}$[1]. Fig. 3.1(a) shows the enthalpy per particle as a function of Monte Carlo time calculated using a modified Hamiltonian. As is clear from Fig. 3.1(a), the Monte Carlo time needed to obtain an accurate sampling of the free energy barrier (i.e. the time needed to perform a large number of barrier crossings) is large even for this rather small system size.

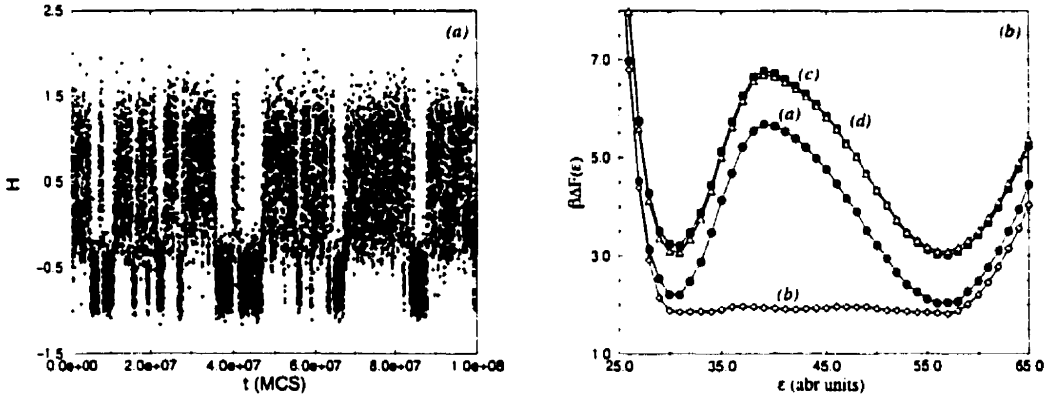


Figure 3.1: Simulation data for the model defined in Eq. (2.10) for a system size of $L = 16$ at a temperature of $T = 0.969T_{\mathrm{M}}$ (a) The enthalpy per particle as a function of Monte Carlo time (calculated using the modified Hamiltonian). (b) The different histograms calculated using a modified Hamiltonian. Curve (a) ($\bullet$) the initial estimate of the shape function $f(\varepsilon)$. Curve (b) ($\diamond$) the spectral free energy function for the modified Hamiltonian. Curve (c) (solid $\square$) the spectral free energy of the original system. Curve (d) ($\triangle$) the spectral free energy function at coexistence.

Fig. 3.1(b) gives the different histograms obtained from the simulations using the modified Hamiltonian. As an initial estimate for the shape function, $f(\varepsilon)$, a rescaled form of the spectral free energy function $\mathcal{F}(\varepsilon)$ calculated for a system size of $L = 14$ (see Eq. (3.35)) is used. The simulations sample the distribution function of the modified Hamiltonian $\tilde{\mathcal{P}}(\varepsilon, x_{\mathrm{c}})$ and the corresponding spectral free energy function, $\tilde{\mathcal{F}}(\varepsilon)$, is calculated. Here, $\varepsilon$ is the internal energy per particle and $x_{\mathrm{c}}$ is the relative cholesterol concentration. Based on Eq. (3.33), the distribution function of the original Hamiltonian is obtained and the corresponding spectral free energy function is calculated. Finally, we use the reweighting technique defined in Eq. (3.22) to obtain

[1]For a definition of $T_{\mathrm{M}}$ see Section 5.1.

the distribution function, the corresponding spectral free energy function $\mathcal{F}(x_c)$, $\mathcal{F}(\varepsilon)$ and the values of $T$ and $\Delta\mu$ at coexistence. The initial shape function $f(\varepsilon)$ and the different spectral free energy functions are all shown in Fig. 3.1(b).

Fig. 3.1 demonstrates that the Umbrella sampling is indeed able to remove the free energy barrier between the two coexisting phases and hence allows for an efficient sampling of both the free energy barrier and the two equilibrium phases.

## 3.2 *The Random Lattice Description*

In this section, the random lattice algorithm is introduced. The algorithm provides the basic representation for the translational degrees of freedom, upon which the specific microscopic models of Chapter 2 are constructed so as to take into account the conformational degrees of freedom and their coupling to the translational degrees of freedom. The description is, to a large extent, similar to the dynamic-triangulated random network applied in the study of fluid membrane conformations (Boal and Rao [92]; Kroll and Gompper [92]; Jeppesen and Ipsen [93]). In the following, we will use the word random-lattice when referring to the dynamic-triangulated random network representation of the translational degrees of freedom of a two-dimensional system.

A full microscopic (or first-principles) treatment of the translational degrees of freedom would be ideal. Such a treatment is, however, computationally demanding and severely limits numerical studies involving translational degrees of freedom[1]. Consequently, different approximation schemes are usually employed, depending on the nature and scope of the study. For example, lattice-gas models are used to describe systems of interacting particles and gas-liquid transitions. In these models, the structure and the occupation of lattices account for the hard-disk repulsion, the short-range nature of the molecular interactions, and the translational entropy. Despite the simplifications underlying these models, they are able to capture the generic thermodynamic properties of gas-liquid transitions for which the full translational invariance of the system is preserved. It is necessary to invoke a different kind of

[1] Recent molecular dynamics calculations for pure lipid bilayers in both the **so** and **ld** include: (Heller, Scheaffer and Schulten [93]; Chu et al. [95]; Tu, Tobias and Klein [95]; Tu et al. [96]). However such studies cannot as yet be used to examine the regions of phase transition due to the large calculational times required for systems of sufficiently large size.

approximation scheme, however, if breaking of the translational symmetry occurs, as is the case with solid-liquid phase transitions.

In the present work, we have developed a simple description based on the idea of representing microscopic spatial configurations of many-particle systems by configurations of a *randomly-varying* triangular lattice. This *random-lattice* description is formulated in such a way that it is adequate both for describing collective phenomena, manifesting the interplay between the conformational (in our case lipid chain conformational) and translational degrees of freedom in a class of two-dimensional systems, and suitable for computer simulations. It is different from conventional lattice descriptions, in that the lattice structure is dynamic: it can be seen as the result of "fluidizing" a *regular* triangular lattice through sampling over non-regular triangular lattice configurations with a fixed global topology. The global topology is here given by the Euler characteristics of the regular triangular lattice[1]. The phase space for the translational degrees of freedom includes both the fluid phases, which have full translational symmetry, and the solid phases which represent a broken symmetry. The algorithm enables us to access both types of phases. Our description is also different from conventional off-lattice descriptions in that it only provides a restricted phase space: those microscopic configurations that correspond to large density fluctuations on short length scales are effectively excluded. This approximation is, nevertheless, sufficient for describing condensed fluid phases of systems of hard-disk particles with short-range interactions.

The translational degrees of freedom of a 2D many-particle system are conveniently represented by the planar coordinates, $(x, y)$, of the particles. A particle configuration is therefore given by $\{(x_n, y_n), n = 1, ..., N\}$, where $N$ is the total number of particles. When dealing with interactions between particles, the most important information required concerns the local environment of each individual particle, such as the distribution of other particles in its neighbourhood and their distances from it. In conventional simulations that explicitly deal with the translational degrees of freedom, it is usually one of the most time-consuming steps to obtain and update this

[1]The Euler characteristic of the regular triangular lattice with periodic boundary conditions is given by $\chi = N - L_E + N_T = 0$, where $N$ is the number of lattice sites, $L_E$ is the number of bonds and $N_T$ is the number of triangles.

information from the microscopic configurations. In this Section, we describe an algorithm which handles structural information in a manner that is distinctly different from conventional off-lattice algorithms, and which at the same time achieves high computational efficiency.

### *3.2.1 Detailed Description of the Algorithm*

Our algorithm is a version of the dynamic-triangulation algorithm used for modelling fluid membranes (Dammann et al. [95]), adapted to 2D planar systems of many particles. The algorithm performs two essential tasks: 1) it generates the phase space associated with the translational degrees of freedom, and 2) it generates and retains a compact data structure that allows efficient access to structural information contained in each microscopic configuration. The data structure is based on triangulation of each spatial configuration of the particles. This triangulation is implemented as follows. An ordered configuration in which the particles are positioned on a regular triangular lattice is used as an initial state in which each site is linked to its six nearest neighbours by tethers. The lattice configuration is then represented by a network of tethers forming triangles; the term "triangulation" refers to this representation. Each site in the random lattice is occupied by a hard disk and a model particle is associated with every hard disk. The phase (or configuration) space can then be explored through a random updating (or stochastic evolution) of configurations of the lattice, which consists of three steps to be described in the following Subsections. All these steps are subject to the standard Metropolis Monte Carlo (MC) acceptance criterion Eq. (3.3). The central data structures in the random lattice algorithm and a detailed description of the updating methods for the random lattice are given in Appendix A.1.

*(a) Particle Moves*

The first step in the MC updating procedure is the "particle move", which is illustrated in Fig. 3.2. A particle is chosen at random and its center is subject to a random displacement $(\delta x, \delta y)$ where

$$\begin{aligned} \delta x &= (2\zeta_x - 1)\delta r_{\mathrm{MAX}} \\ \delta y &= (2\zeta_y - 1)\delta r_{\mathrm{MAX}} \ . \end{aligned} \tag{3.36}$$

$\zeta_x$ and $\zeta_y$ are random numbers, $0 \leq \zeta_{x(y)} \leq 1$. The value of $\delta r_{\mathrm{MAX}}$ is adjusted during the simulations so that approximately 25 % of the moves are accepted. The acceptance criterion of 25 % is found to ensure that the range of particle displacements is sufficiently large to allow for an efficient sample of the phase space. Moves which would result in an overlap of hard disks are always rejected. Another constraint is that the length of every tether is not allowed to exceed a maximum value $l_{\mathrm{max}}$.

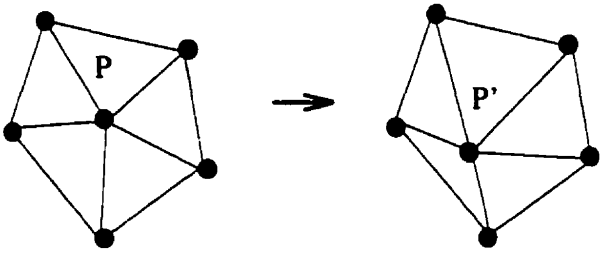


Figure 3.2: Particle move. The hard disk at position P is moved to position P'.

*(b) Link Flip*

The second step is referred to as the "link flip." In every configuration of the random lattice, each tether (or link) is one diagonal of a quadrilateral formed by the two adjacent triangles. In the "link flip", a tether is chosen at random; this tether is replaced by a tether along the other diagonal of the quadrilateral if the length of the replacement does not exceed $l_{\mathrm{max}}$, and is kept otherwise. A "link flip" is illustrated schematically in Fig. 3.3.

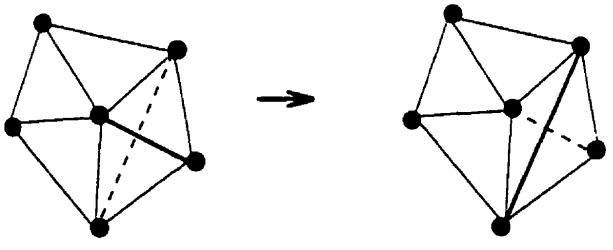

Figure 3.3: A tether (shown as a thick line) is replaced by another tether along the diagonal provided that the length of the new tether does not exceed $l_{max}$.

The combination of the particle move and the link flip makes the lattice "dynamic" (or random) in the sense that its configuration evolves through stochastic variations

in both the local connectivity of the lattice and the real-space coordinates of the particles. This ensures both particle diffusion across the whole system and fluctuations in local particle distribution, as required in any description of the translational degrees of freedom.

*(c) Change of System Size*

In the constant $(N, P, T)$ ensemble used in the simulations it is necessary to allow the area of the 2d system to fluctuate. In our simulations this is achieved via a third step in the MC procedure – a random uniform expansion or contraction of the whole system (McDonald [72]). In this step, a random change in the size of the system is generated by rescaling the length as follows

$$\delta L = (2\zeta - 1)\delta L_{\mathrm{MAX}} \ , \tag{3.37}$$

where $\zeta$ is a random number, $0 \leq \zeta \leq 1$, and the coordinates of all particles are rescaled accordingly. If the distance between any two particles after the rescaling is smaller than the hard-disk diameter, the change is always rejected. The maximum possible size change, $\delta L_{\mathrm{MAX}}$, is adjusted during the simulation to give an acceptance ratio of about 50 %. The criterion of a 50 % acceptance ratio is found to ensure an efficient sample of the phase space.

In this MC updating procedure for change of system size, the probability of accepting a move from a state with an area $A_i = L^2$ to a state with an area $A_f = (L + \delta L)^2$ is determined by $\min(1, e^{-\beta \Delta H})$, where $H$ defined as $H = H_{\mathrm{model}} + H_{\mathrm{HD}}$. $H_{\mathrm{model}}$ is the microscopic model Hamiltonian describing the interactions between the particles and

$$H_{\mathrm{HD}} = PA - \mathrm{k_B} T N \ln A \ . \tag{3.38}$$

The first term in $H_{\mathrm{HD}}$ represents the energy associated with the lateral pressure, $P$, and the second term reflects the degeneracy of a microscopic configuration of $2N$ translational degrees of freedom. A derivation showing that the Hamiltonian defined by Eq. (3.38) does indeed generate the constant $N - P - T$ ensemble is given in Appendix A.2.

In order for the simulational algorithm to obey detailed balance, we combine all of the updating procedures in a random manner so that the symmetry of the Markov

chain generated by the algorithm is maintained (see section 3.1.1). This means in practice that there must be no preferred sequential order in the way the different updating procedures are performed (Frenkel and Smit [97]). We define for our simulations, a time unit of one Monte Carlo step (MCS), which is the time needed to perform on average one complete pass through steps (a), (b) and (c), and one complete run through changing the molecular type or conformational state of each particle in the system.

A sufficiently large number of the simulation steps then generates a configuration (phase) space that is characteristic of the translational degrees of freedom of the system. It is important to emphasize that the given Hamiltonian $H_{\text{model}}$ describing the microscopic interactions between particles is included in the acceptance criterion of Eq. (3.3) for all of the three steps in the MC update for the random lattice.

### 3.2.2 The Hard Disk Model

The value of $l_{max}$ is kept fixed during the simulations. This constraint on the maximum tether length ensures that configurations where two tethers cross are excluded from the configurational space accessed by the algorithm. The main data structure used in our algorithm describes the position of each individual particle relative to its tethered neighbours. This is referred to as the "link structure." When the tether length is bounded, a one-to-one mapping can be efficiently established from a given link structure to a nearest-neighbour structure. It can be expected that the constraint on the tether length prevents the algorithm from accessing the *entire* phase space spanned by the 2D translational degrees of freedom, since those microscopic configurations that correspond to large fluctuations in the particle density are not compatible with this constraint. In order to assess the validity of this approximation, we have revisited the system of non-interacting hard disks by studying the solid-liquid transition in this system in the presence of our constraint. This solid-liquid transition is solely driven by the configurational entropy associated with the 2D translational degrees of freedom. Moreover, a recent simulation study by Lee and Strandburg ([92]) using a full off-lattice algorithm provides quantitative information on the transitional properties and presents numerical evidence that the transition is of first-order (although this subject still remains a contentious issue). A numerical study of this

system using our random-lattice algorithm therefore allows us to assess quantitatively any restrictive effect that the constraint may have on the representation of the translational degrees of freedom. We expect that, once the constraint is effectively removed by allowing a large value for the maximum tether length, our algorithm should lead to results that are consistent with those obtained by using the full off-lattice algorithm (Lee and Strandburg [92]; Fernández, Alonso and Stankiewicz [95]).

In the following, we give a short summary of the results of our study of the hard-disk system with the random-lattice algorithm. A hard-disk system with $N = L^2 = 12^2$ particles was simulated for two cases with respect to the constraint of the maximum tether length. In the first case, a strong constraint was employed in the algorithm; in the second case, this constraint was relaxed. In the case of the relaxed constraint the algorithm was modified to include a cell-list structure to facilitate a fast check of steric interactions between neighbouring hard disks (Allen and Tildesley [87]). During the simulations, the structure factor of the system was calculated as

$$S(\vec{k}) = \left\langle \sum_{i,j} e^{-i(\vec{R}_i - \vec{R}_j)\cdot\vec{k}} \right\rangle \quad , \tag{3.39}$$

where $\vec{R}_{i,j}$ is a two-dimensional vector giving the position of disk $i$ ($j$) and $\langle \ldots \rangle$ denotes a thermal average. In Fig. 3.4, $S(\vec{k})$ is shown for different values of the reduced lateral pressure, $P^* = \frac{Pd^2}{k_B T}$, where $d$ is the hard-disk diameter. For the constrained case, there is a clear change in lateral order as the value of the reduced pressure is changed from 8.75 to 9.75, as indicated in Figs. 3.4(a) and 3.4(b). Using the reweighting histogram method (Ferrenberg and Swendsen [88]), we found the position of the transition to be at $P^* \simeq 9.15$. We also estimated the change in the average area per molecule across the transition to be $\Delta a = a_l - a_s \simeq 0.014$, where $a_{s(l)} = \frac{A_{s(l)}}{d^2 N} \frac{2}{\sqrt{3}}$ and $A_{s(l)}$ is the total area of the solid (liquid) phase. As the constraint on the tether length is relaxed, the lattice-melting event shifts to a value of the reduced pressure between 8.25 and 8.75, as illustrated in Figs. 3.4(c) and 3.4(d). Again, by using the reweighting histogram method, the position of the solid-fluid transition is found to be located at $P^* \simeq 8.55$, and the value of the area change across the transition is estimated to be $\Delta a \simeq 0.052$.

These results demonstrate that, as the constraint is relaxed, our simulation data tend toward the results for $P^*$ obtained from other off-lattice studies of the hard-disk system (Lee and Strandburg [92]). For example, the work reported in Ref. (Lee

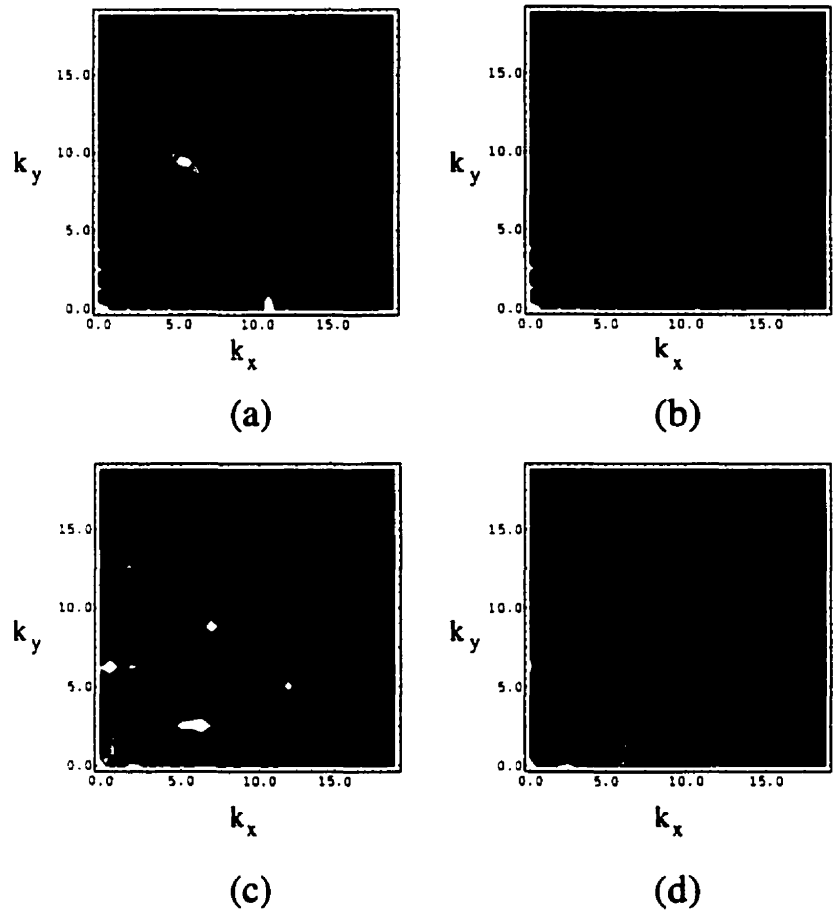


Figure 3.4: Contour plot of the structure factor $S(\vec{k})$ in the $(k_x, k_y)$ plane calculated for the hard-disk system of size $N = 144$. In (a) and (b) $\langle l_{\max} \rangle \simeq 1.73d$ and $d = 0.6$. Here $\langle \cdots \rangle$ denotes a thermal average. In (c) and (d) $\langle l_{\max} \rangle \simeq 7d$ and $d = 1.0$. The value of the reduced lateral pressure is (a) $P^* = 9.75$, (b) 8.75, (c) 8.75 and (d) 8.25. The position of the first Bragg-peak is at a $k$-value of $2\pi/d$, which for the system (a) corresponds to $|k| \simeq 10.5$ and (c) $|k| \simeq 6.28$.

and Strandburg [92]) estimates that $P^* \simeq 8.0$ and $\Delta a \approx 0.05$ in the limit of $L \to \infty$. Our results also show that the essential characteristics of the transition remain largely intact in the random-lattice algorithm, although imposing the constraint of maximum tether length results to a certain extent in changes in transition quantities, such as the small shift in the transition pressure. However, since we have not in the present work performed a systematic finite-size analysis or a detailed study of the relaxation times (Fernández, Alonso and Stankiewicz [95]), we will not make a closer comparison with the results from other theoretical work on the hard-disk melting transition.

# 4

# RESULTS FOR PURE SYSTEMS

In this chapter, we describe the phase behaviour of the single component models, Models I-III, defined in Chapter 2 as obtained from the Monte Carlo simulations. The presentation falls naturally in two parts. The first part contains the results of the simulational study of Ising Models I and II, and the second part describes the results for the extended Doniach model, Model III.

## *4.1 Details of the Simulations*

Before presenting the numerical results obtained from the simulation studies of the microscopic models of Chapter 2, we describe the statistical-mechanical formulation of the problem in terms of thermodynamic ensembles and the simulation procedures.

The systems under consideration consist of a total number of $N$ particles confined in a simulational box with periodic boundary conditions. All simulations were performed using the Monte Carlo Metropolis algorithm defined in Eq. (3.3), for fixed $N$, $T$ and surface pressure $\Pi$.

The simulations were initialized using a lattice configuration which was crystalline (regular triangular) and the internal degrees of freedom were disordered. This initial configuration was then equilibrated by the Metropolis Monte Carlo algorithm to a high-temperature disordered state in both the translational and internal degrees of freedom. The high temperature equilibrium state then served as the initial state for the simulations at lower temperatures. In the case of a cooling experiment the equilibrium states at lower temperatures were reached by cooling down from the high-temperature state in small temperature steps. In each of the cooling steps, several Monte Carlo updating steps (Monte Carlo steps per particle, MCS) were discarded before the measurement of various physical quantities of the equilibrated system was

started. Depending on the particular model, the number of MCS used to reach the equilibrium high-temperature state was between 30,000 and 200,000. The number of MCS discarded in the subsequent temperature steps was between 10,000 and 200,000. The measurement of various physical quantities was performed over a simulation period of 30,000 to $5 \cdot 10^6$ MCS for simulations within the canonical ensemble (see below) and over a simulation period of $10\text{-}200 \cdot 10^6$ MCS for the simulations within the semi-grand canonical ensemble.

### *4.1.1 Statistical Mechanical Ensembles*

The acceptance criterion and the class of Monte Carlo trial moves for the Monte Carlo algorithm of Eq. (3.6) is specific to the statistical ensemble to be generated in the Monte Carlo simulations. For the single component systems defined by the Models I-III, the natural ensemble is the constant $N - P - T$ ensemble. In Appendix A.2, it is shown that acceptance criterion defined by the Hamiltonian of Eq. (3.38) does indeed generate the distribution function corresponding to this ensemble.

For the Models III-IV which contain two types of molecular species, two different statistical mechanical ensembles were used: (a) the semi-grand canonical ensemble, in which the relative number of "sterol" particles was controlled by a parameter, $\mu_\Delta$, the difference between the chemical potentials of "lipid" and "sterol" particles, and could therefore fluctuate; and (b) the canonical ensemble, in which the number of "sterol" particles, and thus the "sterol" concentration, $x_c$, was fixed. The two formulations are complementary to one another. The canonical ensemble in our formulation is similar to the constant $N - P - T$ ensemble defined above.

The semi-grand canonical ensemble is generated by using the Monte Carlo Metropolis acceptance criterion with the model Hamiltonian modified as:

$$H_{semi-grand} = H_{model} + \mu_\Delta N_{sterol} \quad , \tag{4.1}$$

where $N_{sterol}$ is the number of sterol molecules in the system and $\mu_\Delta$ is the difference in chemical potential between the lipids and the sterol particles. The terminology *semi-grand* canonical ensemble refers to the fact that the total number of particles is kept fixed in the simulations and that only the relative concentration of sterol

particles is a fluctuating quantity as opposed to the grand canonical ensemble where the total number of particles is a fluctuating quantity.

The simulations based on the semi-grand canonical ensemble immediately give the equilibrium probability distribution as functions of $T$ and $\mu_\Delta$, for relevant quantities such as the "sterol" concentration. The phase diagram of the system, both in the ($\mu_\Delta$, $T$) representation and in the ($x_c$, $T$), can then be unambiguously obtained from these probability distributions.

## 4.2 Ising Model I and Ising Model II on a Random Lattice

Ising Models I and II were formulated to describe two-dimensional systems where both internal (spin) and translational degrees of freedom are present and are coupled through microscopic interactions. Consequently, characterization of the phase behaviour of these model systems requires knowledge of the macroscopic behaviour of *both* types of degrees of freedom. As the macroscopic behaviour of the translational degrees of freedom is described as either solid (**s**) or liquid (**l**) and that of the spin degrees of freedom is characterized as either (spin) ordered (**o**) or (spin) disordered (**d**), each model system can in principle have four different phases: a solid-ordered (**so**) phase, a solid-disordered (**sd**) phase, a liquid-ordered (**lo**) phase, and finally a liquid-disordered (**ld**) phase. We use this terminology below in our description of the phase behaviour of the models. Our simulation study of the models concentrates on identifying these phases in parameter spaces of the models, locating the boundaries between the different phases and characterizing the nature of the thermodynamic singularities associated with the phase boundaries.

### 4.2.1 Ising Model I.

For Ising Model I, a convenient choice for the parameter space is given by a reduced lateral pressure, defined as $Pd^2/J_0$, and a scaled temperature $T/T_C$, where $T_C$ is the critical temperature of the spin transition in the Ising model on the regular triangular lattice. The simulation study of Ising Model I was performed for a range of values of the reduced lateral pressure and the reduced temperature. The results show that the four phases described above are indeed all present in the region of the parameter

space explored. Moreover, the phase boundaries separating these four phases are simply two intersecting lines. One line is predominantly controlled by the solid-liquid thermodynamic singularity and is considered to be a first-order line. This line will be termed as the "lattice-melting" transition, while the second line is mainly associated with a critical order-disorder transition of the spin system. Specifically, the low-pressure, high-temperature phase is the **ld** phase, and the low-temperature high-pressure phase is the **so** phase. The low-pressure intermediate phase is the **lo** phase; and the high-pressure intermediate phase is the **sd** phase. For low pressures, e.g., $Pd^2/J_0 = 10.0$, the critical Ising spin transition has a higher temperature than the lattice-melting transition. As the pressure increases, the temperature difference between the two transitions decreases. At the point of intersection, where $Pd^2/J_0 = 30.0$, the two transitions coincide in temperature. For higher pressures, e.g., $Pd^2/J_0 = 50.0$, this ordering in temperature is reversed and the lattice-melting transition has a higher temperature than the Ising spin transition.

In order to investigate the critical behaviour of the Ising spin transition for this model and to compare it to that of the regular-lattice Ising model, a detailed finite-size scaling analysis of the simulation data for this transition was carried out. The scaling relations for the thermodynamic response functions $C_P$ and $\chi$ are given in Section 3.1.2, Eq. (3.12). Fig. 4.1 shows the results of the analysis of three sets of simulation data obtained for three different values of the lateral pressure, $Pd^2/J_0 = 10.0$, 30.0 and 50.0, as cited in the previous paragraph. The total number of particles, $N = L^2$, varied in the finite-size scaling analysis from 64 to 400. In our analysis, the value of $\chi_{MAX}$ ($C_{P,MAX}$) was taken as an average of the maximum value of the susceptibility (the specific heat) over five different simulation runs. The value of $\delta\chi$ was taken as the average value of the half width over the five different $\chi$ curves[1]. As is clear from Fig. 4.1, the critical exponents $\gamma$ and $\nu$ found from the finite-size scaling analysis are, within the statistical error of the calculations, consistent with those of the 2D regular-lattice Ising model ($\gamma = 7/4, \nu = 1$) (Stanley [71]).

[1]More accurate values of these three quantities can obviously be obtained by performing longer simulations in conjunction with the Ferrenberg-Swendsen reweighting technique (Ferrenberg and Swendsen [88]). For the present purpose, it is however sufficient to use the peak position and the height of the response functions as estimates for $\chi_{MAX}(L)$, $C_{P,MAX}(L)$ and $\delta\chi(L)$.

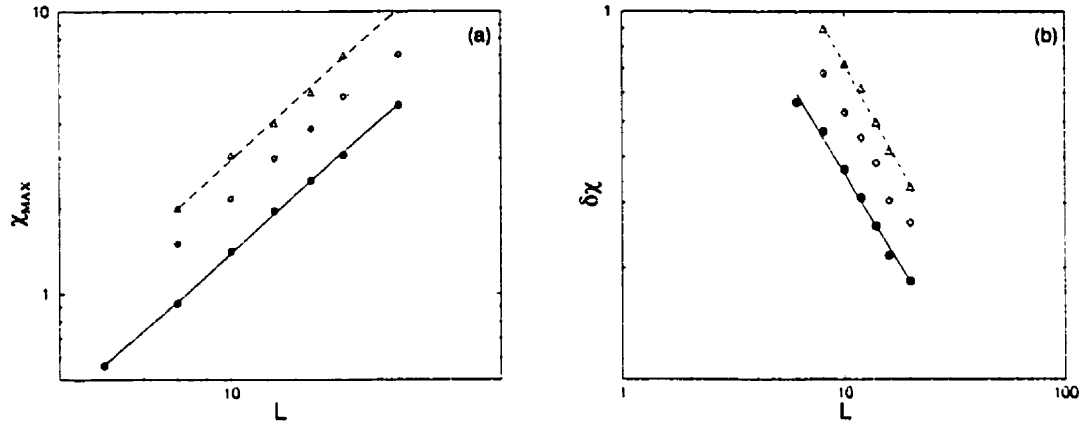


Figure 4.1: Finite-size scaling plots for Ising Model I in the cases of three different values of $Pd^2/J_0$. (a) $\chi_{MAX} \sim L^{\gamma/\nu}$ and (b) $\delta\chi \sim L^{-1/\nu}$. The upper curve ($\triangle$) corresponds to $Pd^2/J_0 = 10.0$, the middle curve ($\circ$) to $Pd^2/J_0 = 30.0$, and the lower curve ($\bullet$) to $Pd^2/J_0 = 50.0$. For clarity the three curves are shifted along the vertical axis. (a) The values for the ratio of the exponents $\gamma$ and $\nu$ for the three curves are $1.76 \pm 0.02$, $1.73 \pm 0.02$, $1.78 \pm 0.05$, respectively. (b) The corresponding values of the exponent $1/\nu$ are $0.98 \pm 0.04$, $1.06 \pm 0.06$ and $1.09 \pm 0.05$, respectively.

It would be much more demanding to perform a finite-size scaling analysis of the specific heat (data not shown) because of the very weak singularity and the influence of a non-singular term in $C_P$ which cannot be neglected at finite $L$. However, the $C_P$-data for the larger system sizes gives a weak dependence of $C_{P,MAX}(L)$ on $L$, indicative of a small specific-heat exponent, $\alpha \sim 0$, consistent with the logarithmic singularity ($\alpha = 0$) associated with the regular-lattice Ising critical behaviour. We thus conclude that, within the range of lateral-pressure values studied in our simulation, the Ising Model I defined on the *dynamic* random lattice belongs to the same universality class as the regular-lattice Ising model.

Overall, the simulation study of Ising Model I shows that there is no significant macroscopic manifestation of the microscopic coupling between the spin and the translational degrees of freedom. This observation can be rationalized as follows. In this model, the particle-particle interaction has no distance dependence, and the microscopic coupling between the two types of degrees of freedom is only facilitated through the fluctuating local connectivity of the lattice. In the condensed systems considered here, not only are the fluctuations in the local connectivity of the lattice small, but there is also no change in the macroscopic value of the local connectivity as the systems change from solid to liquid state. In other words, the microscopic coupling

does not give rise to a strong coupling between the spin and the translational degrees of freedom that alters the characteristics of their corresponding thermodynamic singularities and macroscopic phase behaviour.

### 4.2.2 *Ising Model II.*

Ising Model II describes a more complex type of microscopic coupling between the spin and the translational degrees of freedom: In addition to the coupling through the fluctuating local connectivity, there is also coupling through the distance-dependent ($R_0$) spin-spin interaction. The emphasis of our study of this model is to investigate whether the more complex microscopic coupling will lead to intricate coupling at the macroscopic level, and in turn, to more complex phase behaviour.

Indeed, Ising Model II was found to have more complex phase behaviour, in particular with respect to the coupling of the degrees of freedom at the macroscopic level. Displayed in Fig. 4.2 is the phase diagram for the model, given in the parameter space of the reduced pressure and the scaled temperature for a fixed $\frac{R_0}{d} = 1.41$.

The phase diagram was obtained from simulation data and our analysis of that data. Again, as in Ising Model I, the four principal phases are all present, and the remnant of the phase diagram of Ising Model I can be seen in the low-pressure and high-pressure regions of the parameter space, where the lattice-melting transition and the critical spin transition are decoupled and where **lo** and **sd** phases intervene between the **so** and the **ld** phases. However, the phase boundaries separating these phases no longer consist of two intersecting lines alone. A new phase boundary directly separating the **so** and the **ld** phases, is now present, as indicated by the solid line between the two special points, $t_1$ and $t_2$. These two points are in fact tricritical points (see below) and their locations, ($\frac{Pd^2}{J_0}\Big|_{t_1} = 35$, $\frac{T}{T_C}\Big|_{t_1} = 0.945$) and ($\frac{Pd^2}{J_0}\Big|_{t_2} = 40$, $\frac{T}{T_C}\Big|_{t_2} = 1.035$), as indicated in the phase diagram are only estimates (which include finite-size effects) [1]. Along this phase boundary, which is of first order, the translational degrees of freedom override the spin degrees of freedom and the

[1] To determine the precise locations of the two tricritical points requires a detailed analysis based on finite-size scaling theory, which however, is computationally very demanding and outside the scope of the present work. The important point is that we were able to establish the existence of these two points.

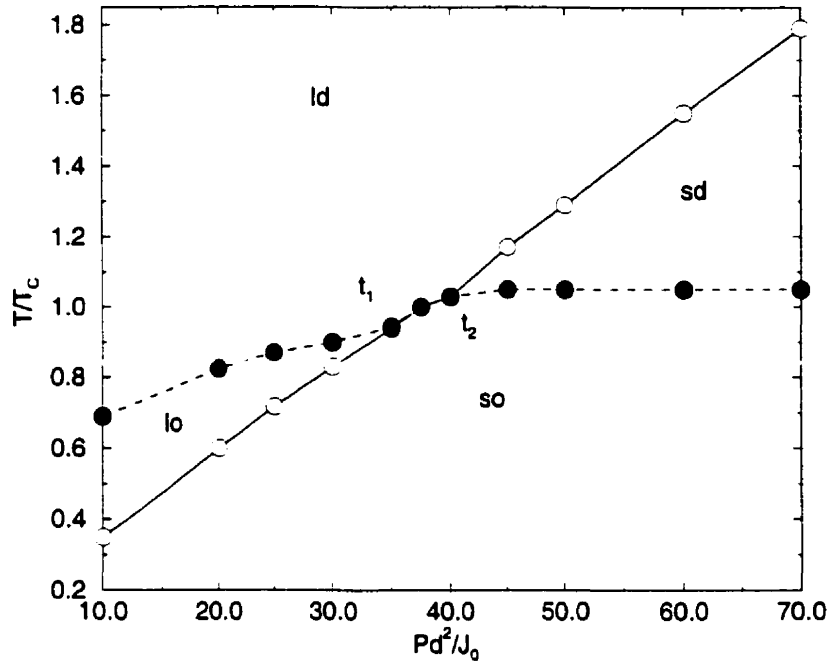


Figure 4.2: The phase diagram for Ising Model II for $R_0/d = 1.41$. The dashed phase boundary line (•) corresponds to the critical Ising-like transitions from a spin-ordered (**o**) to a spin-disordered (**d**) phase. The solid boundary line (○) corresponds to the first-order lattice-melting transition from a solid (**s**) phase to a liquid (**l**) phase. $t_1$ and $t_2$ are the two tricritical points described in the text. Between the two tricritical points the spin order-disorder singularity is coupled to the lattice melting and is of first order.

lattice-melting transition preempts the critical spin transition, leading to a first-order singularity also in the spin order parameter.

Presented in Figs. 4.3-4.5 is a collection of simulation data obtained for Ising Model II, which corroborates the phase diagram. Fig. 4.3(a) shows the change of area (per molecule) with temperature for a set of values of pressure that cover the parameter range investigated. An abrupt change in the area takes place at a specific pressure-dependent temperature for all the pressure values considered. The corresponding response function, the reduced area compressibility, $K^* = K/\beta d^2$, given in Fig. 4.3(b), displays the signature of the same singularity. The sharpness of the peaks is taken as the indication of a first-order lattice melting transition.

The critical spin order-disorder transition, existing in both the low-pressure ($P < P_{t_1}$) and the high-pressure ($P > P_{t_2}$) regions, is identified principally from the simulation data such as those shown in Fig. 4.4. The temperature dependence of the

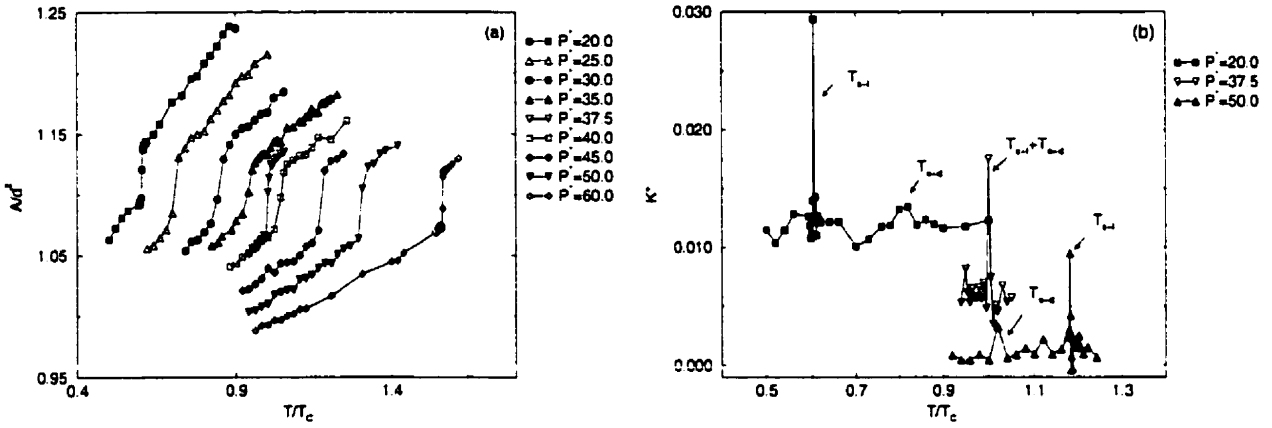


Figure 4.3: a) Area, $A$, per particle, and (b) the corresponding reduceced area compressibility, $K^* = K/\beta d^2$, of Ising Model II for different values of the lateral pressure $P^* = Pd^2/J_0$. The system size is $N = 256$ and $R_0/d = 1.41$. The temperature is given in units of the critical temperature, $T_C$, of the regular lattice Ising model. For clarity, the $K$ curves are shifted along the vertical axis by multiples of 0.005.

spin order parameter is given in Fig. 4.4(a), for a set of pressure values. Both at low values and high values of the pressure, the spin order parameter varies steeply, but *continuously*, at a particular pressure-dependent temperature concomitantly with the occurrence of a peak at the same temperature in the spin susceptibility function, $\chi$, in Fig. 4.4(b). This particular temperature is thus determined for each value of the pressure, giving the location in the parameter space of the critical spin transition.

As expected, the specific heat, $C_P$, which carries information about energy fluctuations arising from both the translational and spin degrees of freedom, display peaks at both transitions, as Fig. 4.5 clearly demonstrates. The identification of the solid and liquid characteristic of the phases has also been confirmed by analysis of the structure factor, $S(\vec{k})$ (data not shown). $S(\vec{k})$ has clear Bragg peaks in the solid phase and displays only diffuse rings in the liquid phase.

The simulation data suggests that the critical temperature of the spin transition separating the **lo** and the **ld** phases in the low-pressure region has an observable pressure dependence, whereas the temperature of the critical spin transition separating the **so** and **sd** phases in the high-pressure region coincides with the critical temperature of the regular-lattice Ising model (as expected).

In order to investigate the critical behaviour of the spin transitions in more detail in both the low-pressure and the high-pressure regions, we also performed finite-size

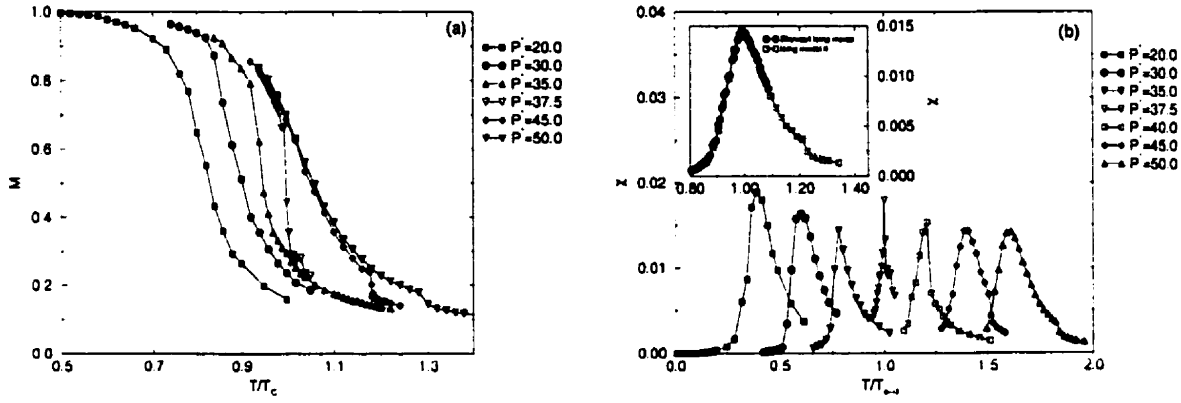


Figure 4.4: (a) Spin order parameter, $M$, and (b) the corresponding susceptibility, $\chi$, of Ising Model II for different values of the lateral pressure $P^* = Pd^2/J_0$. The system size is $N = 256$ and $R_0/d = 1.41$. $M$ is shown as a function of $T/T_C$, whereas $\chi$ is given as a function of $T/T_{c-d}$, where $T_{c-d}$ is determined by the peak position of $\chi$. For clarity the $\chi$ curves are shifted along the horizontal axis. The actual peak position for the different curves are $0.825T_C$, $0.89T_C$, $0.98T_C$, $1.00T_C$, $1.03T_C$, $1.05T_C$ and $1.05T_C$ respectively. The inset in (b) shows a comparison between $\chi$ of the regular-lattice Ising model and $\chi$ of Ising Model II for $P^* = 50.0$.

scaling analysis of the simulation data on the spin susceptibility $\chi$ in the low-pressure region, based on the scaling hypothesis described in Eq. (3.12), and the result of the analysis is shown in Fig. 4.6. This figure shows that the universal Ising critical behaviour is unaltered by the fluctuations in the density (or local connectivity of the random lattice). On the high-pressure side of the tricritical point $t_2$, both the universal and non-universal behaviour of the critical transition is expected to be identical to that of the regular-lattice Ising model. This is confirmed by the data shown in the inset in Fig. 4.4(b), which demonstrate that, in this pressure region, the susceptibility, as a function of $T$ fits perfectly in shape to the susceptibility of the regular-lattice Ising model in the neighbourhood of the critical temperature.

The phase boundary between the two special points, $t_1$ and $t_2$ (see Fig. 4.2), distinguishes the phase behaviour of Ising Model II from that of Ising Model I. It lies directly between the **so** and **ld** phases. The first-order nature of this phase transition is indicated by the discontinuous change in the area $A$ (for example, see Fig. 4.3(a) for $Pd^2/J_0 = 37.5$) at the transition temperature, and more interestingly, by a corresponding sharp change in the spin order parameter (see Fig. 4.4a for $Pd^2/J_0 = 37.5$) that is distinctly different from the temperature-dependence of the spin order param-

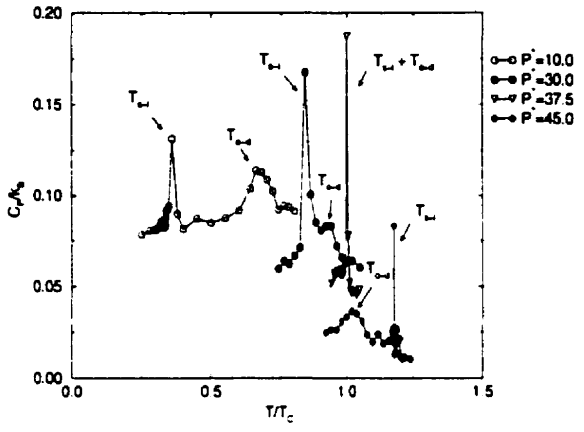


Figure 4.5: Specific heat, $C_P$, per particle of Ising Model II as a function of $T/T_C$ for different values of the lateral pressure $P^* = Pd^2/J_0$. The system size is $N = 256$ and $R_0/d = 1.41$. For clarity the $C_P$ curves are shifted along the vertical axis by multiples of 0.025. For low values of the lateral pressure $P^*$ ($P^* = 10.0$ and $P^* = 30.0$) the temperature of the critical spin transition, $T_{o-d}$, is higher than the lattice-melting temperature $T_{s-l}$. At higher values of $P^*$ ($P^* = 45.0$) $T_{s-l}$ is higher than $T_{o-d}$. For intermediate values of $P^*$ ($P^* = 37.5$) the two transitions are coupled and $T_{o-d} \simeq T_{s-l}$.

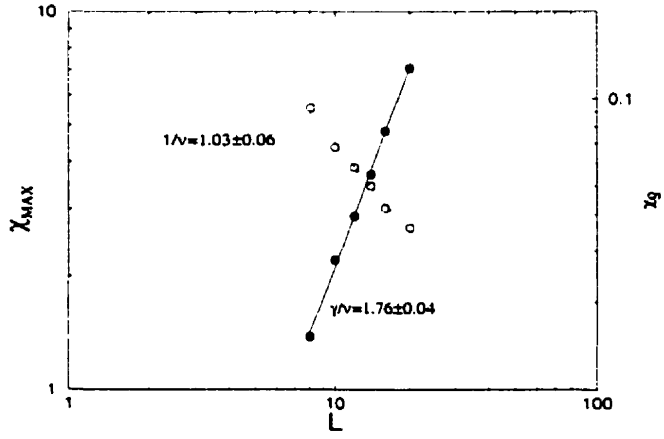


Figure 4.6: Finite-size scaling plots for Ising Model II for $Pd^2/J_0 = 20.0$. $\chi_{MAX}$ is the maximum value of the spin susceptibility and $\delta\chi$ is the half width of the $\chi$ curve. The values of $\chi_{MAX}$ and $\delta\chi$ were determined as described in the text. The value of the exponent $\gamma/\nu$ is $1.76 \pm 0.04$ and the value of the exponent $1/\nu$ is $1.03 \pm 0.06$

eter at lower and higher values of the pressure.

In order to demonstrate unambiguously that the spin order-disorder singularity is a *first-order* singularity, i.e., that it is slaved by the lattice melting, we calculated the two-dimensional probability distribution function, approximated by the histogram, $\mathcal{P}(A, M)$ (for a fixed system size), which is displayed in Fig. 4.7. The statistics underlying this histogram were obtained from $8 \cdot 10^6$ MCS[1]. The histogram clearly exhibits a two-state (spin-ordered and spin-disordered) structure, indicating coexisting so and ld phases and a finite interfacial tension. Since the line of the critical spin transition is terminated from both the low-pressure and the high-pressure sides at $t_1$

[1] A more satisfactory analysis would be a detailed finite-size scaling analysis of the two-dimensional histogram, $\mathcal{P}(A, M)$. However, due to the extensive statistics which an analysis of this kind would require, we have not performed such a systematic finite-size scaling analysis.

and $t_2$, these two points are tricritical points.

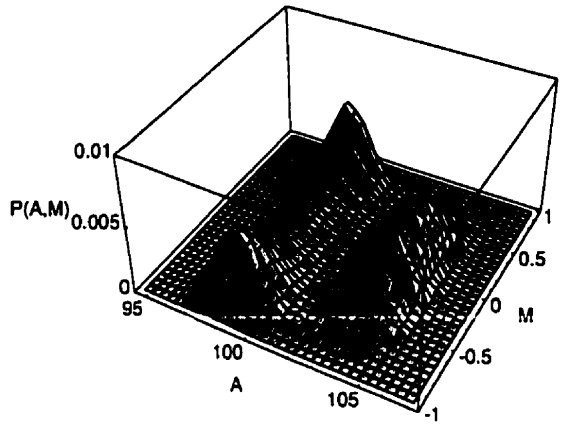


Figure 4.7: The two-dimensional histogram $\mathcal{P}(A, M)$, where $A$ is the total area of the system and $M$ is the spin order parameter, obtained for Ising Model II at parameter values $Pd^2/J_0 = 37.5$ and $T = 1.012T_C$ where the spin singularity is coupled to the lattice-melting. The system size is $N = 256$. The histogram is obtained by extrapolation from a nearby temperature using the reweighting technique of Ferrenberg and Swendsen. The sampling time to obtain the histogram was $8 \cdot 10^6$ MCS.

A last, but no less important, observation which we have made from the simulation data concerns the interplay between the two types of degrees of freedom in the low-pressure and the high-pressure regions. Although in these regions, the first-order singularity associated with the translational degrees of freedom is decoupled from the critical singularity arising from the spin degrees of freedom, as manifested in the two separate transitions corresponding to the lattice melting and the critical spin transitions, respectively, there is evidence that the macroscopic behaviour of one type of degree of freedom is affected by the thermodynamic singularity arising from the other. For example, the critical spin fluctuations at the spin transitions, both in the low-pressure region and in the high-pressure region, enhance the density fluctuations, as indicated in Fig. 4.3(b) by the peaks in the area compressibility occurring at the spin transitions although they are less pronounced than the peaks related to the lattice-melting transitions. Vice versa, at the lattice-melting transitions, the spin degrees of freedom are expected to display a weaker first-order singularity, the signature of which is too weak to be identified unambiguously from the simulation data.

A simple argument based on mainly mean-field considerations puts all the above observations and analysis into perspective, in relation to the phase behaviour of Ising Model I. As described in Section 2.1, in Ising Model II a new length scale, $R_0$, is introduced to define the range of the spin-spin interaction. It is mainly the interplay between this new length scale and the length scale, $l(P)$, set by the density (or

pressure) of the system, that gives rise to the phase behaviour of Ising Model II, which is more complex than that of Ising Model I. If $l(P)$ is always smaller than $R_0$, there is then no difference between the thermal average values of the local coordination number and the number of the interacting nearest neighbours, whether the system is in solid or liquid state; and the phase behaviour of Ising Model II is effectively the same as the phase behaviour of Ising Model I. If, however, $l(P)$ for low pressures is larger than $R_0$, then the average value of the number of interacting nearest neighbours in the liquid state can be smaller than that in the solid state.

At very low pressures, the lattice-melting takes place before any critical fluctuations in the spin degrees of freedom set in, taking the system from the **so** phase to the **lo** phase. The critical spin transition occurs at a higher temperature, well separated from the lattice-melting transition, as in Ising Model I. However, due to the reduced number of interacting particles in this case, the transition temperature is suppressed compared to that of the solid-state critical spin transition. In this region of the phase diagram, the macroscopic behaviour of the spin degrees of freedom is expected to have properties similar to the annealed and bond-diluted regular-lattice Ising model at low dilution (Stinchcombe [83]). As the pressure increases, the lattice-melting temperature increases and reaches at a point ($t_1$) the temperature of the critical spin transition, which is still lower than the critical temperature in the solid state. Beyond this point, the lattice-melting dictates the macroscopic behaviour of the spin degrees of freedom, altering it discontinuously from the ordered state characteristic of the solid-state spin order parameter to the disordered state described by the bond-diluted and annealed Ising model, rather than the regular lattice Ising model, and thereby rendering it a *first-order* singularity. At point $t_2$, the lattice-melting temperature coincides with the critical temperature of the solid-state (regular-lattice) Ising model, and the first-order singularity in the spin degrees of freedom turns into the critical singularity again. In the high-pressure region, the lattice-melting temperature, being bounded from below by that of the non-interacting hard-disk system, is higher than the critical temperature for the magnetic transition. $l(P)$ becomes irrelevant to the critical magnetic transition which separates the **so** and **sd** phases. The phase behaviour in this region is again similar to the phase behaviour of Ising Model I

in the high-pressure region.

## 4.3 Model III: Doniach's Model on a Random Lattice

As discussed in the Introduction and Section 2.2, Model III – Doniach's model defined on the random lattice – was constructed as a minimal model that describes phase equilibria in phospholipid-bilayer systems which are characterized by translational degrees of freedom as well as internal degrees of freedom corresponding to the different conformational states of lipid-acyl chains. In this model, the spin degrees of freedom represent the chain conformational degrees of freedom. The principal (dimensionless) parameters in the model are the following four: $Pd^2/J_0$, $R_0/d$, $V_0/J_0$ and $k_BT/J_0$ (see Fig. 2.1). Our simulation study of the model explored the two-dimensional parameter space spanned by $V_0/J_0$ and $k_BT/J_0$, for fixed values of the other two parameters, $Pd^2/J_0 = 0.925$, and $R_0/d = 1.41$, and the simulation results are summarized in the phase diagram given in Fig. 4.8.

The topology of the phase diagram, characterized by three phase boundaries merging at a triple point, $t_1$, resembles the low-pressure part of the topology of the phase diagram of Ising Model II, with the difference that the spin or chain conformational order-disorder transition in this model is first order, driven by the internal or conformational entropy and it thus referred to as the chain-melting transition. This distinct topology indicates that, again, as in Ising Model II, the thermodynamic singularity arising from the lattice melting can be either coupled or decoupled from the singularity associated with the chain-melting, depending on the values of the parameters. The three phase boundaries, all being of first order and corresponding to a lattice-melting transition, a chain-melting transition and a transition at which *both* melting processes take place, divide the explored region of the parameter space into three phases, the **so**, **lo** and **ld** phases. The three insets in the figure show, respectively, a characteristic microscopic configuration of each phase.

Fig. 4.9 displays a selection of the simulation data that led to the construction of the above phase diagram. The data shown consists of the temperature dependence of the various thermodynamic quantities, the area per particle, $\langle A \rangle$, the area compressibility, $K$, the specific heat per particle, $C_P$, and the enthalpy per particle, $\langle H \rangle$, and

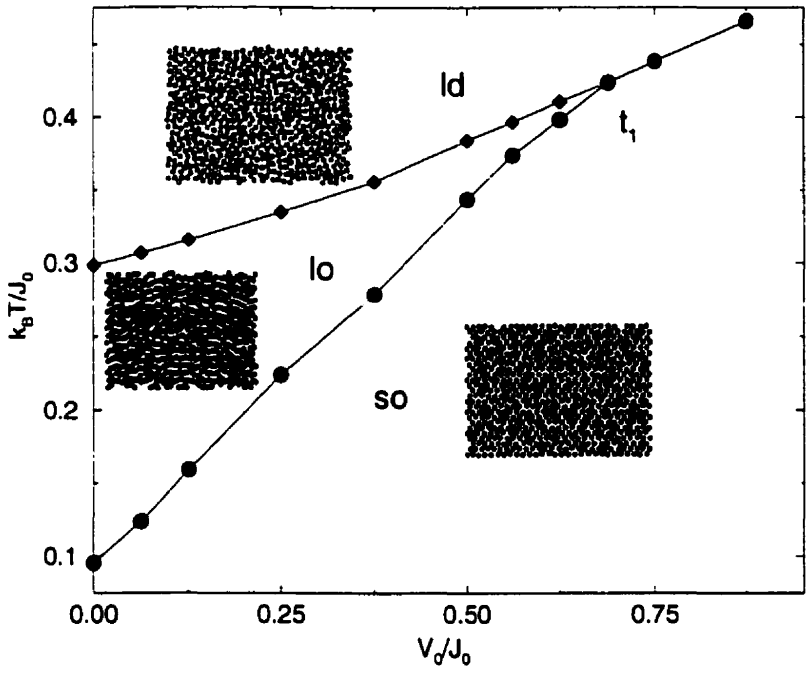


Figure 4.8: Phase diagram for the extended Doniach model, Model III. All three phase boundaries are first-order phase boundaries. The insets show snapshots of typical micro-configurations for the three different phases labeled **so** (solid-ordered), **ld** (liquid-disordered), and **lo** (liquid-ordered). Chains in the disordered state are plotted as (○) and chains in the ordered chain state as (●). The three snapshots are not given to scale. In comparison with experiments the **so-lo** phase line is interpreted as the sub-main phase transition and the **lo-ld** phase line as the main phase transition in long-chain phospholipid bilayers. $t_1$ is the triple point described in the text.

was obtained for a system with $N = 256$ particles and for the following specific values of the model parameters: the internal entropy, $s = k_B \ln D_d = 14.4 k_B$, the conformational energy of the chain disordered state, $E_d/J_0 = 1.303$, and $V_0/J_0 = 0.25$. The data clearly indicates that two distinct first-order phase transitions take place at two different temperatures. At the lower temperature, $T_{s-l} = 0.218 J_0/k_B$, a low-enthalpy, lattice-melting transition takes the system from the **so** phase into the **lo** phase. At the higher temperature, $T_{o-d} = 0.335 J_0/k_B$, the chain-melting transition changes the system from the **lo** phase to the **ld** phase.

Our calculation also showed that in the region of the parameter space where the two melting processes are decoupled, i.e., $V_0/J_0 < V_0/J_0|_{t_1}$, the temperature of the chain-melting transition, $T_{o-d}$, actually depends on the model parameters in a rather simple way. Explicitly, $T_{o-d}$ can be determined as the solution to the equation

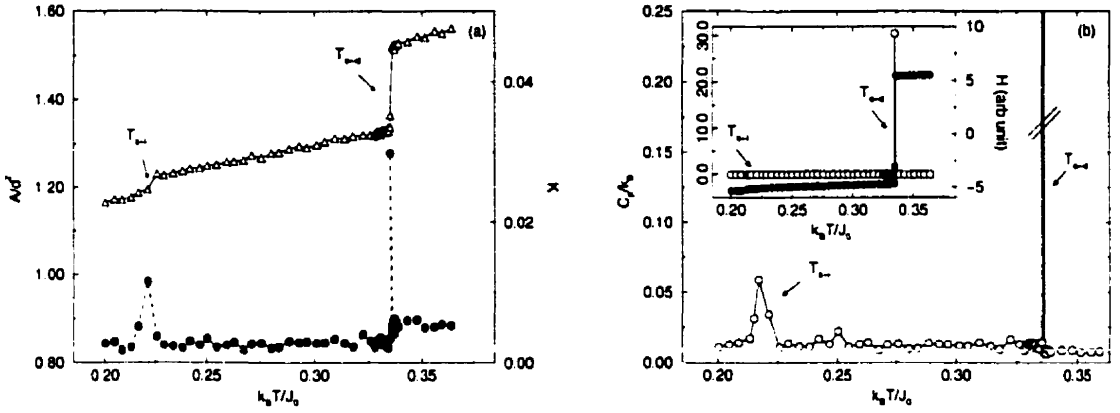

Figure 4.9: Simulation data of the extended Doniach model, Model III, for a system size of $N = 256$ and parameter values $Pd^2/J_0 = 0.925$, $V_0/J_0 = 0.25$ and $R_0/d = 1.41$. (a) shows the area per particle, $A$ ($\Delta$), and the area compressibility, $K$ ($\bullet$). (b) shows the heat capacity per particle, $C_P$. The inset in (b) shows the full scale curves for the heat capacity (o) and the enthalpy per particle (- - -). $T_{o-d}$ is identified as the chain melting transition and $T_{s-l}$ as the sub-main transition in long-chain phospholipid bilayers.

$$-\frac{1}{2}\left[E_d + \frac{\langle z_i \rangle}{2}(J_0 + \langle q_i \rangle V_0) - k_B T_{o-d} \ln D_d\right] + P\Delta\langle A \rangle = 0 \quad , \tag{4.2}$$

where $\langle z_i \rangle$ is the mean value of the local coordination number of the dynamic lattice, and $\Delta\langle A \rangle$ is the change in the surface area per particle as the system undergoes the spin order-disorder transition. $\langle q_i \rangle$ is the mean fraction of the nearest-neighbour pairs that interact with the strength of the deeper square well, a quantity which most significantly reflects the interplay between the translational and the chain-conformational degrees of freedom. It is quite straightforward to understand this result. The Hamiltonian of Model III, as defined in Eq. (2.8), can be written as a diluted Ising model in an effective external temperature-dependent field, $h_{(i)\,eff}(T)$, similar to the original Doniach lattice model. However this field, depends on $z_i$ and $q_i$ as follows

$$h_{(i)\text{eff}}(T) = -\frac{1}{2}\left[E_d + \frac{z_i}{2}(J_0 + q_i\, V_0) - k_B T_{o-d} \ln D_d\right] \quad . \tag{4.3}$$

It thus is a *fluctuating* quantity of the random lattice via the fluctuations in $z_i$ and $q_i$. For the systems simulated with periodic boundary conditions, the local coordination number $z_i$ is conserved on average, i.e., $\langle z_i \rangle = 6$. Furthermore, for a dense 2D liquid system, $z_i$ was found to have a very narrow distribution around 6. Similarly, the fluctuations of $q_i$ about its mean value were also found to be small. Hence, the chain-

melting transition temperature is well approximated by the temperature set by the condition $\langle h_{\rm eff}(T_{\rm o-d})\rangle + P\Delta\langle A\rangle = 0$, which corresponds to that given by Eq. (4.2). For small values of $V_0/J_0$ the gap between the **so-lo** and the **lo-ld** phase boundaries is quite large and the **lo** states close to the chain-melting transition contains many "defects" – interacting pairs having interparticle distances larger than $R_0$ and hence has a rather small value of $\langle q_i\rangle$. For instance, for $V_0/J_0 = 0.25$, we find $\langle q_i\rangle = 0.77$ for the **lo** states just below the chain-melting transition. As we move closer to $t_1$, the number of the defects in the **lo** states decreases, and for $V_0/J_0 = 0.625$ we find $\langle q_i\rangle = 0.96$. Beyond the triple point the low-temperature phase remains crystalline ordered, due to the strong interactions imposed by larger values of $V_0$, and the number of pair defects is essentially zero. Increase in temperature leads to the chain-melting process, which makes the particle-particle interaction ineffective and consequently brings about the lattice-melting process. The phase boundary is then determined by the chain-melting process, for which Eq. (4.2), with $\langle q_i\rangle = 1$, still gives a reasonable valid description.

The enthalpy change across the lattice-melting transition can be found from the enthalpy histogram at the transition temperature. An estimate of the enthalpy change per particle, $\Delta H_{\rm s-l}$, leads to a value of approximately $0.35{\rm k_B}$ per particle for the corresponding entropy change, $\Delta S_{\rm s-l}$. In contrast, the chain-melting transition exhibits a much larger latent heat, corresponding to an entropy change per particle of approximately $14{\rm k_B}$. The heat content in the lattice melting is thus only a few percent of the heat content in the spin order-disorder transition for the chosen set of model parameters.

The dependence of the lattice-melting transition temperature on $V_0/J_0$ is apparent from the phase diagram. The transitional entropy also was found to have a systematic dependence on the parameter. As the value of $V_0/J_0$ is increased from below towards the triple-point value, the simulation data given in Fig. 4.10 shows a steady increase in $\Delta S_{\rm s-l}$ with the parameter value.

Our study of Model III predicts for lipid-bilayer systems a generic picture of the phase behaviour, or more specifically, of the mode in which the chain conformational and molecular translational degrees of freedom are coupled at macroscopic level. In

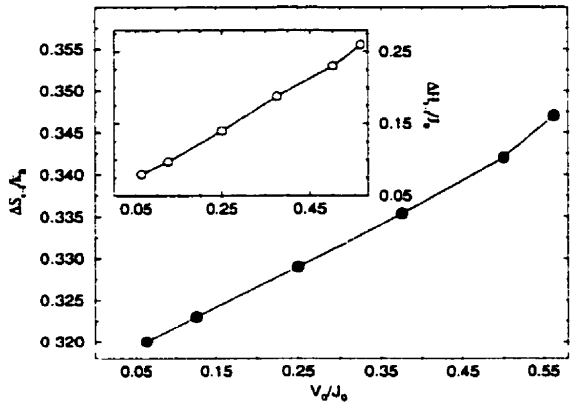


Figure 4.10: Entropy change at the lattice-melting (or sub-main) transition, $\Delta S_{s-l}$, for different values of the model parameter $V_0/J_0$ in Model III, (see Fig. 4.8). The inset in the figure gives the corresponding values of the transitional enthalpy $\Delta H_{s-l}$

particular, it is shown that the loss of the lateral or in-plane ordering, represented by the lattice-melting transition, can take place without the complete loss of the collective ordering in chain conformations; consequently, an intermediate phase, the **lo** phase, can exist [1]. There is no *a priori* reason why the lattice-melting transition and the chain-melting transition should be simultaneous, although it is generally accepted that the main transition in phospholipid bilayers involves both the lattice-melting and the chain-melting processes.

In a recent *high-sensitivity* calorimetric study by Jørgensen (Jørgensen [95]) a new and distinct sub-main transition was shown to be present in fully hydrated multilamellar bilayers of long-chain lipids in the homologous series of di-acyl phosphatidylcholines, $DC_nPC$, with $17 \leq n \leq 20$. The experimental data shows that the entropy change per lipid molecule across this sub-main transition, $\Delta S_{sm}$, is very small, being in the range between $0.22k_B$ and $0.56k_B$. Our model calculations offer an interpretation of this newly-discovered sub-main transition in terms of a decoupling of the lattice-melting transition from the chain-melting transition. As discussed in a recent

[1]The phase diagram for Model III (the Doniach model) of Fig. 4.8 which is applicable to the phase behaviour of pure lipid bilayers is given in terms of the **so**, **lo** and **ld** phases. The generic phase behaviour shown in this diagram was first found using a lattice model (Mouritsen and Zuckermann [87b]) which combined a Pink model ([80]) and a 30-state Potts model. The pink model is an extension of the Doniach model involving 10 conformational states and thus describes the chain degrees of freedom, while the Potts model represents the translational degrees of freedom. The combined Pink-Potts model was examined on a regular lattice and therefore cannot give a true physical representation of the lattice melting.

paper (Nielsen et al. [96a]), the latent heat, or correspondingly, the transitional entropy predicted by our study of Model III for the lattice-melting transition compares favorably with the experimental data for the sub-main transition. This implies that Model III, despite of its minimal nature captures some of the essential mechanisms underlying the interplay between the chain-conformational and the translational degrees of freedom in lipid-bilayer systems.

## 4.4 *Discussion*

Motivated by the rich phase behaviour of lipid-bilayer systems, the work reported in this chapter is the result of an investigation of the equilibrium phase behaviour in two-dimensional dense many-particle systems where both translational and internal degrees of freedom are present and are coupled through microscopic interactions. We first developed a random-lattice algorithm given a full description of the translational degrees of freedom for a dense two-dimensional system. We then formulated, and studied using computer-simulation techniques, a series of three statistical mechanical models. These models treat the internal degrees of freedom essentially as Ising spin variables, but with different emphasis and levels of complexity in the description of the microscopic coupling to the translational degrees of freedom. The models were shown to lead to quite rich phase behaviour although they only describe microscopic interactions in a minimal and generic manner. The most important feature in the phase behaviour of these models is that, depending on the model parameters, phase transitions associated with the internal degrees of freedom can be either coupled to, or decoupled from, the first-order phase transition in the translational degrees of freedom corresponding to the lattice-melting process, thus manifesting at the macroscopic level the interplay between the two types of degrees of freedom. In particular, as in Model II, when the internal degrees of freedom are strongly coupled to the translational degrees of freedom in a macroscopic manner, their order-disorder singularity in the conformational degrees of freedom is slaved by the singularity leading to the first order lattice melting transition and the order-disorder transition becomes first order. This is in contrast to the critical singularity which occurs when the coupling is weak at the macroscopic level. It is further shown that in the case of weak coupling, the

universal critical behaviour of the internal degrees of freedom remains unchanged, in the sense that it is in the same universality class as the regular-lattice Ising model. Finally, we discussed the prediction of one of the models, Model III, in relation to a recent experimental observation of a new sub-main phase transition in phospholipid bilayer systems.

We conclude this chapter with a final remark on the prospects of the type of random-lattice models as proposed in the chapter. The formulations of such models are quite general and may be applied to any two-dimensional dense systems where different types of degrees of freedom are present and relevant. In particular, this approach should open up new possibilities in studies of structural and thermodynamic properties of complex systems such as multicomponent lipid bilayers - a highly biologically-relevant example being lipid-cholesterol mixtures, as will be shown in the next chapter.

# 5

# Results for Lipid–Sterol Mixtures

This chapter contains details of our simulations of the generic phase behaviour of the models for the series of lipid-sterol mixtures as defined in Section 2.3. The description is written in two parts. First we give the results for the analysis of the lipid-cholesterol system and next the results for the analysis of the series of lipid-sterol systems.

## 5.1 *Model IV, Lipid-Cholesterol Mixtures*

In this section, we give the results of Monte Carlo simulations for the phase diagrams and physical quantities of lipid-cholesterol bilayers. The simulations were based on the model of Section 2.3 (Eq. (2.10)) and the techniques described in Chapter 3 were applied. The principal thermodynamic control parameters for the simulations are the temperature $T$, and either the cholesterol concentration, $x_c$, or $\mu_\Delta$, the effective chemical potential controlling the equilibrium cholesterol concentration. We define $x_c = \frac{N_c}{N}$, where $N$ is the total number of particles in the system and $N_c$ is the number of cholesterol molecules. This definition is related to the molar definition, $x_c^m$, commonly used in experimental work, by $x_c^m = \frac{2x_c}{1+x_c}$, since each lipid molecule contains two chains. The other parameters in the model were fixed at specific values in all simulations. For convenience, the unit for energy was chosen to be $J_0 \equiv V^l_{o-o}$, the strength of the longer range attraction between chains in the ordered state, as defined by Eq. (2.14); and the unit for lengths is set at the hard-disk diameter, $d$. The surface pressure, $\Pi$, was fixed at $\Pi d^2/J_0 = 6.0$. The excitation energy of the disordered state of lipid chains was chosen as $E_d = 1.303J_0$, and the degeneracy, $D_d$, of the state, was taken to be $\ln D_d = 7.2$. The parameters defining the different interaction potentials as in Eq. (2.13) and Eq. (2.14) were set to the following specific values: $V^s_{o-o} = 1.55J_0$, $V^l_{o-c} = 2.45J_0$, $V^s_{o-c} = -1.75J_0$, $V^l_{d-c} = 0.35J_0$, $V^s_{d-c} = -0.35J_0$, $V^l_{c-c} = 0.5J_0$,

$V^{s}_{c-c} = -1.0J_0$, $V^{l}_{o-d} = 0.5J_0$ and $V^{s}_{o-d} = -0.5J_0$. The radius of the short range square well potential was $R_0/d = 1.3$. The values of $\Pi$, $R_0$, $E_d$ and $\ln D_d$ were chosen so that the latent heat of the main transition and the change in surface area across the main transition are comparable to that measured experimentally for the single-component DPPC bilayer system (G. Cevc [93]). The value for $V^{s}_{o-o}$ was chosen such that the phase transition in the pure "lipid system" is located in the regime where the lateral and the internal degrees of freedom are coupled (see discussion in Section 2.3). Other parameters, $V^{s,l}_{\alpha-c}$ ($\alpha = o, l, c$), were also set at certain values, for which the phase behaviour predicted by the model resembles that of DPPC-cholesterol bilayers. The above values of the parameters, however, are not unique in that the same generic phase behaviour holds for a large set of different parameter values.

### 5.1.1 *Phase Diagrams: Simulations within the Semi-Grand Canonical Ensemble*

In order to calculate phase diagrams for our model system, we performed simulations within the semi-grand canonical ensemble (see Section 4.1.1), using the simulation methods described in Chapter 3.

Figure 5.1 gives the phase diagrams constructed based on our simulation data. Fig. 5.1(a) is presented in terms of two control parameters, the concentration of cholesterol $x_c$ and the reduced temperature $T/T_M$, where $T_M$ is the temperature of the main transition in the pure lipid system, while Fig. 5.1(b) shows a conjugate representation in the parameter space spanned by $\mu_\Delta$ and $T/T_M$. As clearly illustrated in the phase diagrams, the generic thermodynamic behaviour of our model is characterized by three principal phases, an **so** phase, an **ld** phase, and an **lo** phase, defined in the Introduction, by three first-order lines between these three phases and finally, by two special points, a critical point, $P_C$, which terminates the **ld–lo** transition and a triple point, $P_t$, at which all three phases coexist.

Figure 5.2 gives examples of the finite-size analysis of the phase coexistence. This figure shows the spectral free energies, $\mathcal{F}_L(x_c)$, calculated as a function of the system size $L$, for two of the three first-order transitions, corresponding to the **so–lo** and the **ld–lo** coexistence, respectively. In each case, a value of $T$ was chosen and kept fixed

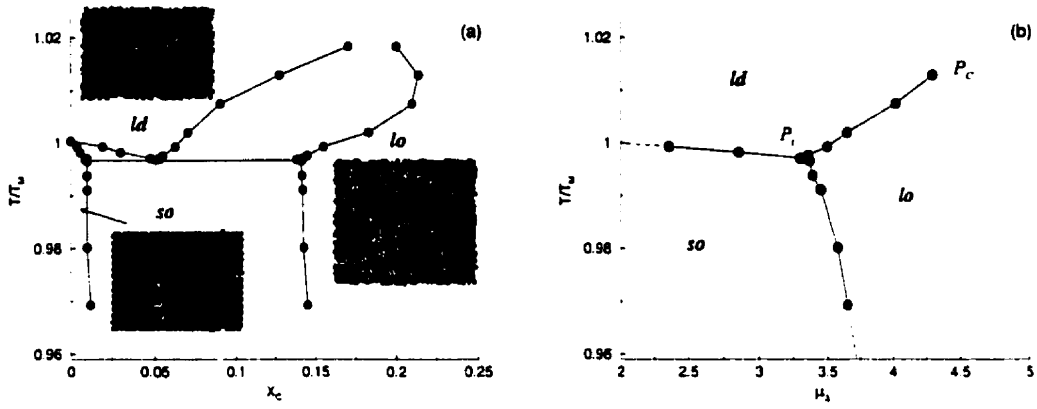


Figure 5.1: Phase diagram for the lipid cholesterol model. (a) The phase diagram as a function of cholesterol concentration $x_C$ and reduced temperature $T/T_M$. The inserts to the figure show different snapshot of micro configurations corresponding of the different phase in the diagram. The snapshots are not given to scale. The different phases labeled in the phase diagram are; **so**, solid ordered (gel), **ld**, liquid disordered (fluid) and **lo** liquid ordered where the first letter refers to the lateral order of the phase and the second letter refers to the conformational order of the phase. (b) The phase diagram as a function of $\mu_\Delta$ and $T/T_M$. $P_C$ and $P_t$ are the critical point of the **ld-lo** coexistence region and the triple point respectively described in the text.

in the simulations of systems of different sizes while the parameter $\mu_\Delta$ was tuned and a specific value, $\mu^*_\Delta(T;L)$, was determined for each system size from the "coexistence" condition, which is specified by two equal-energy minima in $\mathcal{F}_L(x_c)$.

The figure shows a monotonic increase with system size $L$ in the "interfacial energy", $\Delta\mathcal{F}_L(x_c)$, defined as the height of the maximum relative to the minima of the spectral free energy function, indicating the existence of a first-order transition (Lee and Kosterlitz [91]). The magnitude of the free energy barrier between the coexisting phases can be obtained from the curves in the figure. For example, for a system of size $L = 20$, $\Delta\mathcal{F}_L(x_c)_{\mathbf{ld-lo}} \simeq 3k_BT$ and $\Delta\mathcal{F}_L(x_c)_{\mathbf{so-lo}} \simeq 4.5k_BT$.

The finite-size analysis also provides evidence for the presence of a critical point terminating the **ld–lo** coexistence. In Fig. 5.3 we show the finite-size analysis of the simulation data for three different temperatures close to the critical point of the **ld-lo** coexistence region. The inserts in the figure show the variation of the spectral free energy as a function of system size for all three temperatures. For the lowest temperature, $T = 1.007T_M$ (Fig. 5.3(a)), the finite-size analysis shows a linear increase of the energy associated with an interface between the **ld** and the **lo** phase, indicating the existence of a first-order phase transition. The gradient of the linear

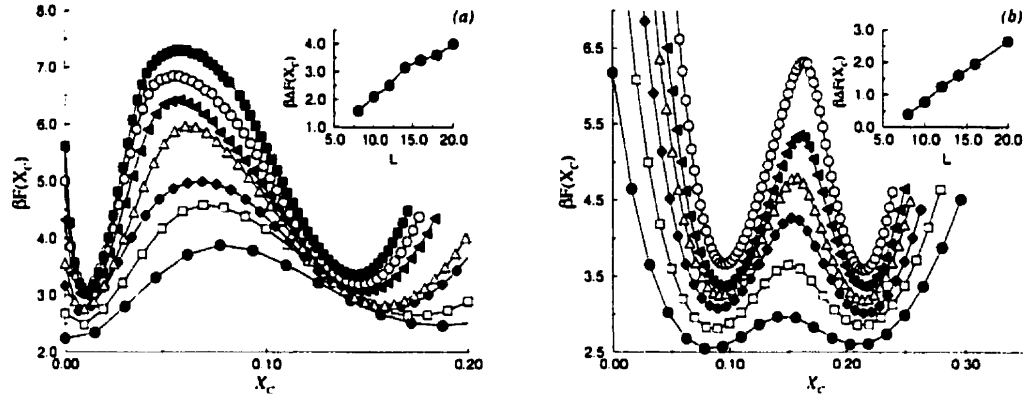


Figure 5.2: Finite size scaling plot of $\beta\mathcal{F}_L(x_C)$. (a) $T = 0.969T_M$ (**so-lo** phase coexistence). The system sizes are $L$ = 8, 10, 12, 14, 16, 18 and 20. (b) $T = 1.007T_M$ (**ld-lo** phase coexistence). The system sizes are $L$ = 8, 10, 12, 14, 16, and 20. The inserts to the figures show the barrier height $\beta\Delta\mathcal{F}(x_C)$ as a function of system size. The lines connecting the points in the two inserts are guides to the eye.

relation corresponds to the interfacial tension between the two coexisting phases. For the highest temperature, $T = 1.018T_M$ (Fig. 5.3(c)), $\Delta\mathcal{F}_L(x_c)_{\mathbf{ld-lo}}$ decreases as a function of system size $L$, demonstrating the absence of a phase transition for this temperature. Finally, the results for $T = 1.013T_M$ (Fig. 5.3(b)) suggest that the "interfacial energy" at this temperature for large system sizes approaches a constant value, indicating that the critical point of the **ld-lo** coexistence region is located close to $T = 1.013T_M$.

A precise determination of the line of the three-phase coexistence, requires systematic simulations for different system sizes, which turns out to be impractical. We have, therefore, contented ourselves with making a good estimate from a single histogram calculated for a sufficiently large system. Figure 5.4 shows the histogram $\mathcal{P}(\varepsilon, x_c)$ for a system of size $L = 18$ at a temperature $0.997T_M$. The histogram demonstrates the coexistence of the three distinct phases: the **so** phase, with a low internal energy and low cholesterol concentration; the **ld** phase, with a high internal energy and a modest cholesterol concentration; the **lo** phase, with an intermediate internal energy and a relatively high cholesterol concentration. Based on this result we estimate the location of the three phase line to be close to $T \simeq 0.997T_M$ and the concentration of cholesterol in the three coexisting phases to be, respectively, $x_{c,\mathbf{so}} \simeq 0.010$, $x_{c,\mathbf{ld}} \simeq 0.053$ and $x_{c,\mathbf{lo}} \simeq 0.143$.

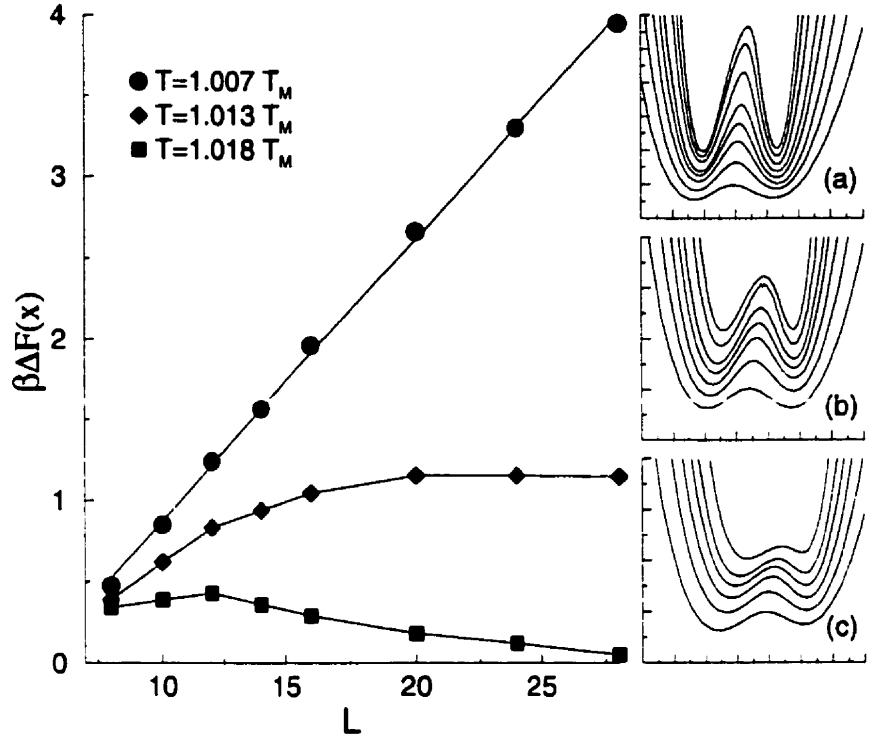


Figure 5.3: Finite size scaling plot of $\beta\Delta\mathcal{F}_L(x_C)$ at three temperatures close to the critical point of the **ld-lo** coexistence region. (a) $T = 1.007T_M$, (b) $T = 1.013T_M$ and (c) $T = 1.018T_M$. The system sizes are $L$=8,10,12,14,16,20,24 and 30. The inserts to the figure show the spectral free energy $\mathcal{F}_L(x_C)$ for the different system sizes. The line connecting the point in (a) is a linear fit to the barrier height as a function of system size. The lines connecting the point in (b) and (c) are guides to the eye.

The coexistence region between the **so** and the **ld** phases is very narrow and both the three phase coexistence line the main transition point of the pure lipid system are strongly dependent on system size. It is therefore quite time consuming to obtain histograms of the distribution function at coexistence, which have sufficient accuracy for finite size scaling analysis. We have thus used the Ferrenberg Swendsen reweighting technique (Ferrenberg and Swendsen [88]) to estimate the locations of the boundaries of the **so-ld** coexistence region. Specifically, we have through the reweighting procedure extrapolated the probability distribution functions obtained from the three-phase histogram to higher temperatures.

The phase diagrams in Fig. 5.1 exhibit all the characteristics of macroscopic uncoupling of the translational and the chain-conformational degrees of freedom: the appearance of the **lo** phase, and the two uncoupled transitions associated with this

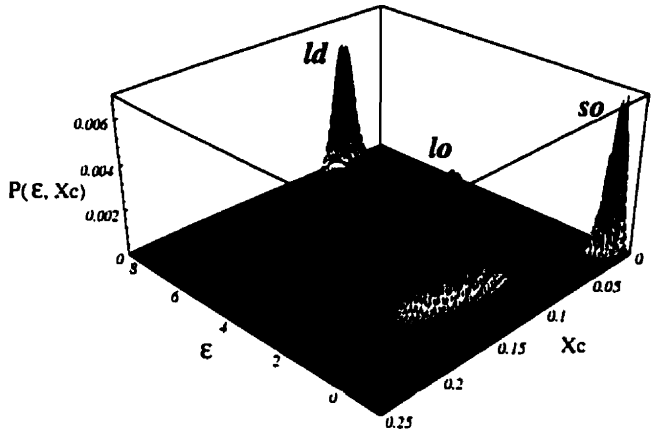


Figure 5.4: The histogram $\mathcal{P}(\epsilon, x_c)$ for a system size of $L = 18$ and $T = 0.997$. The three coexisting phases are located at cholesterol concentration of $x_c = 0.010$ (**so**), $x_c = 0.053$ (**ld**) and $x_c = 0.143$ (**lo**).

phase specifically, the **so–lo** and the **ld–lo** transitions. These two transitions correspond to the ordering processes of the translational and the chain-conformational degrees of freedom, respectively. It is clear that this phenomenon is a macroscopic consequence of the dual-natured interaction of the cholesterol molecule with the translational and chain-conformational degrees of freedom of the lipid molecules. When Fig. 5.1(a) is considered together with our understanding of the **so–ld** transition in the pure lipid system as described in Ref. (Nielsen et al. [96b]) and displayed in Fig. 4.8, it provides clues as to how the dual effect of cholesterol is macroscopically manifested in the system. In the one-component lipid system, the **so–ld** transition is predominantly driven by the conformational entropy associated with the disordered state of the lipid chains, and the transition temperature, $T_M$, is determined by the competition between the conformational-entropy effect and the strength of the effective interactions between conformationally ordered chains. Incorporation of cholesterol into the lipid system creates a complex picture of the macroscopic ordering phenomena. Below $T_M$, the **so** phase can only solubilize very low concentrations of cholesterol without loosing its quasi long-range translational order, due to the "crystal-breaking" function of cholesterol. Once the concentration reaches certain small, temperature-dependent, values, the "crystal-breaking" function of cholesterol does indeed cause a breakdown of the global packing order of the chains, and the loss of the long-range translational order. This breakdown in turn affects the chain-ordering process, as it also implies a reduction in the strength of the effective cohesive interactions between chains in the conformationally ordered state. The reduced effective

interaction strength thus sets a maximal temperature for the macroscopic ordering of chain conformations, and this maximal temperature is essentially the temperature of the three-phase line. Below this temperature, the cohesive interaction between chains, albeit at its reduced strength, dominates over the conformational-entropy effect and sustains a macroscopic conformational order, even though the translational order is lost. The "chain-ordering" tendency of cholesterol, or the high affinity of cholesterol for conformationally ordered chains, results in relatively high solubility of cholesterol in the lipid matrix, corresponding to the wide miscibility gap between the lipid-rich **so** and the cholesterol-rich **lo** phases. In contrast, above the temperature of the three-phase coexistence, and for intermediate cholesterol concentrations, the effect of conformational entropy takes precedence over both the cohesive interactions and the chain-ordering effect of cholesterol, thus favoring the **ld** phase as the equilibrium phase. Under this entropy dominance, the chain-ordering effect of the cholesterol translates into its low affinity for lipid molecules with disordered chains as reflected in the moderate solubility of cholesterol molecules in the **ld** phase. At high enough cholesterol concentrations, however, the chain-ordering effect wins the competition over the entropy effect, reinstating the macroscopic order in the lipid chain conformations, i.e., the **lo** phase. This ordering event, which only involves the conformational degrees of freedom, is manifested in the reasonably wide region of the **ld**–**lo** coexistence.

### 5.1.2 *Simulations within the Canonical Ensemble; a Structural Analysis*

In this section, we present results of a detailed structural analysis of the various phases described above. The results have all been obtained by performing simulations within the canonical ensemble as described in Section 4.1.1. In the simulations, we calculate the following structure factors

$$S_T(\vec{q}) = \frac{1}{N}\{\langle \rho_T(\vec{q})\rho_T(-\vec{q})\rangle - \langle \rho_T(\vec{q})\rangle^2 \delta_{\vec{q},\vec{0}}\}$$
$$S_O(\vec{q}) = \frac{1}{N}\{\langle \rho_O(\vec{q})\rho_O(-\vec{q})\rangle - \langle \rho_O(\vec{q})\rangle^2 \delta_{\vec{q},\vec{0}}\}$$

$$S_C(\vec{q}) = \frac{1}{N}\{\langle \rho_C(\vec{q})\rho_C(-\vec{q})\rangle - \langle \rho_C(\vec{q})\rangle^2 \delta_{\vec{q},\vec{0}}\} \tag{5.1}$$

$$S_{O-C}(\vec{q}) = \frac{1}{N}\{\langle \rho_O(\vec{q})\rho_C(-\vec{q}) + \rho_C(\vec{q})\rho_O(-\vec{q})\rangle - 2\langle \rho_O(\vec{q})\rho_C(\vec{q})\rangle\, \delta_{\vec{q},\vec{0}}\} .$$

Here, $\rho_T(\vec{q})$ is the Fourier transform of the total density operator, $\rho_T(\vec{r}) \equiv \sum_i \delta(\vec{r}-\vec{r}_i)$ and $\rho_G(\vec{q})$, $\rho_C(\vec{q})$ the Fourier transforms of the partial density operators $\rho_\alpha(\vec{r}) \equiv \sum_i \delta(\vec{r}-\vec{r}_i)\mathcal{L}_{\alpha i}$ for the lipid chains in the ordered state ($\alpha$ = o) and the cholesterol molecules ($\alpha$ = c) respectively. $\langle\cdots\rangle$ denotes a thermal average and $N$ is the number of particles.

Figures 5.5-5.10 summarize the calculated structure factors characterizing the lateral structure of the various thermodynamic phases. Each simulation was performed for a system size of $N = 1600$ and the thermodynamic average of the structure factor contains $10^5$ different microconfigurations with a time interval of 100 MCS between two consecutive configurations.

Fig. 5.5(a) and Fig. 5.5(b) show, for the **so** and the **ld** phase, respectively, the structure factors $S_T(\vec{q})$ and $S_O(\vec{q})$ as well as the circular averages of $S_T$, $S_O$, $S_C$ and $S_{G-C}$. In Fig. 5.5(a) the plots of $S_T(\vec{q})$ and $S_O(\vec{q})$ give a clear signal of a solid hexagonal phase characterized by a lattice spacing close to $d$. In Fig. 5.5(b) the plot of $S_T(\vec{q})$ demonstrates the liquid characteristics of the **ld** phase. The average interparticle distance can be determined from the position of the first diffuse scattering ring, and an estimate gives a value of $< r >$ close to $1.115d$.

Figure 5.6 displays both the total structure factor, $S_T$, and the two partial structure factors, $S_O$, and, $S_C$, calculated at $T = 0.969T_M$ and $x_C = 0.165$ where the system is in the **lo** phase. The characteristics of the phase, as far as its lateral structure is concerned, is unambiguously that of a liquid. More systematic analysis of the **lo** phase is summarized in Figure 5.7. The three upper figures show the circular averages of $S_T$, $S_O$, $S_C$ and $S_{O-C}$ calculated at three different locations in the parameter region where the **lo** phase exists. The three lower figures are the corresponding snapshots of microconfigurations. The collective ordering in lipid chain conformations can be observed directly from the snapshots. The figure at the right hand side further demonstrates the "rigidifying" effect of the cholesterol. The high degree of

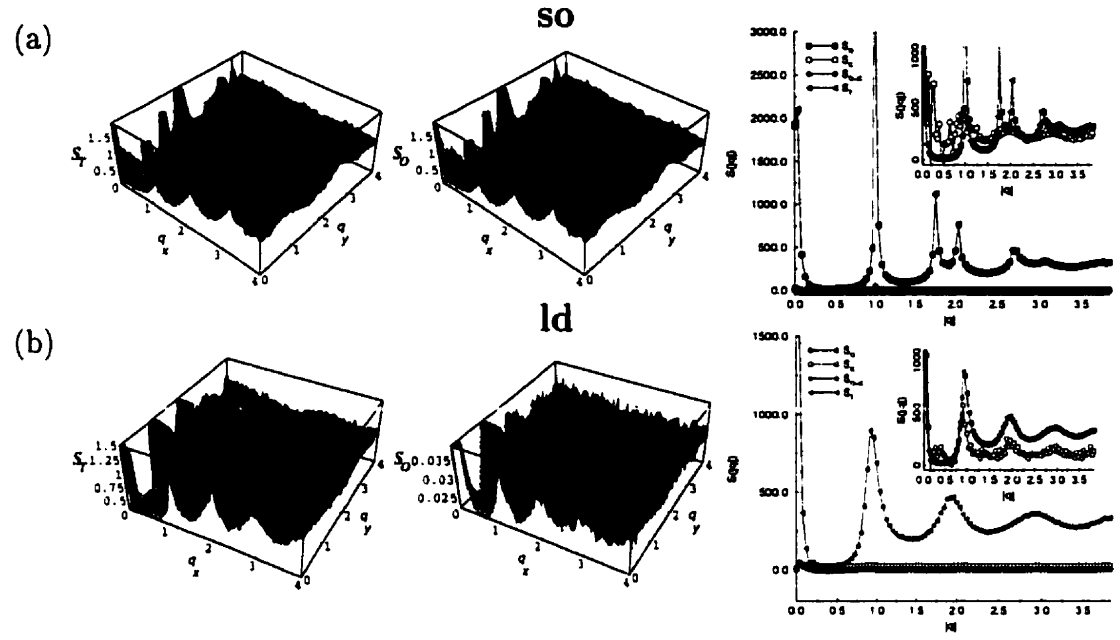


Figure 5.5: The structure factors $S_T(\vec{q})$ and $S_O(\vec{q})$ calculated within the **so** phase and the **ld** phase, respectively. The upper three figures show the results for $T = 0.969T_M$, $x_c = 0.010$ (**so** phase). The lower three figures show results for $T = 1.007T_M$, $x_c = 0.085$ (**ld** phase). The figure to the left shows $S_T(\vec{q})$, the middle figure $S_O(\vec{q})$ and the figure to the right the circular averages for $S_T$, $S_O$, $S_C$ and $S_{G-C}$. The $q$-values are given in units of $2\pi/d$. The Bragg peaks in the upper figure show the structure of an hexagonal ordered solid phase with a lattice spacing around $d$. The diffuse rings in the lower figure show the existence of the liquid phase. The average inter-particle distance can be determined from the position of the first ring and gives a value of around $1.115d$.

chain ordering as illustrated in the snapshot is stabilized only by the incorporated cholesterol, as the pure lipid system is in the **ld** phase at this temperature. Clearly, the appearance of the **lo** phase as a stable equilibrium phase is a macroscopic manifestation of the dual molecular function of cholesterol. When present at relatively high concentrations, cholesterol destroys the quasi long-range translational order and at the same time either induces or reinforces macroscopic order in the lipid chain conformations.

Figure 5.7 offers more information on the details of the lateral structure of the **lo** phase. The three graphs of $S_C(\vec{q})$ all exhibit a diffuse ring located close to $|q| = 0.4 \cdot 2\pi/d$. The intensity of the ring increases with the concentration of the cholesterol. An examination of the corresponding snapshots gives indications of the structures that give rise to these rings. It appears that most of the cholesterol molecules and a significant fraction of the lipid chains aggregate with their own

**lo**

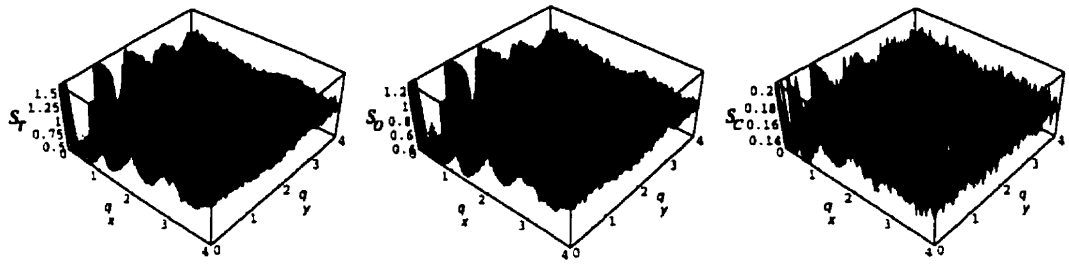

Figure 5.6: The structure factors $S_T(\vec{q})$, $S_O(\vec{q})$ and $S_C(\vec{q})$ calculated at $x_c = 0.165$, $T = 0.969T_M$ within the **lo** phase. The $q$-values are given in units of $2\pi/d$.

species to form one-dimensional thread-like micro-structures. The physical reason for this particular structure lies in the difference between the interaction potential between two cholesterol molecules (Fig. 2.2(d)) and that between a cholesterol molecule and an ordered lipid chain (Fig. 2.2(b)). The relatively weaker cholesterol-cholesterol interaction gives the cholesterol a tendency to minimize nearest neighbour contacts between its own kind in exchange for maximal number of contacts with ordered lipid chains. The formation of the thread-like micro-structures allows this tendency to be expressed to an appreciable extent at high concentrations of the cholesterol. The data for $S_{O-C}$ indicate that the average distance between an ordered lipid chain and a cholesterol molecule is about $1.3d$. In two neighbouring thread-like structures where the cholesterol molecules are separated by one lipid chain, the distance between the cholesterol molecules is then about $2.6d$ (see Fig 5.8).

A configuration as the one shown in Fig. 5.8 ought to give rise to a diffuse ring in the structure factor located at $|q| \approx 0.4 \cdot 2\pi/d$. Furthermore, this signal should be more appreciable in $S_C(\vec{q})$ than in $S_O(\vec{q})$, due to the relatively higher fraction of those cholesterol molecules forming the thread-like structure out of the total number of the cholesterol molecules. This picture is consistent with the simulation results.

Finally, Fig. 5.9 and Fig. 5.10 show the structure factors calculated inside the **so − lo** and **ld − lo** coexistence region, respectively. The structure factor $S_T(\vec{q})$ in Fig. 5.9 gives a clear signal of both a liquid and a solid phase. $S_C(\vec{q})$, the partial

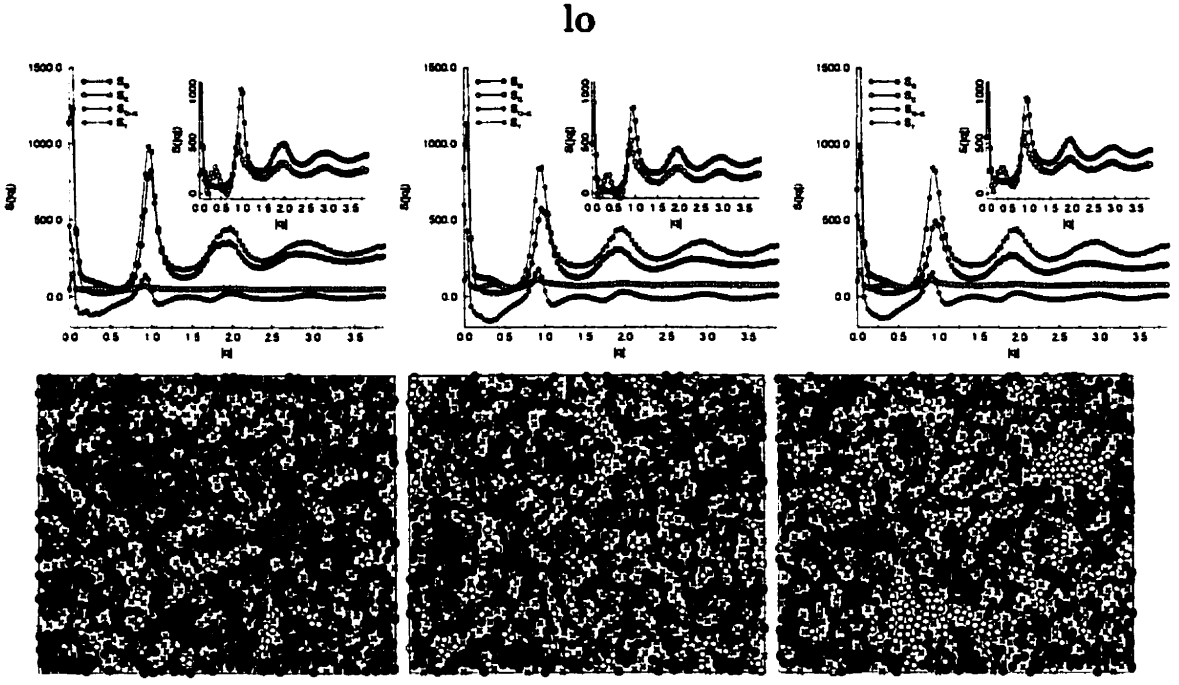


Figure 5.7: The structure factor calculated at different locations within the **lo** phase. The upper three figures show the circular averages of $S_T$, $S_O$, $S_C$ and $S_{O-C}$ calculated at (from the left) $x_c = 0.165$, $T = 0.969T_M$, $x_c = 0.250$, $T = 0.969T_M$ and $x_c = 0.250$, $T = 1.007T_M$. The $q$-values are given in units of $2\pi/d$. The lower three figures show snapshots of the microconfigurations of the corresponding phases. In the snapshots, a lipid chain in the ordered state is shown as (•), a lipid chain in the disordered state as (○) and a cholesterol molecule as (×).

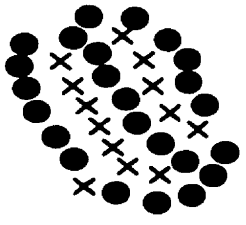

Figure 5.8: Snapshot of two neighbouring thread-like micro structures where the cholesterol molecules are separated by one lipid chain. The snapshot is a part of the snapshot given in Fig. 5.7 for $x_C = 0.250$, $T = 0.969T_M$. A lipid chain in the ordered state is shown as (•), and a cholesterol molecule as (×).

structure factor related to the cholesterol, on the other hand displays only the diffuse properties of a liquid, showing that cholesterol only dissolves in the liquid **lo** phase.

The structure factors in Fig. 5.10, corresponding to the **ld-lo** coexistence, show no sign of a structural difference between the two coexisting phases. This result further supports the characterization of the **lo** phase as a liquid phase.

### 5.1.3 Discussion

The experimentally observed equilibrium phase behaviour of bilayer systems of binary mixtures of phospholipids and cholesterol is characterized by a macroscopic uncou-

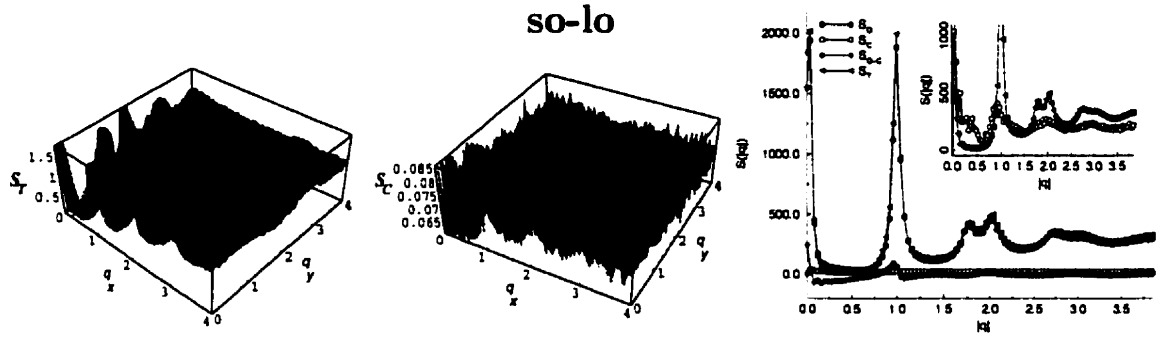


Figure 5.9: The structure factors $S_T(\vec{q})$ (left figure) and $S_C(\vec{q})$ (middle figure) calculated at $x_c = 0.075$ and $T = 0.969T_M$ within the region of phase coexistence of the **so** and the **lo** phases. The figure to the right gives the circular averages of $S_T$, $S_O$, $S_C$ and $S_{O-C}$. The $q$-values are given in units of $2\pi/d$.

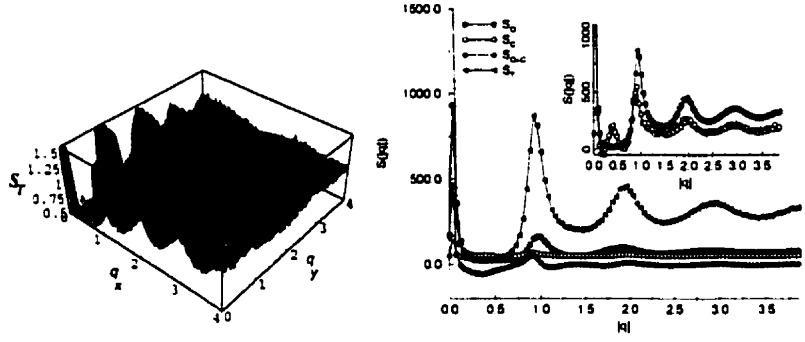


Figure 5.10: The structure factors calculated at $x_c = 0.17$ and $T = 1.010T_M$ within the region of phase coexistence of the **ld** and the **lo** phases. In the figure to the left is shown $S_T(\vec{q})$, the figure to the right gives the circular averages of $S_T$, $S_O$, $S_C$ and $S_{O-C}$. The $q$-values are given in units of $2\pi/d$.

pling of the translational degrees of freedom from the internal molecular, specifically, the chain conformational degrees of freedom. This phenomenon provides a context for investigating the generic physics involved in the interplay between translational and internal molecular degrees of freedom, both at the microscopic level and at the macroscopic level. To this end, we formulated a microscopic model to describe a two-dimensional system composed of two distinct types of "model molecules", representing lipid molecules and cholesterol, respectively, and we have carried out a statistical mechanical study of the model to investigate the equilibrium phase behaviour based on Monte Carlo computer simulations.

The model differs in an essential way from the earlier *lattice* models developed

to describe the phase behaviour of lipid-cholesterol mixtures in that it provides an off-lattice, and therefore more realistic, representation of the translational degrees of freedom in terms of a specific random-lattice algorithm. Naturally, this feature enables us to better characterize and make predictions concerning the macroscopic behaviour of the translational degrees of freedom, i.e. the lateral structures of different thermodynamic phases of the model system.

Given our aim of elucidating *generic* behaviour of the interplay between the configurational and translational degrees of freedom together with the considerable computational effort required for the explicit treatment of translational degrees of freedom, the remaining of the ingredients of the model were tailored to correspond to *minimal* descriptions of the relevant microscopic physics. The chain conformational degrees of freedom and the associated phase space are represented by only two molecular conformational states. Cholesterol is treated as a simple substitutional impurity. Its molecular function in a lipid bilayer is described, based on an earlier hypothesis (Ipsen et al. [87]; Ipsen, Mouritsen and Zuckemann [89]; Ipsen, Mouritsen and Zuckemann [90]), to be dual, both as a "crystal breaker" and as a "chain rigidifier." This molecular mechanism forms in our opinion a microscopic basis for the interplay between translational and conformational degrees of freedom. The microscopic interactions, those between a cholesterol molecule and a lipid chain in particular, were all designed to only contain features that are essential and necessary for describing both the phase behaviour of one-component lipid systems and the dual molecular function of cholesterol.

Our rather extensive and systematic study of the minimal model based on Monte Carlo computer simulations has led to a phase diagram for the model system. This phase diagram displays the same topology as the experimentally obtained phase diagram (Vist and Davis [90]). Particularly, the theoretical phase diagram demonstrates that the proposed microscopic model does indeed provide a picture of microscopic physics underlying the ability of cholesterol to uncouple the macroscopic ordering processes of the translational and chain conformational degrees of freedom already at very low concentrations. The fact that the model is a minimal model suggests that the *macroscopic* uncoupling between translational and chain conformational de-

grees of freedom in these systems may not depend sensitively on the details of the *microscopic* physics and should, therefore, be a generic phenomenon. It has indeed been argued that the phase behaviour of the DPPC-cholesterol bilayer system contains some generic features for mixtures of lipids and cholesterol or cholesterol-like molecules (Ipsen et al. [87]; Thewalt and Bloom [92]; Linseisen et al. [93]), although more concrete experimental evidence is yet to be obtained.

In addition, our study provides detailed information on the lateral structure of the different phases. The structure of the cholesterol-rich phase is of particular interest, since it has been the subject of a long and continuing debate in the experimental literature (Finegold [93]). The structure factor that we have obtained from the simulations clearly shows that the **lo** phase is indeed a liquid phase. More interestingly, the partial structure factors associated with cholesterol molecules and ordered lipid chains, respectively, show signatures of an additional structure that is characterized by length scales roughly twice that of the average distance between nearest neighbours. Inspection of the related microscopic configurations leads to an interesting observation: the cholesterol molecules and those lipid chains that are in direct contact with them tend to form "thread-like" structures. In these structures, each molecule tends to align linearly with its own species. This tendency becomes more pronounced at higher cholesterol concentrations (data not shown). The "threads" are short, involving only a few molecules, and there is no sign of long-range orientational correlations. The origin of this behaviour can be understood as follows. At low and intermediate temperatures as compared with the temperature of the main transition in the one-component system of lipid, the system in the **lo** phase consists of cholesterol and chains in the ordered state only. Therefore, the model effectively becomes an off-lattice antiferromagnetic Ising model with a spin-exchange interaction of strength $\frac{1}{4}V_{o-o}(R_{ij}) + \frac{1}{4}V_{c-c}(R_{ij}) - \frac{1}{2}V_{o-c}(R_{ij})$ subject to an external field[1]. Even though this

[1] In the case where the **lo** phase consists of only cholesterol and chains in the ordered state the microscopic Hamiltonian Eq. (2.10) can be rewritten as an Ising model in an external field. If we associate the Ising spin $S = +1$ state with a chain in the ordered state and the Ising spin $S = -1$ state with a cholesterol molecule, the occupation variables $\mathcal{L}_{io}$ and $\mathcal{L}_{ic}$ can be expressed as $\mathcal{L}_{io} = (1 + S_i)/2$, $\mathcal{L}_{ic} = (1 - S_i)/2$. Rewriting Eq. (2.10) in terms of the Ising spin variable we get $H = \sum_{(i<j)}(V_{o-o}/4 + V_{c-c}/4 - V_{o-c}/2)S_iS_j + \sum_i h(T,P)S_i$. Noting that the interaction potentials

model has not been studied, a related antiferromagnetic Ising model defined on a lattice with elastic deformability, has been shown to display a low-temperature striped phase, in which spins of the same sign line up to form stripes (Gu et al. [96]). The characteristic periodicity in the stripe phase is twice that of the average lattice spacing (Gu et al. [96]). The presence of the "thread-like" structures revealed by our simulations has some experimental support, particularly from fluorescence (Rogers, Lee and Wilton [79]; Mitchell and Litman [98]) and X-ray diffraction (Hui and He [83]) studies. The results of the earlier fluorescence and X-ray diffraction studies were interpreted as support for a structural model where lipid and cholesterol molecules formed stoichiometric complexes and moreover, the complexes aligned themselves linearly (see (Presti [85]) for a review of the earlier studies). In contrast, our theoretical study as well as both the fluorescence study by D.C. Mitchell and B.J. Litman ([98]) and the X-ray diffraction study by Hui and He ([83]) specifically shows, that the partial alignment of molecules as observed in the simulations does not require a chemically specific mechanism such as the formation of stoichiometrical complexes. It is important to note that the "thread-like" structures in the **lo** phase are not the ripple structures observed in experimental systems in **so-lo** coexistence region (Mortensen et al. [88]). The ripple structures involve much larger length scales as well as non-planar membrane surface configurations[1].

$V_{o-o}$ and $V_{o-c}$ have very similar strength and that the strength of the interaction potential $V_{c-c}$ is relatively small, we see that the model becomes an antiferromagnetic Ising model in an external temperature- and pressure-dependent field. ($V_{o-o}$, $V_{o-c}$ and $V_{c-c}$ are all attractive interaction potentials.)

[1]Note that bilayers in our model are considered to be flat. An interpretation of ripple structures has recently been given in terms of a mesoscopic phenomenological model for lipid bilayers (Hansen, Miao and Ipsen [98]).

## 5.2 *Lipid-Sterol Mixture Systems*

In this section, we extend the model of Eq. (2.10) to the series of lipid-sterol systems discussed in Section 2.4. In order to make contact with experimental results, we focus on lipid-cholesterol and lipid-lanosterol bilayer systems. In particular we choose values of the parameters for the model in such a way that the calculated phase diagrams for both systems will have the same characteristics as the experimental ones. At this point, it should be noted that the parameter values chosen as characteristic for a particular lipid-sterol system are not unique. In fact, the same generic phase behaviour can be found for a range of different parameter values. The parameter values used in this section differ from the values used in Section 5.1 above for lipid-cholesterol mixtures (Nielsen et al. [98]). The reason is as follows: experimental observations suggest that the main transition in DPPC lipid bilayers lies close to a critical point (Morrow, Whitehead and Lu [92]). The parameters used in the present section therefore lead to a main transition temperature of the pure lipid system which is close to that of the Ising critical point. This change in parameter values as compared to Section 5.1 does however not change the generic phase behaviour of the model.

The results of the present section are expressed in terms of thermodynamic phase diagrams and thermodynamic observables in the same way as for the analysis of the lipid-cholesterol system presented in Section 5.1. The thermodynamic control parameters are again the temperature $T$, and either the global sterol concentration, $x_{\text{sterol}}$, or $\mu_\Delta$, the effective chemical potential controlling the equilibrium sterol concentration. The other parameters are kept fixed at specific values in all the simulations. For convenience, the length scale is set at the hard-disk diameter, $d$, and the unit of energy is defined to be $J_0$[1]. Thus, the surface pressure, $\Pi$, is fixed at $\Pi d^2/J_0 = 3.0$. The excitation energy of the disordered state of lipid chains is chosen as $E_{\text{d}} = 2.78 J_0$, and the degeneracy, $D_{\text{d}}$, of the disordered state, is taken to be $\ln D_{\text{d}} = 12.78$. The radius of the short range square well potential of Eq. (2.13) is given by $R_0/d = 1.3$. The values of $\Pi$ and $R_0$, are chosen so that change in surface area across the main-transition is comparable to that of the single component DPPC bilayer system (G. Cevc [93]).

[1] In order to convert the energy and length scales into units relevant for lipid bilayer systems, $J_0$ should be of the order $10^{-20} J$ and $d$ of the order 5 Å.

$E_d$ and $\ln D_d$ have the same values as for the 10th state of the Pink Model (Pink, Green and Chapman [80]) and are determined such that the latent heat of the main-transition is comparable to that of the single component DPPC bilayer system. The interaction potential is defined in terms of $V^l$ (the longer range square well potential of Eq. (2.14)) and $V^s$ (the short range square well potential of Eq. (2.13)). The parameters defining the interaction potentials are summarized in Table 5.1.

| | | $V_{o-o}$ | $V_{o-d}$ | $V_{d-d}$ | $V_{c-c}$ | $V_{c-d}$ |
|---|---|---|---|---|---|---|
| (a) | l | 0.40 $J_0$ | -0.15 $J_0$ | 0.20 $J_0$ | 0.20 $J_0$ | 0.00 $J_0$ |
| | s | 0.45 $J_0$ | 0.40 $J_0$ | -0.20 $J_0$ | -0.15 $J_0$ | -0.065 $J_0$ |

| | | Cholesterol | Intermediate | Lanosterol |
|---|---|---|---|---|
| (b) | $V^l_{o-\alpha}$ | 0.85 $J_0$ | 0.825 $J_0$ | 0.75 $J_0$ |
| | $V^s_{o-\alpha}$ | -0.625 $J_0$ | -0.60 $J_0$ | -0.525 $J_0$ |

Table 5.1: Interaction parameters for the model potential of the three lipid-sterol systems in units of $J_0$. (a) The parameter values for the interaction potential,$V_{o-o}$, between two lipid chains in the ordered state, the interaction potential, $V_{o-d}$, between a lipid chain in the ordered state and a lipid chain in the disordered state, the interaction potential, $V_{d-d}$, between two lipid chains in the disordered state, the interaction potential, $V_{c-c}$, between two cholesterol molecules, and the interaction potential, $V_{c-d}$, between a lipid in the disordered state and a cholesterol molecule. Note that these values are identical for all three lipid-sterol systems. (b) The parameter values for the interaction potential,$V_{o-\alpha}$, between a lipid chain in the ordered state and the three different sterol molecules, $\alpha$ being either *chol*, *int* or *lan*, respectively.

In the following, we refer to the three systems treated in this section as being specific to lipid systems containing cholesterol, intermediate sterol and lanosterol, where the intermediate sterol is a sterol on the evolutionary pathway between lanosterol and cholesterol. We are aware that the molecular description in the model is highly approximate and that the model cannot therefore describe the molecular difference between the three specific sterols in any detail. However, based on the phase behaviour of the model system as obtained by numerical simulations, we find that the results for the three specific sets of parameters corresponding to cholesterol, intermediate sterol and lanosterol do indeed give a reasonable description of the differences between the three lipid-sterol systems when compared to experimentally obtained phase diagrams. We will therefore in this section refer to the three lipid-sterol mixtures specifically as

lipid-cholesterol, lipid-intermediate sterol, and lipid-lanosterol mixtures.

The value for $V^{s}_{o-o}/V^{l}_{o-o}$ was again determined so that the phase transition of the pure lipid system is located in the regime where the translational and the internal degrees of freedom are coupled (see discussion in Section 2.3). For the lipid-cholesterol system, the values for $V^{s,l}_{\alpha-c}$ ($\alpha = o, l, c$) were determined so that the phase behaviour of the equilibrium lipid-cholesterol system resembles that of the DPPC-cholesterol bilayer. For the lipid-lanosterol system, the values for $V^{s,l}_{o-lan}$ were chosen so that the difference in lipid chain order parameter at high sterol concentration between the lipid-cholesterol and the lipid-lanosterol system is comparable to the experimentally observed difference in the PPetPC-cholesterol and the PPetPC-lanosterol systems (see Fig. 2.3). Finally, the values for $V^{s,l}_{o-int}$ in the lipid-intermediate sterol system are chosen so that the rigidifying effect on the lipid chains due to the three sterols follows the relation *cholesterol* > *intermediate* ≫ *lanosterol.*

### 5.2.1 *Phase Diagrams; Simulations within the Semi-Grand Canonical Ensemble*

The series of simulations reported here were performed within the semi-grand canonical ensemble similar to those described in Section 5.1.

In Fig. 5.11, we show the phase diagrams for the three different sterol systems based on the simulation results. The diagrams on the left in Fig. 5.11 give the results in terms of the two control parameters $x_{sterol}$ (where $x_{sterol} = x_{chol}$, $x_{int}$ or $x_{lan}$), the concentration of sterol, and the reduced temperature $T/T_{\rm M}$, where $T_{\rm M}$ is the main transition temperature for the pure lipid system. The diagrams to the right in Fig. 5.11 show the same results in terms of the difference in chemical potential, $\mu_{\Delta}$, between the lipid chains and the sterol molecules, and $T/T_{\rm M}$. From the figure, it is clear that small modifications in the strength of the interaction potential between the lipid chains in the ordered state and the sterol molecules lead to a series of phase diagrams which exhibit considerable topological differences.

For the phase diagrams in Fig. 5.11(a), the strength of the interaction between cholesterol and a lipid chain in the ordered state is comparable to the interaction strength between two lipid chains both in the gel state. The phase diagrams are

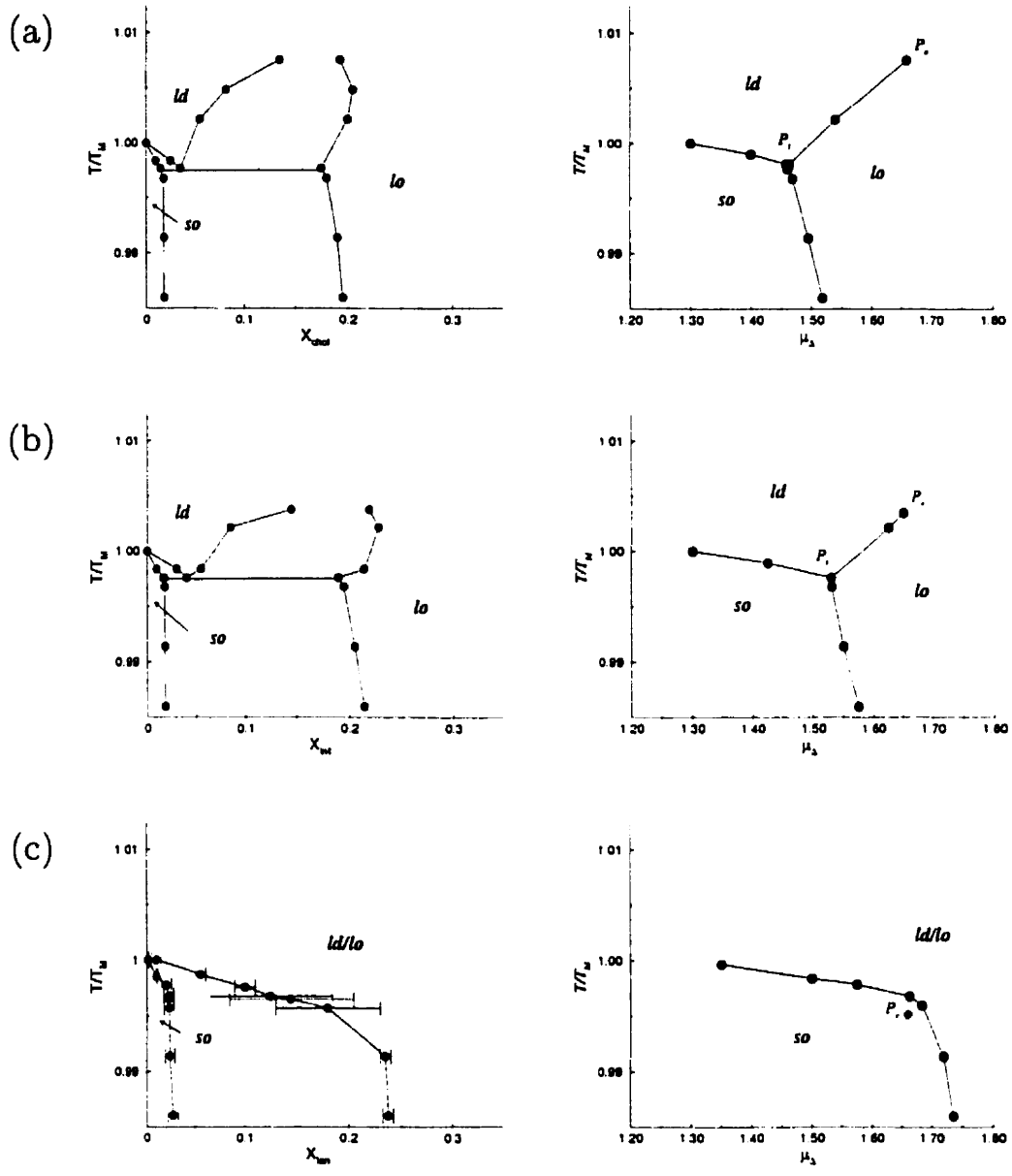


Figure 5.11: Phase diagrams for the lipid-sterol mixture model for three different sterols. (a) lipid-cholesterol mixture, (b) lipid-intermediate sterol mixture, (c) lipid-lanosterol mixture. The left part of the figure gives the phase diagrams as a function of sterol concentration $x_{sterol}$ and reduced temperature $T/T_M$. The right part of the figure gives the phase diagrams as a function of $\mu_\Delta$ and $T/T_M$. The different phases labeled in the phase diagrams are the **so**, solid ordered (gel), **ld**, liquid disordered (fluid), and **lo**, liquid ordered phases, respectively, where the first letter refers to the lateral order of the phase and the second letter refers to the conformational order of the phase. The points $P_c$ and $P_t$ are the critical point of the **ld-lo** coexistence region and the triple point, respectively, and the point $P_c$ in the right part of (c) is the critical point of the metastable **ld-lo** coexistence region described in the text. The error bars given in the left phase diagram in (c) are due to finite size effects as described in the text.

similar to those calculated for the model proposed earlier for the lipid-cholesterol system (Nielsen et al. [98]) (see Section 5.1) and they again show the characteristics of a macroscopic uncoupling of the translational (lateral) and the chain conformational (internal) degrees of freedom due to the inclusion of cholesterol. The strength of the interaction between a lipid chain in the ordered state and a cholesterol molecule is capable of stabilizing the **lo** phase up to high temperatures and the phase diagram is characterized by a substantial miscibility gab between the **lo** phase and the **ld** phase in the region above the three-phase line. The **ld-lo** coexistence region is found to terminate in a critical point, $P_c$, at $T = 1.0075T_{\mathrm{M}}$, $\mu_\Delta = 1.659$. The point of three-phase coexistence, $P_t$, is located close to $T = 0.9977T_{\mathrm{M}}$, $\mu_\Delta = 1.460$ and the concentration of cholesterol in the three coexisting phases is $x_{chol,\mathbf{so}} = 0.015$, $x_{chol,\mathbf{ld}} = 0.035$, and $x_{chol,\mathbf{lo}} = 0.175$, respectively.

For lipid-intermediate sterol systems, the lipid-sterol interaction was taken to be weaker than for the lipid-cholesterol systems and the critical point, $P_c$, of the **ld-lo** coexistence region is found to shift to lower temperatures and slightly higher sterol concentrations as compared to the lipid-cholesterol system. Figure 5.11(b) shows a miscibility gab between the **ld** and the **lo** phases above the three-phase line. The critical point, $P_c$, is located close to $T = 1.0035T_{\mathrm{M}}$, $\mu_\Delta = 1.651$ and the three-phase line, $P_t$, in found to be located close to $T = 0.9976T_{\mathrm{M}}$, $\mu_\Delta = 1.527$ with corresponding sterol concentrations in the coexisting phases being $x_{int,\mathbf{so}} = 0.017$, $x_{int,\mathbf{ld}} = 0.040$, and $x_{int,\mathbf{lo}} = 0.190$, respectively. The **ld-lo** coexistence region is thus reduced substantially as compared to the phase diagram in Fig. 5.11(a), whereas the change in the temperature of three-phase coexistence only displays a minor shift.

Finally, for Fig. 5.11(c) the strength of the interaction between the ordered lipid chains and the sterol molecules is made too weak to stabilize the **lo** phase at high temperatures and the phase diagram shows the absence of a miscibility gab between the **lo** and the **ld** phases. The phase diagram for this sterol system hence has no three-phase line. The critical point, $P_c$, terminating the **ld-lo** coexistence region is located below the solid-liquid phase line at $T = 0.9952T_{\mathrm{M}}$, $\mu_\Delta = 1.66$. The **ld-lo** coexistence region is found to be metastable and thus we cannot define two distinct fluid phases for this system.

The results displayed in Fig. 5.11 were obtained from a detailed finite-size analysis. In Fig. 5.12-5.13, we give several results from this analysis. The procedure employed in the finite-size scaling analysis for the model is similar to that described in Section 5.1 (Nielsen et al. [98]).

The graphs in Figure 5.12 show the finite size scaling plot of $\beta\mathcal{F}_L(x_{chol})$ for the lipid-cholesterol (left side) and $\beta\mathcal{F}_L(x_{int})$ for the lipid-intermediate sterol (right side) systems for different temperatures. Figure 5.12(a) and (b) indicate the existence of a first order transition for both the lipid-cholesterol and the lipid-intermediate sterol system at the two temperatures (Lee and Kosterlitz [91]). The magnitude of the free energy barrier between the coexisting phases can be obtained from the curves in the figure. For example, for a system of size $L = 20$, $\Delta\mathcal{F}_L(x_{chol})_{\mathbf{ld-lo}} \simeq 3.5k_BT$ and $\Delta\mathcal{F}_L(x_{chol})_{\mathbf{so-lo}} \simeq 4.0k_BT$ for the lipid-cholesterol system. Figure 5.12(c) gives the spectral free energy $\beta\mathcal{F}_L(x_{chol})$ and $\beta\mathcal{F}_L(x_{int})$ calculated for different system sizes, $L$, at a temperature close to the critical point of the **ld-lo** coexistence region. The figure demonstrates that the "interfacial energy" at this temperature for large system sizes approaches a constant value. This indicates that the critical point, $P_c$, of the **ld-lo** coexistence region is located close to $T = 1.0075T_M$, $\mu_\Delta = 1.659$ for the lipid-cholesterol system and close to $T = 1.0035T_M$, $\mu_\Delta = 1.651$ for the lipid-intermediate sterol system. The critical point of the **ld-lo** coexistence region is thus shifted for the intermediate sterol system to a lower temperature as compared to the lipid-cholesterol system.

Figure 5.13 gives examples of the finite-size scaling analysis for the lipid-lanosterol system. In Fig. 5.13(a), the plot of the "interfacial" energy indicates the existence of a first order transition between the **so** and the **lo** phases. In Fig. 5.13(b), we show the finite-size dependence of $\beta\mathcal{F}_L(\varepsilon)$ at a temperature of $T = 0.9952T_M$. The figure shows that the interfacial energy at this temperature approaches a constant value for large system sizes, thus indicating the existence of a **ld-lo** coexistence region terminating in a critical point close to $T = 0.9952T_M$, $\mu_\Delta = 1.660$. The plot in Fig. 5.13(c), on the other hand, suggests that the **ld-lo** coexistence region is only metastable with respect to the **so** phase. In this figure, we plot the finite-size dependence of $\beta\mathcal{F}_L(\varepsilon)$ for $T = 0.9952T_M$ and $\mu_\Delta = 1.660$ calculated for a series of relatively small system sizes. The

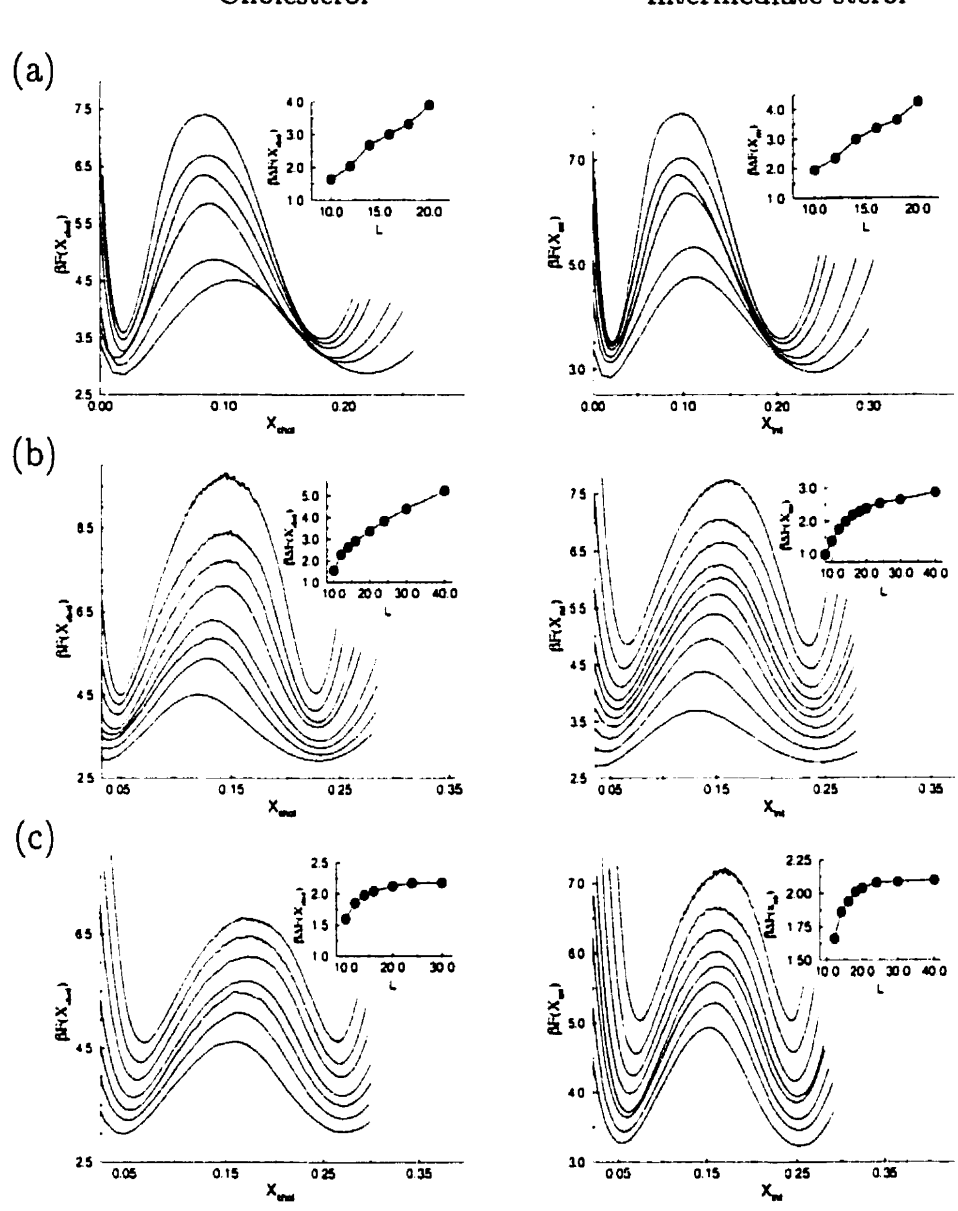


Figure 5.12: Finite size scaling plot of $\beta\mathcal{F}_L(x_{chol})$ and $\beta\mathcal{F}_L(x_{int})$ for the lipid-cholesterol (left side) and the lipid-intermediate sterol (right side) systems. (a) Lipid-cholesterol system at $T = 0.9968T_M$, lipid-intermediate sterol system at $T = 0.9860T_M$ (**so-lo** coexistence region). System sizes are $L$ = 10, 12, 14, 16, 18 and 20. (b) Lipid-cholesterol system at $T = 1.0035T_M$, Lipid-intermediate sterol system at $1.0022T_M$ (**ld-lo** coexistence region). System sizes are $L = 8$ (for the intermediate sterol), 10, 12, 14, 16, 20, 24, 30 and 40. (c) Lipid-cholesterol system at $T = 1.0075T_M$ (close to the point of the **ld-lo** coexistence region). The system sizes are $L$ = 10, 12, 14, 16, 20, 24 and 30. Lipid-intermediate sterol system at $T = 1.0035T_M$ (close to the critical point of the **ld-lo** coexistence region). The system sizes are $L$ = 12, 14, 16, 18, 20, 24, 30 and 40. In the insert to the figures is shown the interfacial free energy $\Delta\beta\mathcal{F}_L(x_{chol})$ and $\Delta\beta\mathcal{F}_L(x_{int})$ as a function of system size. The line connecting the points is a guide to the eye.

spectral free energy functions shown in Fig. 5.13(c) were calculated at $T = 0.9952T_{\mathrm{M}}$ for values of $\mu_{\Delta}$ close to the melting curve and reweighted to the specific value of $\mu_{\Delta} = 1.66$ by use of the Ferrenberg-Swendsen reweighting technique (Ferrenberg and Swendsen [88]). As the figure shows, the free energy of the **so** phase is lower than that of the two liquid phases, suggesting that the **ld-lo** coexisting region is only metastable with respect to the **so** phase. Due to the difficulties associated with simulations of solid-liquid phase transitions for large system sizes described in Section 3.1.5, we have not been able to perform a finite-size analysis of the solid-liquid phase transition up to sufficiently large system sizes in order to conclude rigorously whether the results given above represent the thermodynamic limit of the system. The limited finite-size analysis nevertheless suggests that the **ld-lo** coexisting region remains metastable with respect to the **so** phase as the system size is increased. The lipid-lanosterol system thus has no region of **ld-lo** phase coexistence and the stable phases in the lipid-lanosterol bilayer systems are those of the solid ordered **so** phase and the liquid (**ld/lo**) phase. In the phase diagram of Fig. 5.11(c), the metastable **ld-lo** coexistence region is indicated as a metastable phase coexistence line terminating at $P_c$ below the **so**-(**lo/ld**) transition line.

The presence of the metastable **ld-lo** coexistence region in the vicinity of the solid-liquid melting transition curve gives rise to large error bars in the estimated values for the concentration of lanosterol in the liquid phase for temperatures close to $P_c$. In the vicinity of $P_c$, the spectral free energy of a finite system indicates the presence of three distinct phases (see Fig. 5.13(c)). Only in the thermodynamic limit does the barrier between the **ld** and the **lo** phases vanish and the spectral free energy will then have a shape corresponding to two coexisting phases. For finite systems, we cannot obtain accurate estimates of the lanosterol concentration in the liquid phase based on the loci of the minima in the spectral free energy, $\beta\mathcal{F}_L(x_{lan})$ when the metastable **ld-lo** coexistence region lies close to the solid-liquid melting curve. In the phase diagram of Fig.5.11(c), the error bars on the lanosterol concentration in the liquid phase for temperatures close to $T = 0.9952T_{\mathrm{M}}$ are thus determined from the relative position of the metastable fluid minimum as compared to the position of the stable fluid minimum in the spectral free energy function $\beta\mathcal{F}_L(x_{lan})$ at the specific values

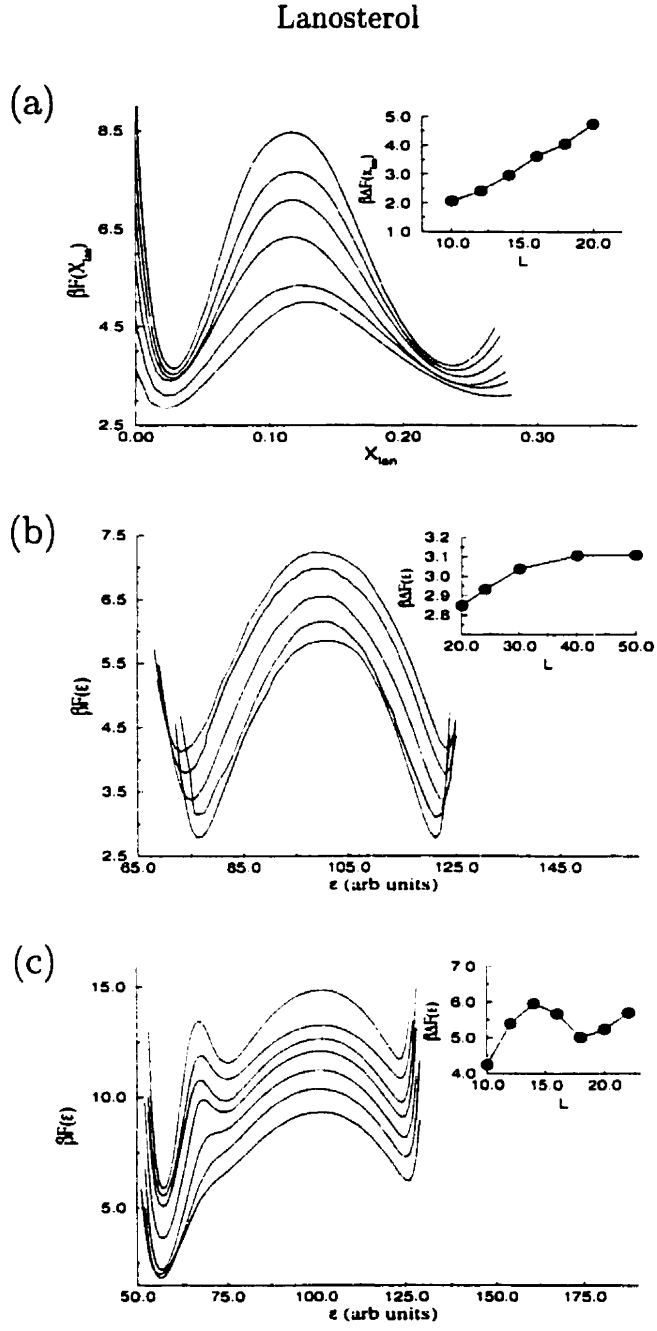


Figure 5.13: Finite size scaling plot of $\beta\mathcal{F}_L(x_{lan})$ and $\beta\mathcal{F}_L(\varepsilon)$ for the lipid-lanosterol system. (a) Finite size scaling plot of $\beta\mathcal{F}_L(x_{lan})$ for $T = 0.9860T_{\rm M}$ (**so-lo** coexistence region). System sizes are $L$ =10, 12, 14, 16, 18 and 20. (b) Finite size scaling plot of $\beta\mathcal{F}_L(\varepsilon)$ for $T = 0.9952T_{\rm M}$. System sizes are $L$ = 20, 30, 40 and 50. For clarity the curves have been shifted down along the $y$-axis so that the largest $L$ is the lowest curve. (c) Finite size scaling plot of $\beta\mathcal{F}_L(\varepsilon)$ for $T = 0.9952T_{\rm M}$ and $\mu_\Delta = 1.66$. The system sizes are $L$ = 10, 12, 14, 16, 18, 20 and 22. In the insert to the figures is shown the interfacial free energy $\Delta\beta\mathcal{F}_L(x_{lan})$ or $\Delta\beta\mathcal{F}_L(\varepsilon)$ as a function of system size. The lines connecting the points are guides to the eye.

of $T$ and $\mu_\Delta$. A detailed finite size analysis up to much larger system sizes in order to estimate the lanosterol concentration in the liquid phase in the thermodynamic limit would clearly give more accurate results. Such an analysis is however very time consuming and beyond the scope of the present work and the above estimate is sufficient for our purpose.

The phase diagram in Fig. 5.11(a) for the lipid-cholesterol system has a topology similar to the experimentally obtained phase diagram for the DPPC cholesterol bilayer system. This close resemblance between the theoretical and the experimental phase diagram again suggests that the microscopic model proposed for the lipid-cholesterol system does indeed provide a correct picture of the effective mechanism of cholesterol in lipid bilayers. We discussed in Section 5.1 how the minimal model for the lipid-cholesterol system provides new insights into how the dual mechanism of cholesterol as being both a crystal breaker and a lipid chain rigidifier is manifested in the phase behaviour of the lipid-cholesterol mixture system. The reader is referred to Section 5.1 for details.

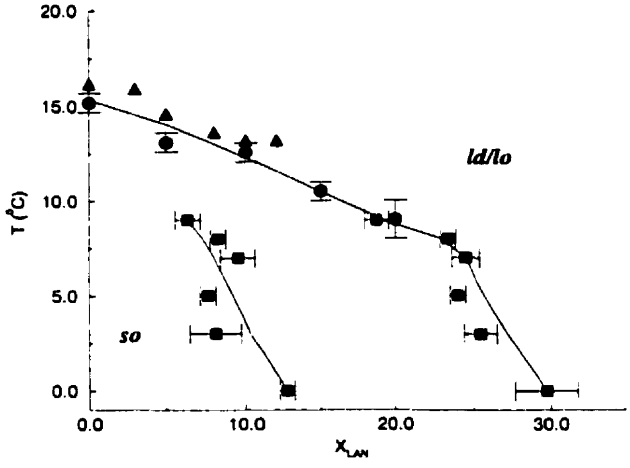


Figure 5.14: Phase diagram for the PPetPC-lanosterol system as obtained form NMR and DCS studies. Filled $\Delta$ are determined from DCS data. $\bullet$ are from NMR data such as the data shown in Fig. 5.15, and filled $\square$ are from $^2$H NMR difference spectroscopy. The lines connecting the points are guides to the eye. Adapted from J. Thewalt [96].

Based on NMR and calorimetry studies, J. Thewalt ([96]) obtained a phase diagram for the PPetPC-lanosterol bilayer system (see Fig. 5.14). PPetPC is a lipid molecule similar to POPC. PPetPC has a double bond at the 6-7 carbon position of the petroselinic acyl chain (Bloom, Evans and Mouritsen [91]). The detailed phase behaviour of the PPetPC-cholesterol system is thus different from that of the DPPC-cholesterol system; however, the generic phase behaviour for the two systems is found

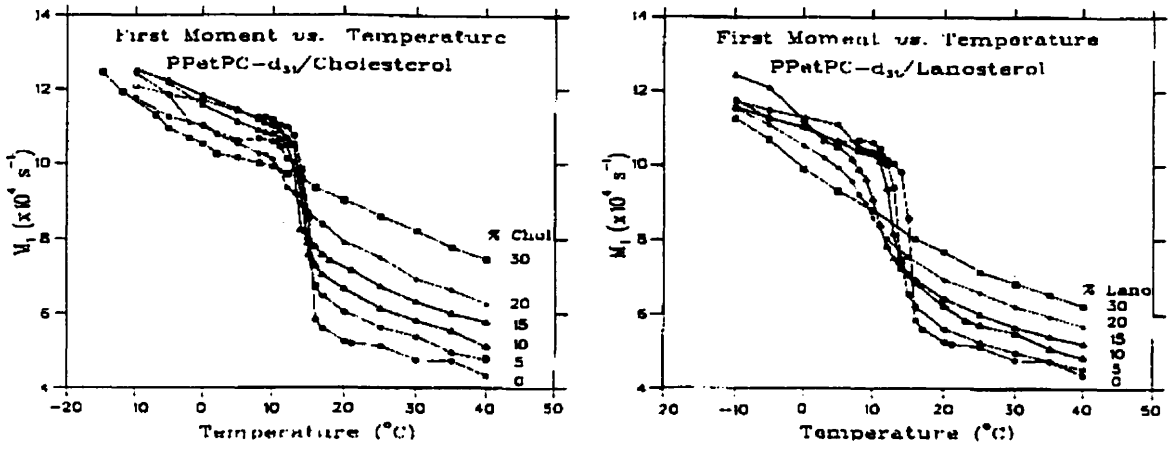


Figure 5.15: The average chain orientational order parameter $\langle |S_{CD}| \rangle$ as a function of temperature for several PPetPC-cholesterol (left) and PPetPC-lanosterol (right) mixtures . A rough estimate of the solid-liquid phase transition can be found as the temperature where the slope of the order parameter curve has its maximum. The constant transition temperature, determined in this manner, for the PPetPC-cholesterol system for concentrations of cholesterol up to 15 % is taken as evidence for the existence of a three-phase line. The constant decrease in transition temperature observed for the PPetPC-lanosterol system as the lanosterol concentration is increased, is, on the other hand, taken as evidence for the absence of a three-phase line. Adapted from J. Thewalt [96].

to be very similar (Thewalt [96]; Bloom and Mouritsen [95]). In the NMR, study one cannot distinguish between the **ld** and the **lo** phases, and the experimental results thus cannot rigorously determine if the PPetPC-lanosterol phase diagram does contain a **ld-lo** coexistence region. The data for the chain order parameter nevertheless suggest that the PPetPC-lanosterol phase diagram has no three-phase line and it does thus not have a **ld-lo** coexistence region (see Fig. 5.15).

The experimental phase diagram of J. Thewalt ([96]) for the PPetPC-lanosterol bilayer system exhibits a topology similar to that of the lipid-lanosterol model system shown in Fig. 5.11(c). This suggests that the model proposed for the lipid-lanosterol system also captures some of the important mechanisms underlying the effects of lanosterol in lipid bilayers and that the differences between cholesterol and lanosterol as proposed in the variation of the model parameters defining the two model systems do indeed picture some of the important differences between the two lipid-sterol systems.

The sole difference between the cholesterol and the lanosterol model molecules within the model picture studied here lies in the strength of the interaction potential between the sterol molecules and lipid chains in the ordered state. The difference

in the interaction strength shown in Fig. 5.11(a) and 5.11(c) is about 11 %, and the difference between the lanosterol and cholesterol model molecules is thus relatively small. This difference is nevertheless the only reason for the topological difference between the phase diagrams of Fig. 5.11(a) and 5.11(c) and the sole reason for the substantial difference between the two lipid-sterol systems.

### 5.2.2 Simulations within the Canonical Ensemble

We have also performed simulations within the canonical ensemble as described in Section 4.1.1. In these simulations, we calculated the structure factors as defined by Eq. (5.1) and the order parameter for the lipid chains defined as;

$$M = \frac{1}{2}(\langle \frac{\sum_i \mathcal{L}_{io} - \mathcal{L}_{id}}{\sum_i \mathcal{L}_{io} + \mathcal{L}_{id}} \rangle + 1) \ , \tag{5.2}$$

where $\mathcal{L}_{io}$ and $\mathcal{L}_{id}$ are the occupation variables for the lipid chains defined in Eq. (2.12) and $\langle \cdots \rangle$ denotes a thermal average. This order parameter is close to unity in the low temperature **so** phase and zero in the high temperature **ld** phase. The thermal average of the structure factors was taken over $5 \cdot 10^4$ different microconfigurations with a time interval of 100 MCS between two consecutive configurations. In the calculation of the thermal average of the order parameter, the system was equilibrated during 200.000 MCS at each value of the temperature and sterol concentration before the thermal average was calculated over a period of 500.000 MCS.

In Fig. 5.16(a), we show the average lipid chain order parameter, $M$, as a function of sterol concentration for the three different sterol systems for $T = 1.0129 T_{\mathrm{M}}$. This temperature is above the critical point of the **ld-lo** coexistence region of the lipid-cholesterol system and all three lipid-sterol systems are in a single phase at this temperature for all sterol concentrations investigated. Figure 5.16(b) shows the average lipid chain order parameter, $M$, for the three different lipid-sterol systems as a function of temperature for $x_{sterol} = 0.225$. This concentration is beyond the **so-lo** and **ld-lo** coexistence regions of both the lipid-cholesterol and lipid-intermediate sterol phase diagrams, and the three systems are in a single phase at this sterol concentration for all the temperatures investigated. Both Figure 5.16(a) and (b) demonstrate the rigidifying effect on the lipid chains of all three sterols. Figure 5.16(a) shows that

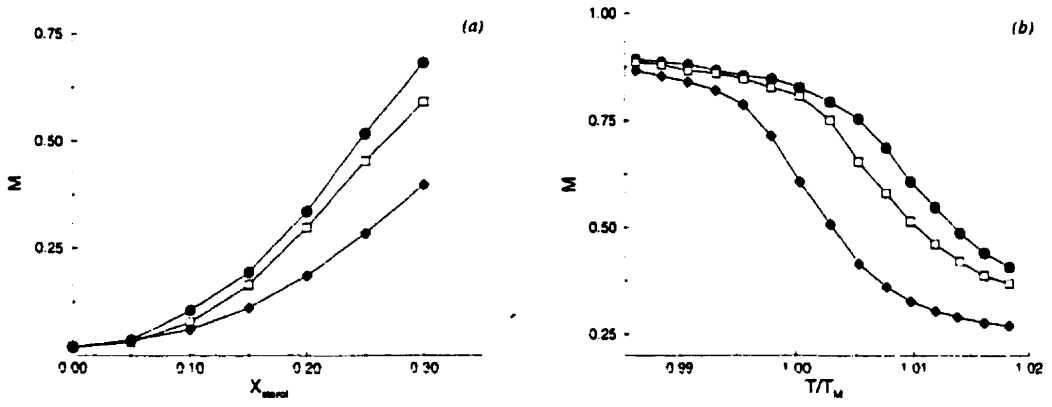


Figure 5.16: Lipid chain order parameter for the three lipid-sterol systems for a system size of $N = 1600$. (•) cholesterol, (□) intermediate sterol and (full ∘) lanosterol. (a) The lipid chain order parameter as a function of sterol concentration calculated using Eq. (5.2) for $T = 1.0129T_{\mathrm{M}}$. (b) The lipid chain order parameter as a function of temperature for $x_{sterol} = 0.225$.

cholesterol at a $x_{chol} = 0.30$ is able to rigidify close to 70 % of the lipid chains, whereas lanosterol at this concentration can rigidify only 40 %. A direct comparison between the experimental data for the chain order parameter (Fig. 2.3) and the simulation results (Fig. 5.16(a)) shows that the difference in chain rigidifying effect between the two model lipid-sterol systems is similar to that of the cholesterol and lanosterol experimental systems. For the experimental systems, we find that cholesterol at a molar concentration of 30 % enhances the chain order parameter by 0.12 units as compared to the pure lipid system. Lanosterol at the same molar concentration enhances the chain order parameter by only 0.07 units. From the simulation results shown in Fig. 5.16(a) we find that cholesterol at a concentration of $x_c = 0.20$ (this concentration corresponds to a molar concentration of $x_c^m = 0.33$) enhances the chain order parameter by 0.325 units as compared to the pure system, whereas lanosterol enhances the chain order parameter by only 0.185 units. If we take the ratio between the two experimental and theoretical values, respectively, we obtain in both cases a value close to 0.57.

Fig. 5.16(b) gives a comparison of the effect on the lipid chains for the three different sterols as a function of temperature at fixed sterol concentration. At low temperatures, all curves tend to the same value of $M$ and the figure shows that the lipid chains in the three lipid-sterol systems are equally ordered at low temperatures.

However, at temperatures above the main transition of the pure lipid system, $T_M$, the three sterols have very different effects on the lipid chains. Cholesterol is capable of maintaining most of the lipid chains in the ordered state up to a temperature of $T = 1.0129T_M$, whereas most of the lipid chains are in the disordered state at this temperature in the lipid-lanosterol system. Since the average lipid chain order parameter in the fluid phase of the lipid membrane is an indirect measure of the mechanical stability of the membrane, the curves in Fig. 5.16 give evidence for the high mechanical stabilizing effect of cholesterol as compared to lanosterol.

Figure 5.17 gives examples of the structure factors characterizing the lateral structure of the high sterol concentration liquid phase of the three sterol systems. The figure shows the partial sterol structure factor $S_{sterol}(|q|)$ of Eq. (5.1) calculated at $T = 1.0022T_M$ and $T = 0.9860T_M$ for $x_{sterol} = 0.225$. At those temperatures and this sterol concentration, the lipid-cholesterol and lipid-intermediate sterol are both in the **lo** phase, which is characterized by a high degree of conformational order in the lipid chains and a high lateral disorder, whereas the lipid-lanosterol system is in the **ld/lo** liquid phase. The figure shows the characteristics of a liquid phase for all three systems. The graphs of $S_{sterol}(|q|)$ for the cholesterol and the intermediate sterol systems show a diffuse ring located close to $0.40 \cdot 2\pi/d$, as was the case for the lipid-cholesterol system investigated in Section 5.1. The origin of this ring is due to the one-dimensional thread-like microdomains formed by the two types of sterols in the lipid bilayer as described in Section 5.1. The graph of $S_{sterol}(|q|)$ for the lanosterol system shows the absence of the diffuse ring at $|q| \simeq 0.40 \cdot 2\pi/d$. In the lipid-lanosterol system, the interaction between the ordered chains and the lanosterol molecules is thus too weak to stabilize the one-dimensional lanosterol microstructures. A comparison between the snapshots given in the lower part of Fig. 5.17, demonstrates the weaker rigidifying effect on the lipid chains of lanosterol as compared to cholesterol. The snapshots show characteristic microconfigurations of the three lipid-sterol systems at $T = 1.0022T_M$ and $x_{sterol} = 0.225$. The plots give evidence for the strong ability of cholesterol and the much weaker ability of lanosterol to rigidify the lipid chains at temperatures above the main transition, $T_M$.

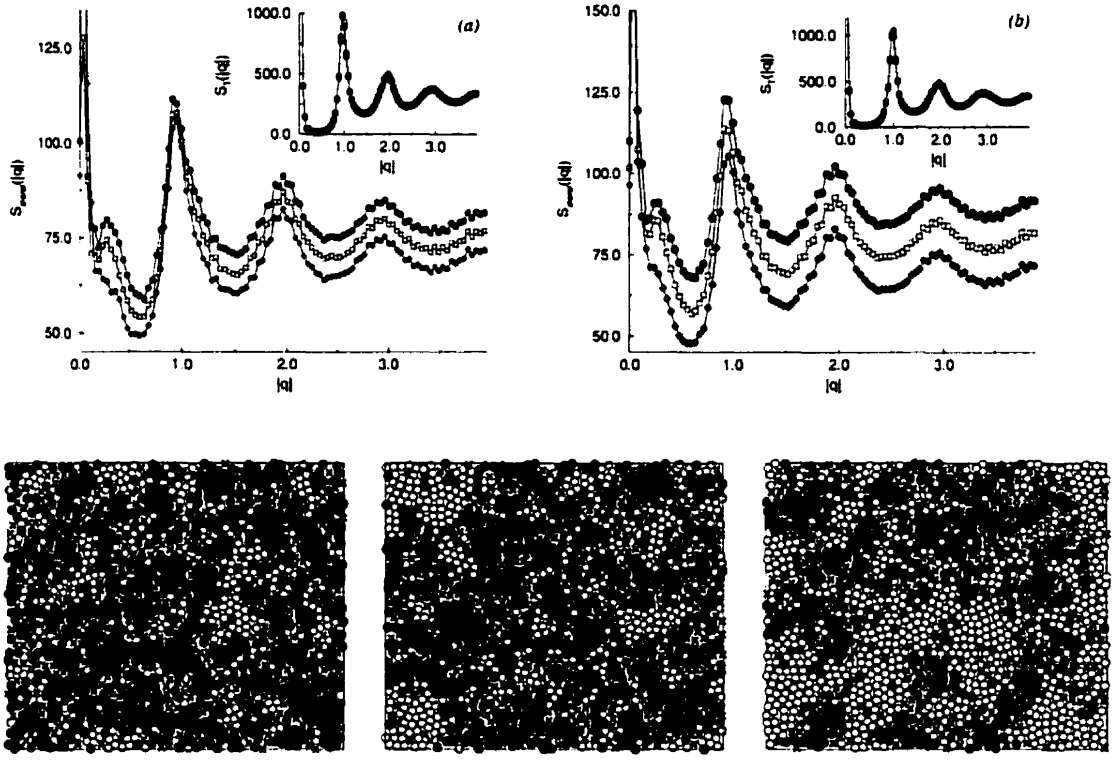


Figure 5.17: The partial sterol structure factor $S_{sterol}(|q|)$ calculated at (a) $T = 1.0022T_{\mathrm{M}}$, $x_{sterol} = 0.225$, (b) $T = 0.9806T_{\mathrm{M}}$, $x_{sterol} = 0.225$ for three sterol systems. $S_{chol}(|q|)$ is shown as (•), $S_{int}(|q|)$ is shown as (□) and $S_{lan}(|q|)$ is shown as (solid ⋄). For clarity the curves for $S_{chol}(|q|)$ and $S_{int}(|q|)$ have been shifted along the $y$-axis. The $|q|$-values are given in units of $2\pi/d$. The insert to the figures shows the total structure factor $S_T(|q|)$ for the three sterol systems. In the three lower figures are shown snapshots of microconfigurations for lipid systems containing cholesterol (left), intermediate sterol (middle) and lanosterol (right) systems calculated at $T = 1.0022T_{\mathrm{M}}$ and $x_{sterol} = 0.225$. In the snapshots, a lipid chain in the ordered state is shown as (•), a lipid chain in the disordered state as (○) and a sterol molecule as (×).

### 5.2.3 *Discussion*

In this section, we investigated a microscopic model describing the phase behaviour of lipid-sterol mixtures. The investigation focused on the application of the model specifically to lipid-cholesterol and lipid-lanosterol mixtures. The effect of the sterol molecules in the lipid bilayer is hypothesized to be a dual mechanism, in that a sterol molecule is both a "crystal breaker" and a "lipid chain rigidifier". The details of the model and the results as applied to lipid-cholesterol mixtures were described in Section 5.1 (Nielsen et al. [98]). In the model, the effective differences between cholesterol and lanosterol are described in a minimal manner by a difference in both the

ability of the sterol molecules to rigidify the lipid chains and in the ability to disrupt the crystalline order. We have calculated phase diagrams and thermal averages of quantities characterizing the different thermodynamic phases for three lipid-sterol systems designed to be specific to the lipid-cholesterol, lipid-intermediate sterol and lipid-lanosterol systems. The phase diagrams of the first and last system display the same topology as the experimentally obtained phase diagrams (Vist and Davis [90]; Thewalt [96]). The theoretical phase diagram for the lipid-cholesterol system shows the presence of a distinct **ld-lo** coexistence region thus demonstrating the ability of cholesterol to uncouple the ordering processes of the chain conformational and the translational degrees of freedom. For the lipid-lanosterol system, on the other hand, the theoretical phase diagram shows the absence of such **ld-lo** coexistence region and we hence predict that lanosterol does not uncouple the transitions associated with the two sets of degrees of freedom. We find for the lipid-lanosterol system that the **ld-lo** coexistence region is metastable with respect to the **so** phase and that the critical point of the **ld-lo** coexistence region is located below the solid-liquid melting curve.

The structural analysis of the **lo** phase for the lipid-cholesterol and the lipid-intermediate sterol systems showed the presence of a diffuse scattering ring at $|q| \simeq 0.4 \cdot 2\pi/d$ in the partial structure factor related to the sterol molecules. The origin of this diffuse ring is the "thread-like" microstructures discussed in Section 5.1 (Nielsen et al. [98]). The structural analysis of the **ld/lo** phase in the lipid-lanosterol system, on the other hand, showed the absence of such a diffuse ring and we conclude that the interaction strength between the ordered lipid chains and the lanosterol molecules is too weak to stabilize the formation of one-dimensional thread-like microdomains in the lipid-lanosterol bilayers.

With regard to the metastability of the **ld-lo** phase coexistence predicted here for lipid-lanosterol bilayers, Wolde and Frenkel ([98]) and Hagen and Frenkel ([94]) reported results on a series of colloidal particle systems exhibiting a generic phase behaviour similar to the series of phase diagrams for the lipid-sterol systems investigated in the present thesis. Hagen and Frenkel showed that the phase behaviour of the hard-core attractive Yukawa system depends strongly on the range of Yukawa interaction (Hagen and Frenkel [94]). They found that the liquid-vapor coexistence

region in the hard-core Yukawa system is only exists for systems where the interaction range of the Yukawa potential is larger than a certain value. For values of the interaction range larger than this specific value, all three phases (solid, liquid and vapor) are present in the calculated phase diagram. As the range of the interaction potential is decreased, the critical point of the liquid-vapor coexistence region is shifted towards the three-phase line, and at a specific value of the interaction range the critical point of the liquid-vapor coexistence region is found to be located at the solid-liquid melting curve. For an interaction range below this specific value, only two stable phases (a solid and a liquid/vapor phase) are present in the system and the liquid-vapor coexistence region lies as a metastable phase coexistence region below the melting curve. Close to the critical point of the liquid-vapor coexistence region, large density fluctuations are present in the system. In the case where the critical point is located in the vicinity of the melting curve, Wolde and Frenkel argue that one should expect large density fluctuations in the solid-liquid phase transition due to the coupling between the critical liquid-vapor transition and the first order solid-liquid transition (Wolde and Frenkel [98]).

The work of Wolde and Frenkel focused on the 'enhancement on protein crystal nucleation by critical density fluctuation" in the context of a phase behaviour of the above kind. They conclude their work by noting that

> ... the phase diagram shown (a phase diagram with a metastable liquid-vapor coexistence region) is likely to be the rule rather than the exception for compact macromolecules. Moreover, it occurs both in the bulk and in (quasi) two-dimensional systems (e.g. in membranes). It is therefore tempting to speculate that nature already makes extensive use of "piggy-back riding" on critical fluctuations to facilitate the formation of ordered structures (Wolde and Frenkel [98]).

In the context of the function of cholesterol in biological membranes, it is tempting to extend the above argument and speculate that Nature has tended to optimize the lipid-sterol interaction strength along the biosynthetic pathway of the different sterols so that the critical point of the **ld-lo** coexistence region is shifted as far away from the solid-liquid melting line as possible. By the synthesis of cholesterol, Nature would

thus have arrived at a sterol with optimal lipid-sterol interactions, resulting in the ability of the sterol to stabilize optimally the **lo** phase and the mechanical properties of the lipid membrane. This point was first made by Bloom and Mouritsen ([88]).

# 6

# MEMBRANE LYSIS

In this chapter, we present the results of the analysis of Model V, which is a model for the stability of lipid membranes in the presence of single or multiple holes. The work presented is based on preliminary results and the presentation has character of a discussion rather than a detailed analysis as was the case in the previous chapters. In this work, we mainly concentrate on the single hole model of Shillcock and Boal ([96]). The results are organized in three parts. First, we give the results for the single hole membrane model with only translational degrees of freedom and compare the results to those obtained by Shillcock and Boal ([96]). Next, we present the results for the stability of single hole membranes described by both translational and conformational degrees of freedom. Finally, we consider the multiple hole model of Shillcock and Seifert ([98]) and discuss whether the effect of multiple holes is greatly overestimated in the work of Shillcock and Seifert. We then present a new phase diagram for the multiple hole membrane model based on numerical simulations.

## *6.1 Thermal Stability of Membranes in Zero Stress*

Here we give the results of Monte Carlo simulations of the single hole model for the thermal stability of membranes at zero stress. Figures 6.1-6.2 show the results of the analysis. The simulations were performed for a system of size $N = 400$ at zero stress ($\sigma = 0$). In this case, the stability of the membrane is controlled by a single parameter, the reduced edge tension, $\lambda^* = \beta\lambda d$. In each simulation, the system was prepared in a triangular lattice configuration, which was equilibrated at a high temperature during 100.000 MCS. After the equilibration, a hole was made in the membrane by removing a randomly chosen tether. The high temperature configuration served as the initial state for the simulations at a given value of $\lambda^*$. In the simulations, the first 100.000

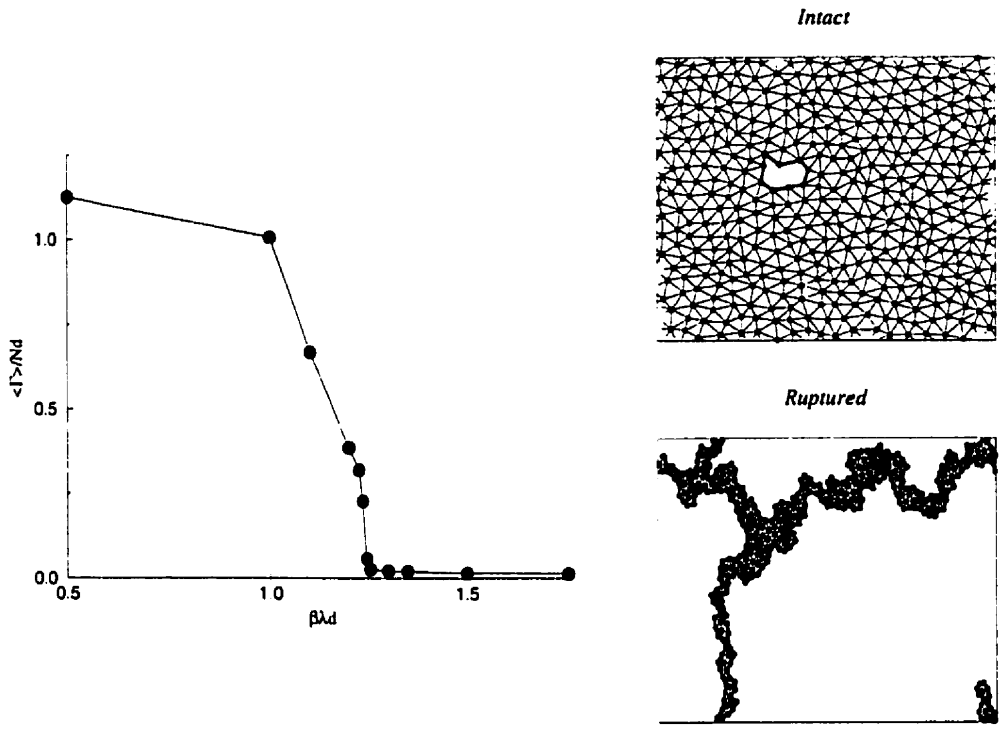


Figure 6.1: The reduced hole perimeter length, $\Gamma/Nd$, as a function of the reduced edge tension, $\lambda^*$, for a system size of $N = 400$. To the right are shown two typical snapshots of microconfigurations for the intact membrane, $\lambda^* = 1.275$, and the ruptured membrane, $\lambda^* = 1.235$, respectively. In the snapshots, the edge of the hole is shown as a thick solid line. The snapshots are not shown to scale.

MCS were discarded before the measurement of various thermodynamic quantities was performed over $1\text{-}10 \cdot 10^6$ MCS. From the simulation results, we calculated the average total area of the bulk membrane and hole, $\langle A \rangle$, the average length of the hole perimeter, $\langle \Gamma \rangle$, and the area compression modulus, $K_A$. The later was calculated from the fluctuation-dissipation theorem as

$$\beta K_A = \frac{\langle A \rangle}{\langle A \rangle^2 - \langle A^2 \rangle} \ . \tag{6.1}$$

Figure 6.1 shows the reduced hole perimeter length, $\Gamma/Nd$, as a function of the reduced edge tension, $\lambda^*$. The figure shows a sharp change in the value of $\Gamma/Nd$ close to $\lambda^* = 1.24$. For values of $\lambda^* > 1.25$ only a small hole is present in the membrane, whereas large holes are present for $\lambda^* < 1.23$. The formation of a large hole in the membrane allows for large area fluctuations in the membrane/hole system. The signal of such large fluctuations is seen in the area compression modulus, $K_A$.

Fig. 6.2(a) gives $\beta K_A d^2$ as a function of the reduced edge tension, $\lambda^*$. For $\lambda^* < 1.23$, the compression modulus is close to zero, whereas it is close to the pure fluid modulus, $\beta K_A d^2 = 18$ (Boal [93]) for $\lambda^* > 1.35$. In Fig. 6.2(b) is shown the area of the bulk membrane and hole, $A$, and the hole perimeter length, $\Gamma$, as a function of Monte Carlo time for $\lambda^* = 1.275$. The graph demonstrates the presence of large fluctuations in $A$ for this value of $\lambda^*$ due to the growth and shrinkage of the hole. For the single hole model at zero stress, we thus reproduce the results of Shillcock and Boal ([96]).

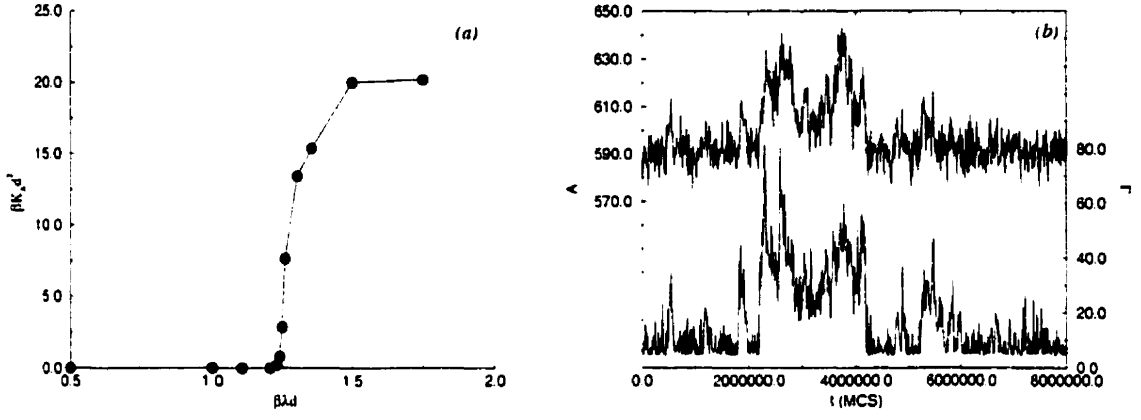


Figure 6.2: (a) The area compression modulus, $\beta K_A d^2$, as a function of reduced edge tension, $\lambda^*$, for a system of $N = 400$. (b) The system area (bulk and hole), $A$, (the upper curve) and the hole perimeter length, $\Gamma$, (the lower curve) as a function of Monte Carlo time for $\lambda^* = 1.275$.

## 6.2 Thermal Stability of Decorated Membranes in the Presence of Holes

We now present the results of the simulations of Model V, which is a model for the thermal stability of membranes decorated with conformational degrees of freedom. The parameters used in the following for the conformational degrees of freedom are those of the lipid-sterol mixture systems described in Section 5.2. The simulations were performed as described in the previous section for a system of size $N = 400$ at zero stress ($\sigma = 0$). In the simulations, we calculate thermal averages of the quantities described in the previous section as well as an effective line tension, $\lambda_{eff}$, associated

with the growth (shrinkage) of the hole defined as

$$\lambda_{eff} = \lambda \mp \left\langle \frac{V(R_l)}{\Delta d} \right\rangle \quad , \tag{6.2}$$

where $\lambda$ is the bare line tension of Eq. (2.15). $R_l$ is the length of the tether $l$ to be removed in the process of growth (shrinkage), $V(R_l)$ is the interaction potential between the particles connected by $l$, and $\Delta d$ is the change in hole perimeter in the growth (shrinkage) process. $\lambda_{eff}$ is a measure for the effective line tension associated with the growth and shrinkage of holes in a membrane which is decorated with internal degrees of freedom.

One should note at this point that the results reported below are calculated for $\sigma = 0$. It is hence not possible to compare directly the results for the intact membrane given here with the results reported in Section 5.2, since the results for the lipid-sterol membrane systems reported in Section 5.2 were obtained for membranes under a lateral pressure of $\beta\sigma d^2 = 3.0$.

Fig. 6.3 shows $\beta\lambda_{eff}d$, $\Gamma$ and $\beta K d^2$ as a function of sterol concentration, $x_{chol}$ and $x_{lan}$, for mixtures of lipid-cholesterol and lipid-lanosterol, respectively. The temperature, $T$, was set to $T = 0.9160T_{\mathrm{M}}$ in all the simulations, where $T_{\mathrm{M}}$ is the main transition temperature of the pure lipid system defined in Section 5.2. At this temperature the pure lipid membrane at zero stress is found to be in the **ld** phase. The value of $\lambda^*$ was set at 0.9, such that the pure lipid membrane system is unstable against rupture. For lipid-cholesterol mixtures, Fig. 6.3(a) shows that $\beta\lambda_{eff}d$ becomes larger than 1.24 for $x_{chol} \geq 0.2$. At high concentrations, cholesterol thus induces an increase in $\beta\lambda_{eff}d$ such that the formation of large holes in the membrane is prevented. Cholesterol is therefore seen to inhibit membrane rupture. For the lipid-lanosterol system, on the other hand, Fig. 6.3(a) shows that $\beta\lambda_{eff}d$ remains below 1.24 for values of $x_{lan}$ up to 0.25 and lanosterol is thus unable to inhibit membrane rupture even at high concentrations. Fig. 6.3(c) gives the reduced area compression modulus, $\beta K d^2$, as a function of sterol concentration for the two lipid-sterol systems. The figure shows that $\beta K d^2$ for the lipid-cholesterol system is close to the pure fluid modulus for high concentrations of cholesterol, again demonstrating the high stabilizing effect of cholesterol. For the lipid-lanosterol system, on the other hand, $\beta K d^2$ is close to zero up to $x_{lan} = 0.25$, showing the weak stabilizing effect of lanosterol.

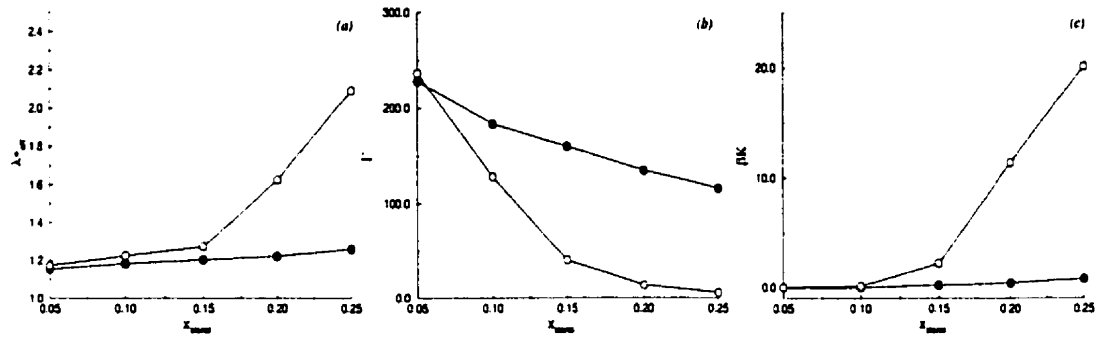

Figure 6.3: (a) The effective line tension, $\lambda^*_{eff} = \beta\lambda_{eff}d$, (b) the average hole perimeter, $\Gamma$, and (c) the area compression modulus, $\beta K d^2$, as function of sterol concentration for lipid-cholesterol (o) and lipid-lanosterol (•) mixtures. The system size is $N = 400$ and the temperature is $T = 0.9160T_M$.

Fig. 6.4 gives snapshots of microconfigurations for a series of sterol concentrations for lipid-cholesterol and lipid-lanosterol systems. The figure shows the strong stabilizing effect of cholesterol on the lipid membrane as compared to lanosterol. At low concentrations, both lipid-sterol mixtures are unstable against the formation of large holes and the membranes shown in the corresponding snapshots are ruptured. High concentrations of cholesterol inhibit the formation of large holes and the microconfiguration shows the presence of a small hole. For high concentrations of lanosterol, however, the snapshot shows the presence of a large hole, again implying that lanosterol is unable to inhibit membrane lysis even at high concentrations.

## 6.3 Discussion

In this chapter, we presented the preliminary results of an analysis of a model for membrane lysis. We compared the results obtained with those of Shillcock and Boal ([96]) in the case of zero lateral stress and found that we reproduce their results. The stability of the membrane is controlled by the reduced line tension, $\lambda^* = \beta\lambda d$. We find that for $\lambda^* > 1.25$ the membrane stays intact and only a small hole is present in the system. For $\lambda^* < 1.23$, however, a large hole is present and the membrane is thus ruptured. The value of $\lambda^*$ separating the intact membrane from the ruptured one is estimated to be close to 1.24.

By decorating the membrane with a set of conformational degrees of freedom defined by Model IV (see Section 5.2), we were able to analyze the mechanical stabilizing

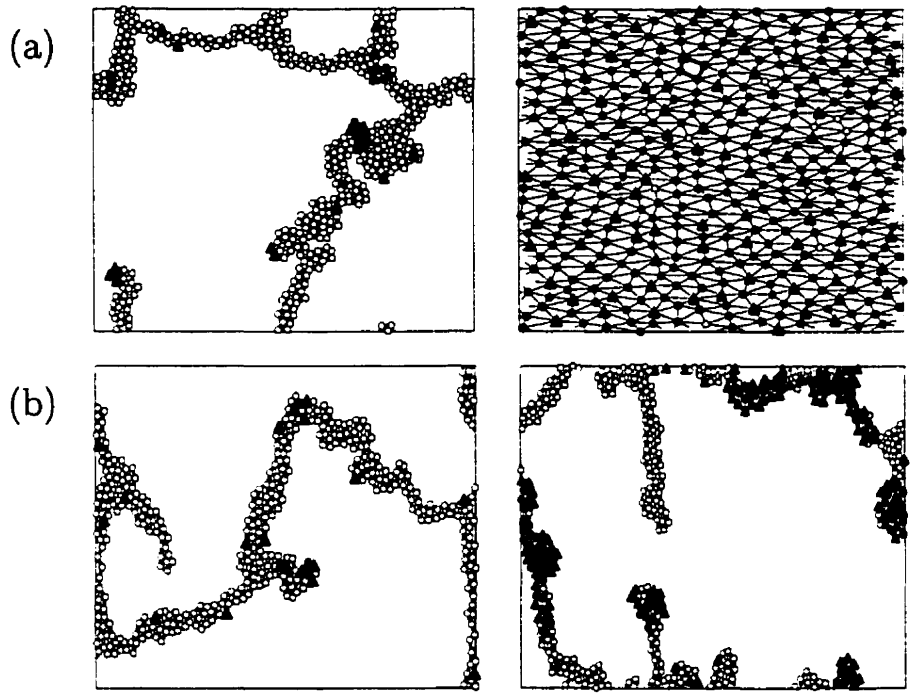


Figure 6.4: Snapshots of characteristic microconfigurations for (a) lipid-cholesterol mixtures, (b) lipid-lanosterol mixtures, at sterol concentrations of 0.05 (left) and 0.25 (right), respectively. $T = 0.9160T_M$. In the snapshots, lipid chains in the ordered state are shown as (•), lipid chains in the disordered state as (○) and cholesterol molecules are shown as (solid △). The snapshots are not shown to scale.

effect of different sterols on the membrane. We found that cholesterol has a significantly higher stabilizing effect on the lipid membrane as compared to lanosterol. In the simulations, we analyzed the stability of lipid membranes containing several concentrations of either cholesterol or lanosterol. A concentration of 20 % cholesterol was found to inhibit the formation of large holes in the membrane, hence stabilizing the membrane against rupture. For the lipid-lanosterol system, however, the membrane was shown to be unstable against rupture even at high concentrations of lanosterol, implying that lanosterol is unable to inhibit rupture.

The mechanical stability of lipid vesicles can be modified by the absorption of peptides such as melittin (Benachir et al. [97]). Furthermore, the lysis associated with the absorption of melittin can be viewed as a result of the reduction of the effective line tension induced by melittin. When the melittin content in the membrane exceeds a certain lower value, the effective line tension becomes too small to stabilize the

membrane against lysis. It is found that the lytic power of melittin in POPC vesicles is inhibited by the presence of high concentrations of cholesterol (Benachir et al. [97]). This "healing" effect of cholesterol on the lipid membrane can be viewed as the result of an enhancement of the effective membrane line tension due to the inclusion of cholesterol as demonstrated in our theoretical study. It would clearly be very interesting to analyze the results of an experimental investigation of melittin-induced lysis of lipid vesicles containing lanosterol. Such an investigation could demonstrate whether lanosterol indeed has a significantly weaker "healing" effect on the lipid membrane than that of cholesterol, as predicted by our study. However, such results are not, to our knowledge, available at present.

Now we turn to the multiple hole model for the thermal stability of membranes by J. Shillcock and U. Seifert ([98]). We have performed a limited simulation study of this model and our results are quite different from those reported by Shillcock and Seifert. The multiple hole model of Shillcock and Seifert employs a chemical potential, $\mu$, to control the number of holes present in the membrane. The chemical potential is related to the kinetic barrier against hole formation, $Q$, as $Q = \lambda L_{min} - \mu$ (see Section 2.5.1). Here, $\lambda$ is the line tension and $L_{min}$ is the perimeter length of the new hole. The number of holes present in the membrane can vary in two distinct ways. Holes can be created and resealed in single-hole processes, and holes can coalesce and fragment in two-hole processes. In order for the equilibrium state of the system to be well defined, the chemical potential must be correctly included in both of these processes. In our analysis of the multiple hole model, we find that the results of Shillcock and Seifert can only be reproduced if the chemical potential is not included in the two-hole processes of coalescence and fragmentation (Shillcock [98]). We believe, however, that the chemical potential should be included in both the single-hole and the two-hole processes and a simple example can demonstrate why. If the intact membrane without holes is taken to be the reference state, then we could arrive at a final state with a single large hole present in at least two distinct ways. First, we could create a single hole and let it grow to its final size. The energy of the final state would then be $E_F^1 = \lambda L - \mu$, where $L$ is the perimeter length of the final hole. Second, we could create a series of $N$ holes and subsequently coalesce these

holes into the large final hole. If the chemical potential is not included in the two-hole processes of coalescence and fragmentation, the energy of the final state would be $E_F^2 = \lambda L - N\mu$. This is clearly different from $E_F^1$ and the energy would, in this case, be a path dependent variable, which is clearly incorrect. Only if the chemical potential is included in the two-hole processes would the energy of the final state be path independent and the thermodynamical state of the system well defined.

It turns out that the way in which the chemical potential is implemented in the model of Shillcock and Seifert has very important consequences for the phase behaviour. In Fig. 6.5, we give the phase diagram as obtained from simulations of a small system with $N = 256$. Also shown is the phase diagram as obtained from simulations in the case where the chemical potential is only involved in the single-hole processes. The figure shows that the specific implementation of the chemical potential can change the phase behaviour substantially for small values of $q^*$ $(= \beta Q)$. This limit corresponds to large values of $\mu$ and to situations in which many holes are present in the system.

In our calculations, we find that the presence of multiple holes have a minor effect on the stability of the membrane against rupture. This is in contrast to the results of Shillcock and Seifert ([98]). Using the chemical potential in both the single-hole and the two-hole processes, we find that the scenario for membrane rupture for all values of $q^*$ is that of the formation and growth of a single hole. The stability of the multiple hole membrane is thus essentially identical to that of the single hole membrane.

The snapshots shown to the right in Fig. 6.5 demonstrate the presence of multiple holes in the membrane for small values of $q^*$. The phase behaviour, as described by the phase diagram, however, indicates that the holes only interact weakly. The reason for this weak interaction is the chemical potential. Situations in which many holes are present in the membrane correspond to large values of $\mu$. In the process of coalescence, the length of the hole perimeter remains essentially constant. The energy cost associated with the coalescence is hence $\mu$. In cases where many holes are present in the membrane and the process of coalescence thus could be important, the value of $\mu$ is large and the energy cost associated with the coalescence process is hence so high that the process only rarely occurs. This presents a difficulty in the model of

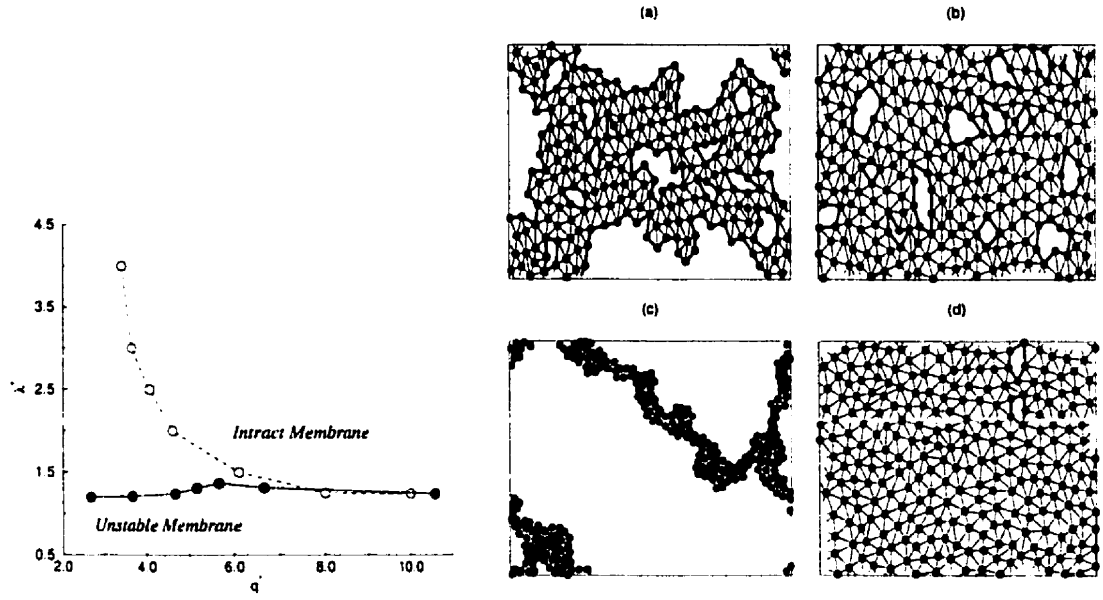


Figure 6.5: Phase diagram for the fluid membrane in terms of the reduced line tension, $\lambda^*$, and reduced barrier height, $q^*$. (•) are the results from the simulation study using the chemical potential in both the single-hole and the two-hole processes. (o) are the results from simulations using the chemical potential only in the single-hole processes. The lines connecting the points are guides to the eye. The snapshots to the right show characteristic microconfigurations at different values of $q^*$ and $\lambda^*$ from the simulation study using the chemical potential in both the single-hole and the two-hole processes. (a) $\lambda^* = 1.2$, $q^* = 3.4$, (b) $\lambda^* = 1.3$, $q^* = 3.9$, (c) $\lambda^* = 1.3$, $q^* = 7.4$, and (d) $\lambda^* = 1.4$, $q^* = 7.7$. The snapshots are not shown to scale.

Shillcock and Seifert, since the stability of the membrane should indeed depend on the presence of multiple holes.

The difficulty in the model of Shillcock and Seifert lies in the use of a chemical potential to induce variations in the barrier against hole formation. We here suggest a model which should give a correct description of the stability of lipid membranes in the presence of multiple holes and which should not suffer from the difficulties associated with the use of a chemical potential. The formulation of the model is inspired by the function of melittin absorbed by lipid membranes. In the model, a change in the barrier against hole formation is induced by the inclusion of melittin-like impurities which have a lower line tension than that of the lipid chains. We associate a line tension with all tethers in the system. The line tension along tethers connected to an impurity is then a certain fraction of the line tension along tethers connecting two lipid chains. The impurities act as nucleation sites for holes. At low impurity concentrations, only few holes will be present in the membrane and the model should

essentially be identical to the single hole model of Shillcock and Boal ([96]). At high impurity concentrations, however, multiple holes should be present. These holes interact strongly through the two-hole processes of coalescence and fragmentation, since basically no energy cost is associated with these processes. We hence expect that the presence of multiple holes should have an important effect on the phase behaviour of the membrane for this model.

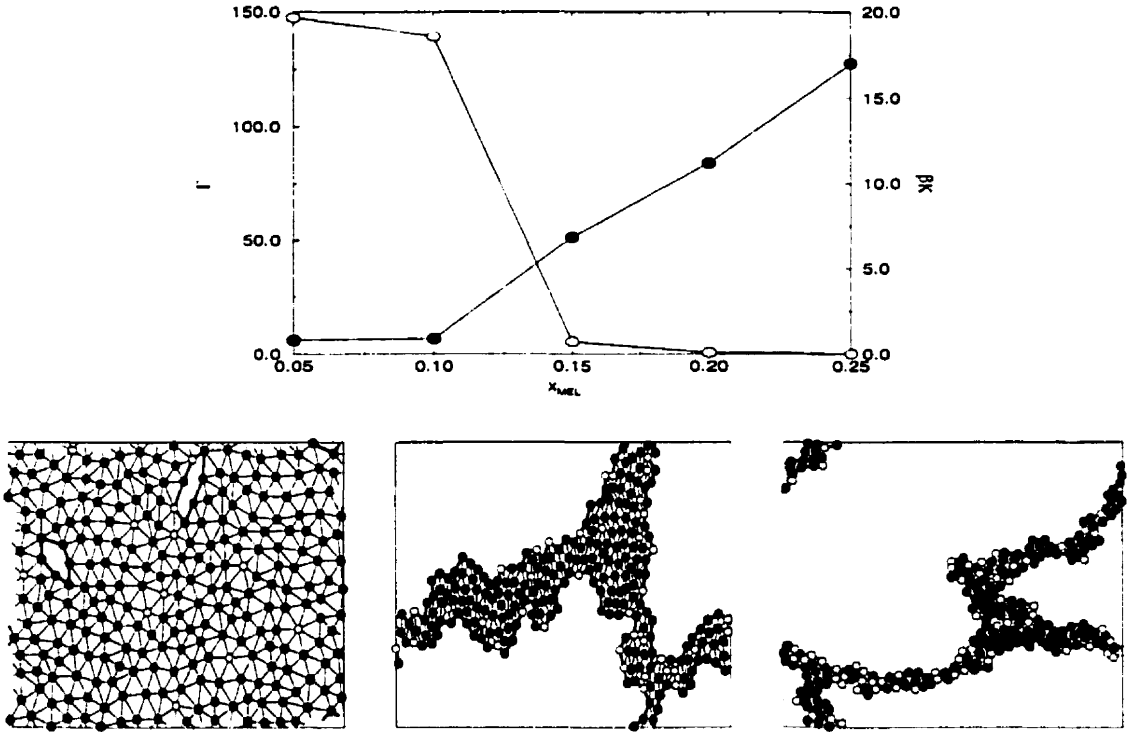


Figure 6.6: The total hole perimeter for all holes, $\Gamma$ (•) and the area compression modulus, $\beta K d^2$ (○), as a function of impurity concentration, $x_{mel}$, for a system of size $N = 256$. The lipid-lipid line tension is $\lambda^* = 1.5$ and the impurity-lipid and impurity-impurity line tension is $0.75 \cdot \lambda^*$. In the lower part of the figure are shown snapshots of characteristic microconfigurations for different concentrations of impurities. $x_{mel} = 0.05$ (left), $x_{mel} = 0.15$ (middle) and $x_{mel} = 0.25$ (right). In the snapshots, lipid chains are shown as (•) and impurities as (○), respectively. The snapshots are not given to scale.

Preliminary simulations show that this is indeed the case. At low impurity concentrations, isolated holes are formed in the membrane at the sites of the impurities. The hole size is found to change rapidly for values of $\lambda^*$ close to 1.24, as was the case for the single-hole model of Shillcock and Boal ([96]). At high concentrations, however, the impurity sites are not isolated and the holes formed at the impurity sites

interact strongly. Fig. 6.6 shows the results obtained from a simulation at $\lambda^* = 1.5$. At this value of $\lambda^*$, the membrane is shown to become unstable against formation of large holes as the concentration of impurities is increased. As is seen from the snapshots of microconfigurations given in Fig. 6.6, the impurities tend to accumulate close to or on the edge of the hole. The results from our preliminary work on the multiple hole model for membrane lysis is hence very promising, and we believe that further investigations which will include a minimal model for the conformational degrees of freedom should allow us to understand better how melittin induces lysis in lipid membranes containing sterols.

# 7

# General Conclusions

In the present thesis, we have investigated a series of microscopic models for two dimensional complex fluid systems. We have developed a random lattice algorithm which provides an effective representation of the translational degrees of freedom of the complex fluids. The main concern of this work has been the investigation of complex systems in which the phase behaviour is determined by an interplay between the translational and conformational degrees of freedom of the fluid systems.

We have investigated a series of five microscopic models. All models are minimal in that they only contain an approximate description of the conformational degrees of freedom of the related model particles and in that the interparticle interaction potentials are designed to contain only features that are necessary for describing systems where the interplay between the two sets of degrees of freedom can manifest itself in the macroscopic phase behaviour. The conformational degrees of freedom are in all models essentially treated as Ising spin variables. Different degrees of complexity in the description of the microscopic coupling between the translational and conformational degrees of freedom, allowed us to study a variety of models related to pure lipid membrane and lipid-sterol membrane systems.

The phase equilibria described by the models, specifically phase diagrams and equilibrium thermal averages of specific quantities, such as structure factors, internal energy, surface area and order parameter characterizing the different phases, were calculated using several Monte Carlo simulation techniques, including histogram- and thermodynamic reweighting techniques, finite-size scaling as well as non-Boltzmann sampling techniques.

The different models were shown to exhibit a rich phase behaviour. Depending on the specific model parameters, the phase transition associated with the conformational

degrees of freedom was found be either coupled to, or uncoupled from, the phase transition associated with the translational degrees of freedom.

The first model investigated was an Ising model defined on a two dimensional fluid surface. The simulation study of this model displayed no macroscopic manifestation of a coupling between the spin and the translational degrees of freedom. For the second model, an Ising model in which the spin degrees of freedom are more strongly coupled to the translational degrees of freedom, the phase transitions in the two sets of degrees of freedom were shown to be macroscopically coupled for certain values of the model parameters. For parameter values for which the two transitions are coupled, the Ising spin transition was shown to be of first order and slaved by the first order lattice melting transition associated with the translational degrees of freedom. In situations where the Ising transition is uncoupled from the transition in the translational degrees of freedom both Ising models were shown to display a critical behaviour identical to that of the regular-lattice Ising model universality class.

For the Model III, a minimal model for the phase behaviour of lipid bilayers, we calculated a phase diagram in terms of temperature and a parameter, $V_0/J_0$, which measures the strength of the coupling between the two sets of degrees of freedom. The point of key importance in the phase diagram is the appearance of two distinct regimes, separated by a triple point, of different types of macroscopic interplay between the two sets of degrees of freedom. A regime of macroscopic coupling between the two sets of degrees of freedom, as observed in most systems of pure lipid bilayers, exists for values of $V_0/J_0$ greater than the triple-point value. However, a regime of macroscopic decoupling also exists as part of the generic thermodynamic behaviour of the model, for values of $V_0/J_0$ smaller than the triple-point value, where two distinct ordering transitions take place successively, separated by an intermediate phase characterized by the translational order of the liquid crystalline (**ld**) phase and the conformational order of the gel (**so**) phase of pure lipid bilayer systems.

Our study of the model for lipid bilayers containing sterols (Model IV) led to a series of phase diagrams expressed in terms of sterol concentration and temperature. We focused on the application of the model to the specific systems of lipid-cholesterol and lipid-lanosterol mixtures. The calculated phase diagrams were shown to have the

same topology as the experimentally obtained phase diagrams. The phase diagram calculated for the lipid-cholesterol displayed the presence of a **ld-lo** coexistence region, thus demonstrating the ability of cholesterol to uncouple the phase transitions associated with the translational and conformational degrees of freedom, respectively. The phase diagram for the lipid-lanosterol, however, showed the absence of a **ld-lo** coexistence region. For the lipid-lanosterol system, our theoretical study thus predicts that lanosterol does not uncouple the phase transitions associated with the two sets of degrees of freedom. We view the metastability of the **ld-lo** coexistence region predicted for the lipid-lanosterol system as a support of the hypothesis on membrane evolution of M. Bloom and O.G. Mouritsen ([88]). Specifically, we suggest that Nature in the process of evolution has tended to optimize the lipid-sterol interaction so as to stabilize optimally the **lo** phase and the mechanical properties of the lipid membrane.

In the analysis of the lipid-sterol systems, we also obtained detailed information on the lateral structure of the various phases. Here, the study of the sterol-rich phase was of particular interest, since this phase for the lipid-cholesterol systems has been the subject of a long and continuing debate in the literature due to its relevance for biological membrane systems. The structure analysis showed that the sterol-rich phase is indeed a liquid phase. More interestingly, for the lipid-cholesterol system, the partial structure factors associated with the cholesterol molecules showed a diffuse ring corresponding to a structure characterized by a length scale of roughly twice the average interparticle distance. We argue that the origin of the diffuse ring is the formation of "thread-like" microdomains in the lipid-cholesterol system. The formation of such microdomains is stabilized by the strong interaction between ordered lipid chains and cholesterol and by the weak interaction between two cholesterol molecules. The structure analysis of the lipid-lanosterol system showed the absence of this diffuse ring, and we thus predict that lanosterol has too weak an interaction with the lipid chains to stabilize the formation of "thread-like" microdomains.

For the model for membrane lysis which includes sterols (Model V), we find that cholesterol has a significantly higher stabilizing effect on the lipid membrane as compared to lanosterol. We find that the inclusion of 20 % cholesterol in the lipid mem-

brane inhibits the formation of large holes and cholesterol is thus found to stabilize the membrane against lysis. Lanosterol, on the contrary, is found to have a weak stabilizing effect on the membrane and inclusion of lanosterol was found to be unable to stabilize the membrane against lysis.

The use of Monte Carlo simulations to calculate the equilibrium phase behaviour of the various models proposed in this thesis turned out to be difficult in situations where simulations up to large system sizes were needed in order to determine the finite size scaling behaviour. This was in particular the case for the model proposed for lipid-sterol mixtures. For this model, our simulation study could not determine rigorously the equilibrium phase diagram for the lipid-lanosterol system due to strong finite-size effects. To circumvent the difficulties associated with finite size effects, we could apply the methods of thermodynamic integration (Frenkel and Smit [97]) combined with the Gibbs-Duhem integration method due to D. Kofke ([93]) to calculate the phase boundaries in the lipid-lanosterol phase diagram. Such an analysis would be highly interesting since it could conclusively determine if the topology of the lipid-lanosterol phase diagram is indeed different from the generic lipid-cholesterol phase diagram, as predicted in this thesis.

We end this thesis with some final remarks on the further applications of the random-lattice simulation approach in general and the models proposed for lipid bilayer systems in particular. The random-lattice algorithm developed in this thesis has proved very powerful in the investigation of dense liquid systems and the minimal model approach put forward in the thesis can readily be applied to a large series of problems related to lipid membrane systems where the interplay between translational and conformational degrees of freedom plays an important role for the phase behaviour. The list of such problems is large: lipid mixtures, lipid mixtures containing sterols and membrane protein systems are just a few. The phase behaviour of all these systems is to some degree controlled by constraints on the packing of the different conformational states of the molecular species and an understanding of the thermodynamic behaviour thus requires a detailed description of the interplay between the translational and conformational degrees of freedom.

Finally, the random lattice algorithm can in a straightforward manner be extended

to include the third spatial dimension and thus extended to give a realistic description of the curved two-dimensional surface of a lipid membrane. This extension should allow for a whole new class of problems to be addressed where the phase behaviour is determined by an interplay between the out-of-plane curvature and the in-plane translational and conformational degrees of freedom.

# APPENDICES

## A.1 The Datastructure of the Random Lattice Algorithm

The central datastructures in the random lattice algorithm are the vertex (hard disk) positions and a "link" structure defining the connectivity of the random lattice.

The vertices are labled $V_i$, $i = 1, \ldots, N$ and the real space positions of a vertex are stored as a matrix $X(i,j)$, for $i = 1, \ldots, N$ and $j = 1, 2$. The number of tethers (or links) in the random lattice is a fixed quantity and the tethers are labeled as $L_i$, $i = 1, \ldots, 3N$ (the number of tethers in the random lattice is 3 times the number of vertices).

The connectivity of the triangulated random lattice is organized as a series of ordered linked lists, each defining the tethers forming a triangle in the random lattice. We associate two numbers $\pm i$ to each tether $L_i$. The triangles in the random lattice

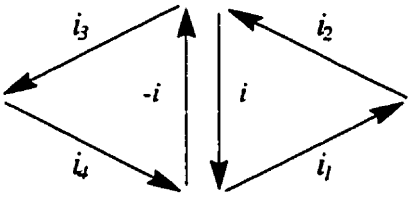


Figure A.1: Linked lists defining the triangulated random lattice. In a cyclic fashion we can locate the tethers in the two triangles sharing $L_i$.

are defined by the linked lists, each of which are organized in such a way that we via the lists can locate all the tethers in the two triangles sharing $L_i$, i.e. $i_1 = \mathcal{N}(i)$, $i_2 = \mathcal{N}(i_1)$, $i_3 = \mathcal{N}(-i)$ and $i_4 = \mathcal{N}(i_3)$ (See Fig. A.1), where $\mathcal{N}$ denotes a operator for stepping one element ahead in the linked list. This relation must hold for all tethers $L_i$ and each linked list must thus satisfy the condition $\mathcal{N}(\mathcal{N}(\mathcal{N}(i))) = i, \forall i$. By using the oriented datastructure and a datastructure defining the vertices at each end of a tether, we can in a cyclic fashion locate the tethers defining the connectivity of any given vertex in the random lattice. We can in this manner locate the nearest neighbour structure of any such vertex.

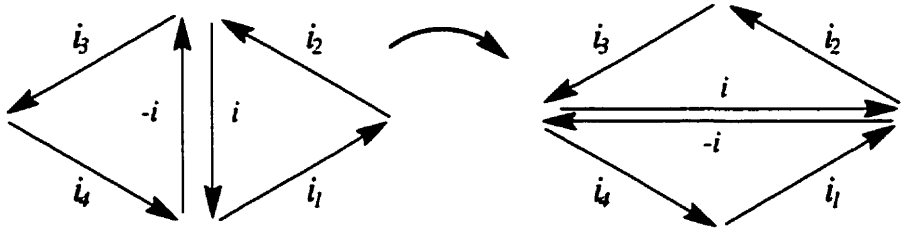


Figure A.2: The update of the linked lists after a link-flip. We only need to make the following changes in the datastructure in order to update the connectivity after a link-flip: $\mathcal{N}(i) = i_2, \mathcal{N}(-i) = i_3, \mathcal{N}(i_1) = -i, \mathcal{N}(i_2) = i_3, \mathcal{N}(i_3) = i$ and $\mathcal{N}(i_4) = i_1$.

The update of the connectivity of the random lattice is described in the link-flip procedure of Section 3.2. In a link-flip procedure two vertices each loose a tether and two other vertices each gain a tether. To keep the random lattice regular we must require that no vertex has less than three tethers connecting it to other vertices, and that two vertices can only be connected once to each other. Further we must also ensure that the length of the new tether is greater than the hard-disk diameter, $d$, and smaller than the maximum tether length $l_{max}$. To update the linked lists after flipping a tether we need only to change $\mathcal{N}(\pm i)$, $\mathcal{N}(i_1)$, $\mathcal{N}(i_2)$, $\mathcal{N}(i_3)$ and $\mathcal{N}(i_4)$ (see Fig. A.2) which makes the link structure a very compact and efficient datastructure.

## A.2 The Isobaric-Isothermal Ensemble

In this appendix, we demonstrate that a Metropolis Monte Carlo simulation based on the Hamiltonian defined in Eq. (3.38) does indeed sample the isobaric-isothermal $N-P-T$ thermodynamic ensemble. The derivation given here follows closely that given by D. Frenkel and B. Smit ([97]), page 103.

The partition function $Z(N,V,T)$ for a classical system of $N$ identical particles in a volume $V$ is given by

$$Z(N,V,T) = \frac{1}{\Lambda^{3N}N!}\int_0^L \cdots \int_0^L d\mathbf{r}^N \exp[-\beta E(\mathbf{r}^N)] \ , \tag{A.1}$$

where $E$ is the energy of the configuration $\mathbf{r}^N$, $\beta$ is the inverse temperature $1/k_BT$ and $\Lambda = \sqrt{h^2/(2\pi m k_B T)}$ is the thermal Broglie wavelength. If we assume that the system is contained in a cubic box of size $L = V^{1/d}$, we can introduce a set of rescaled coordinates $\mathbf{s}_i = \mathbf{r}_i/L$ for $i = 1,\ldots,N$ and rewrite Eq. (A.1) as

$$Z(N,V,T) = \frac{V^N}{\Lambda^{3N}N!}\int_0^1 \cdots \int_0^1 d\mathbf{s}^N \exp[-\beta E(\mathbf{s}^N, L)] \ . \tag{A.2}$$

Now the Helmholtz free energy of the system is

$$\begin{aligned} F(N,V,T) &\equiv -k_BT \ \ln Z \\ &= -k_BT \ \ln\left(\frac{V^N}{\Lambda^{3N}N!}\right) - k_BT \ \ln \int_0^1 \cdots \int_0^1 d\mathbf{s}^N \exp[-\beta E(\mathbf{s}^N, L)] \\ &= F^{id}(N,V,T) + F^{ex}(N,V,T) \ . \end{aligned} \tag{A.3}$$

In the last line, we have identified the two parts of the free energy as an ideal gas contribution and an excess part. Say that the system is allowed to interact with an ideal gas reservoir. The total volume of the system plus the reservoir is fixed at a value $V_0$. The total number of particles is fixed at $M$. The volume of the $N$-particle system is $V$ and the volume of the $M-N$ ideal gas reservoir is then $V_0 - V$. The partition function for the combined system is the product of the partition function for the two subsystems

$$Z(N,M,V,V_0,T) = \frac{V^N(V_0-V)^{M-N}}{\Lambda^{3N}N!(M-N)!}\int_0^1 d\mathbf{s}^{M-N}\int_0^1 d\mathbf{s}^N \exp[-\beta E(\mathbf{s}^N, L)] \ , \tag{A.4}$$

where we have assumed that the thermal wavelength of the ideal gas is equal to $\Lambda$ for the interaction system. We now allow the volume of the $N$-particle system to fluctuate. The most probable value of $V$ will be the value that minimizes the free energy of the combined system. The probability density $\mathcal{N}(V)$ of finding the subsystem with a volume $V$ is given by

$$\mathcal{N}(V) = \frac{V^N(V_0-V)^{M-N}\int_0^1 d\mathbf{s}^N \exp[-\beta E(\mathbf{s}^N, L)]}{\int_0^{V_0} dV' V'^N (V_0-V')^{M-N}\int_0^1 d\mathbf{s}^N \exp[-\beta E(\mathbf{s}^N, L)]} \ . \tag{A.5}$$

In the limit where the size of the reservoir tends to infinity ($V_0 \to \infty$, $M \to \infty$, $(M-N)/V_0 \to \rho$) a small change in the volume of the small system does not change the pressure of the large system and the large system simply acts as a manostat for the small system. In that limit, we can write

$$\begin{aligned}(V_0 - V)^{M-N} &= V_0^{M-N}[1-(V/V_0)]^{M-N} \\ &\to V_0^{M-N}\exp(-(M-N)V/V_0) \\ &\to V_0^{M-N}\exp(-\rho V)\ .\end{aligned} \tag{A.6}$$

Since the reservoir contains only an ideal gas, $\rho$ can be written as $\beta P$. With these substitutions Eq. (A.5) can be simplified as

$$\mathcal{N}_{N,P,T}(V) = \frac{V^N \exp(-\beta PV)\int_0^1 d\mathbf{s}^N \exp[-\beta E(\mathbf{s}^N, L)]}{\int_0^{V_0} dV' V'^N \exp(-\beta PV)\int_0^1 d\mathbf{s}^N \exp[-\beta E(\mathbf{s}^N, L)]}\ . \tag{A.7}$$

We thus find that the probability of locating the small system in a particular configuration $\mathbf{s}^N$ of the $N$ particles at a given volume $V$ is

$$\begin{aligned}\mathcal{N}_{N,P,T}(V) &\propto V^N \exp(-\beta PV)\exp[-\beta E(\mathbf{s}^N, L)] \\ &= \exp\{-\beta[E(\mathbf{s}^N, L) + PV - N\beta^{-1}\ln V]\}\ .\end{aligned} \tag{A.8}$$

It is then clear, that a Monte Carlo algorithm in which a change in the system volume is accepted according to the Metropolis scheme with a Hamiltonian defined by Eq. (3.38) will indeed generate a sampling of phase space corresponding to the isobaric-isothermal $(N-P-T)$ ensemble.

## A.3 Details of the Multiple Hole Algorithm

In this appendix, we give some of the details of the actual implementation of the multiple hole algorithm as described in the Section 2.5.1.

In the insertion or removal procedure for the multiple hole algorithm a vertex is chosen at random among the $N_V$ vertices in the network. An attempt to remove or add a tether is tried with equal probability. A hole is created, if the selected vertex is internal by removing one of the connected tethers at random. An attempt to add a tether to an internal tether always fails. If the selected vertex is external, a tether is removed from the edge of the corresponding hole as described for the single hole simulations. A hole is sealed, when it has only four vertices on the edge and a tether is placed successfully across the hole. Holes are allowed to fragment and coalesce. If the removal of the tether results in a vertex being on the edge of two holes, then an attempt is made to allow the two holes to coalesce. In the same way, if two vertices on the edge of a hole get so close that a tether can be added between them, then an attempt to fragment the hole into two smaller holes is made.

This algorithmic scheme is quite complex and it is therefore appropriate to make some clarifying comments as to how the scheme is implemented so as to obey detailed balance. The move classes defining the particle move, link flip and area change are all identical to the procedures described in Section 3.2.1. In the following, we hence only summarize how detailed balance is ensured in the different move classes connected to the variations in the number of holes and the hole perimeter.

**Creation/Sealing of Holes.** The probability for removing a tether connected to a specific vertex and subsequent create a hole is $1/N_V \cdot 1/N_T$, where $N_V$ is the number of vertices in the network and $N_T$ is the number of tethers connected to the particular vertex. If the move is accepted, the number of tethers connected to the particular vertex will decrease by one. The probability for attempting the reverse move is just $1/N_V$, since the hole will always seal if the number of vertices along the edge is equal to four. In order for the hole creation/sealing procedure to obey detailed balance, the probability for sealing a hole must thus be modified according to $1/(N_T + 1)$.

**Coalescence/Fragmentation of Holes.** The probability for the coalescence of two holes is just $1/N_V$, since coalescence is always attempted if the removal of a tether leads to a vertex being on the edge of two holes. The probability for performing the reverse move, of fragmenting the larger hole into the original two smaller ones, is however $1/N_V \cdot 1/N_{pair}$, where $N_{pair}$ is the number of vertices along the edge of the large hole that are within a distance from the particular vertex to allow for a tether be inserted. Detailed balance for the coalescence or fragmentation procedure is thus only ensured, if the probability for coalescence is modified according to $1/N_{pair}$, where $N_{pair}$ is the total number of vertices along the edge of the combined hole, that can be connected to the selected vertex.

**Removal/Insertion of Tethers.** Since, in the scheme for the multiple hole algorithm, we perform moves at a randomly selected vertex, the probability for the

removal/insertion of tethers at a vertex along the edge of a hole does not depend on the actual number of external vertices in the membrane. The probability for attempting a removal/insertion of a tether is always $1/N_V$. In contrast to the single hole algorithm, the probability for the removal/insertion of tethers along the edge of the holes does thus not need any modification in order to obey detailed balance.

With this implementation of the multiple hole model, we thus ensure that the transition matrix defining the Monte Carlo process for hole creation and sealing as well as hole coalescence and fragmentation is symmetric. This, in turn, ensures that the corresponding Monte Carlo moves obey detailed balance.

# REFERENCES


ALBERTS, B., BRAY, D., LEWIS, J., RAFF, M., ROBERTS, K., AND WATSON, J. D. [89]. *Molecular biology of The Cell.* Garland Publishing, Inc, New York & London, second edition, 1989.

ALDER, B. J. AND WAINWRIGHT, T. E. [62]. *Phys. Rev. Lett.*, **127**, 359 (1962).

ALLEN, M. P. AND TILDESLEY, J. P. [87]. *Computer Simulations of Liquids.* Oxford Science Publications, 1987.

BEN-AV, R., KINAR, J., AND SOLOMON, S. [92]. *Int. J. Mod. Phys.*, **3**, 279 (1992).

BENACHIR, T., MONETTE, M., GRENIER, J., AND LAFLEUR, M. [97]. *Eur. Biophys. J.*, **25**, 201–210 (1997).

BERENZINSKI, V. L. [71]. *Zh. Eksp. Teor. Fiz.*, **61**, 1144 (1971).

BERG, B. A. AND NEUHAUS, T. [92]. *Phys. Rev. Lett.*, **68**, 9 (1992).

BLOOM, M., EVANS, E., AND MOURITSEN, O. G. [91]. *Q. Rev. Biophys.*, **24**, 293 (1991).

BLOOM, M. AND MOURITSEN, O. G. [88]. *Can. J. Chem.*, **66**, 706 (1988).

Bloom, M. and Mouritsen, O. G. [95]. *Handbook of Biological Physics*, volume 1, chapter 2. Elsevier B.V.

BOAL, D. H. [93]. *Phys. Rev. E*, **47**, 4604–4606 (1993).

BOAL, D. H. AND RAO, M. [92]. *Phys. Rev. A*, **45**, 6947 (1992).

BOULATOV, D. V. AND KAZAKOV, V. A. [87]. *Phys. Lett.*, **B186**, 379 (1987).

BOWEN, P. B., BURKE, J. L., CORSTEN, P. G., CROWELL, K. J., FARRELL, K. L., MACDONALD, J. C., MACDONALD, R. P., MACISSAC, A. B., POOLE, P. H., AND JAN, N. [89]. *Phys. Rev. B.*, **40**, 7439 (1989).

CHAIKIN, P. M. AND LUBENSKY, T. C. [95]. *Principles of condensed matter physics.* Cambridge University Press, Cambridge, Great Britain, 1995.

CHU, S., CLARK, M., BALAJ, V., SUBRAMANIAN, S., SCOTT, H. L., AND JAKOBSSON, E. [95]. *Biophys. J.*, **69**, 1230 (1995).

DAMMANN, B., FOGEDBY, H. C., IPSEN, J. H., MOURITSEN, O. G., RISBO, J., SABRA, M. C., SPEROTTO, M., AND ZUCKERMANN, M. J. [95]. *Nonmedical Applications of Liposomes.* CRC Press, Boca Raton, Florida, 1995.

DAVIS, J. H. [79]. *Biophys. J.*, **27**, 339–358 (1979).

DIMITROVA, M. N. AND MATSUMURA, H. [97]. *Coloids Sirf. B. Biointerfaces*, **8**, 287–294 (1997).

DONIACH, S. [78]. *J. Chem. Phys.*, **68**, 4912 (1978).

ESTEP, T. N., MOUNTCASTLE, D. B., BILTONEN, R. L., AND THOMPSON, T. E. [78]. *Biochemistry*, **17**, 1984–1989 (1978).

EVANS, E. [74]. *Biophys. J.*, **74**, 923–931 (1974).

EVANS, E. AND RAWICZ, W. [90]. *Phys. Rev. Lett.*, **64**, 2094–2097 (1990).

FERDINAND, A. E. AND FISHER, M. E. [69]. *Phys. Rev.*, **185**, 832 (1969).

FERNÁNDEZ, J. F., ALONSO, J. J., AND STANKIEWICZ, J. [95]. *Phys. Rev. Lett.*, **75**, 3477 (1995).

FERRENBERG, A. M. AND SWENDSEN, R. H. [88]. *Phys. Rev. Lett.*, **61**, 2635 (1988).

FERRENBERG, A. M. AND SWENDSEN, R. H. [89]. *Phys. Rev. Lett.*, **63**, 1195 (1989).

FINEGOLD, L., EDITOR [93]. *Cholesterol in Membrane Models*. CRL Press, 1993.

FRENKEL, D. AND SMIT, B. [97]. *Understanding molecular simulations,*. Academic Press, 1997.

G. CEVC, E. [93]. *Phospholipids Handbook*. Marcel Dekker, New York, 1993.

GELBART, W. M., BEN-SHAUL, A., AND ROUX, D. [94]. *Micelles, Membranes, Microemulsions and Monolayers*. Partially Ordered Systems. Springer-Verlag, Heidelberg, 1994.

GENNIS, R. B. [89]. *Biomembranes*. Springer-Verlag, Heidelberg, 1989.

GU, L., CHAKRABORTY, B., GARRIDO, P. L., PHANI, M., AND LEBOWIT, J. L. [96]. *Phys. Rev. B.*, **53**(18), 11985 (1996).

HAGEN, M. H. J. AND FRENKEL, D. [94]. *J. Chem. Phys.*, **101**(5), 4093 (1994).

HALSTENBERG, S., HEIMBURG, T., HIANIK, T., KAATZE, U., AND KRIVANEK, R. [98]. *Biophys. J.*, **75**, 264 (1998).

HANSEN, P. L., MIAO, L., AND IPSEN, J. H. [98]. *Phys. Rev. E.*, **58**, 2311 (1998).

HELFRICH, W. [75]. *Z. Naturf.*, **30 c**, 841–842 (1975).

HELLER, H., SCHEAFFER, K., AND SCHULTEN, K. [93]. *J. Phys. Chem.*, **97**, 8343 (1993).

HELLER, W. T., HE, K., LUDTKE, S. J., HARROUN, T. A., AND HUANG., H. W. [97]. *Biophys. J.*, **73**, 239–244 (1997).

HUI, S.-W. AND HE, N.-B. [83]. *Biochemistry*, **22**, 1159 (1983).

IPSEN, J. H., KARLSTRÖM, G., MOURITSEN, O. G., WENNERSTRÖM, H., AND ZUCKERMANN, M. J. [87]. *Biochem. Biophys. Acta*, **905**, 162 (1987).

IPSEN, J. H., MOURITSEN, O. G., AND ZUCKEMANN, M. J. [89]. *J. Chem. Phys.*, **91**, 1855 (1989).

IPSEN, J. H., MOURITSEN, O. G., AND ZUCKEMANN, M. J. [90]. *Biophys. J.*, **56**, 661 (1990).

JEPPESEN, C. AND IPSEN, J. H. [93]. *Europhys. Lett.*, **22**, 713 (1993).

JOÓS, B. [96]. *Dislocations in Solids*, volume 10. North-Holland, Amsterdam, 1996.

JØRGENSEN, K. [95]. *Biochim. Biophys. Acta*, **1240**, 111 (1995).

KOFKE, D. A. [93]. *J. Chem. Phys.*, **98**, 4149–4162 (1993).

KOSTERLITZ, J. M. AND THOULESS, D. J. [73]. *J. Phys. C*, **6**, 1181 (1973).

KROLL, D. M. AND GOMPPER, G. [92]. *Phys. Rev. A*, **46**, 3119 (1992).

LEE, J. AND KOSTERLITZ, J. L. [90]. *Phys. Rev. Lett*, **65**, 137 (1990).

LEE, J. AND KOSTERLITZ, J. L. [91]. *Phys. Rev. B*, **43**, 3265 (1991).

LEE, J. AND STRANDBURG, K. J. [92]. *Phys. Rev. B*, **46**, 11190 (1992).

LEMMICH, J., MORTENSEN, K., IPSEN, J. H., HØNGER, T., BAUER, R., AND MOURITSEN, O. G. [97]. *Eur. Biophys. J.*, **25**, 293 (1997).

LINSEISEN, F. M., THEWALT, J. L., BLOOM, M., AND BAYERL, T. M. [93]. *Chem. Phys. Liquids*, **65**, 141–149 (1993).

LITSTER, J. D. [75]. *Phys. Lett.*, **53A**, 193–194 (1975).

LUDTKE, S. J., HE, K., HELLER, W. T., HARROUN, T. A., YANG, L., AND HUANG., H. W. [96]. *Biochemistry*, **35**, 13723–13728 (1996).

MATSUZAKI, K., SUGISHITA, K., HARADA, M., FUJII, N., AND MIYAJIMA., K. [97]. *Biochim. Biophys. Acta.*, **1327**, 119–130 (1997).

MCDONALD, I. R. [72]. *Mol. Phys.*, **23**, 41–58 (1972).

METROPOLIS, N., ROSENBLUTH, A., ROSENBLUTH, M., TELLER, A., AND TELLER, E. [53]. *J. Chem. Phys.*, **21**, 1087 (1953).

MITCHELL, C. D. AND LITMAN, B. J. [98]. *Biophys. J.*, **75**, 896 (1998).

MORROW, M. R., WHITEHEAD, J. P., AND LU, D. [92]. *Biophys. J.*, **63**, 18–27 (1992).

MORTENSEN, K., PFEIFFER, W., SACKMANN, E., AND KNOLL, W. [88]. *Biochem. Biophys. Acta.*, **945**, 221 (1988).

MOURITSEN, O. G. [91]. *Chem. Phys. Lipids*, **57**, 179 (1991).

MOURITSEN, O. G., DAMMANN, B., FOGEDBY, H. C., IPSEN, J. H., JEPPESEN, C., JØRGENSEN, K., RISBO, J., SABRA, M. C., SPEROTTO, M. M., AND ZUCKERMANN, M. J. [95]. *Biophys. Chem.*, **55**, 55 (1995).

MOURITSEN, O. G. AND ZUCKERMANN, M. J. [87a]. *Chem. Phys. Lett.*, **135**, 294 (1987).

MOURITSEN, O. G. AND ZUCKERMANN, M. J. [87b]. *Euro. Biophys. J.*, **15**, 77 (1987).

NAGLE, F. [73]. *J. Chem. Phys.*, **58**, 252 (1973).

NEEDHAM, D. AND HOCHMUTH, R. M. [89]. *Biophys. J.*, **55**, 1001–1009 (1989).

NEEDHAM, D., MCINTOSH, T. J., AND EVANS, E. [88]. *Biochemistry*, **27**, 4668 (1988).

NELSON, D. R. AND HALPERIN, B. I. [79]. *Phys. Rev. B*, **19**, 2457 (1979).

NIELSEN, M., MIAO, L., IPSEN, J. H., JØRGENSEN, K., ZUCKERMANN, M. J., AND MOURITSEN, O. G. [96a]. *Biochem. Biophys. Acta*, **1278**, 170 (1996).

NIELSEN, M., MIAO, L., IPSEN, J. H., ZUCKERMANN, M. J., AND MOURITSEN, O. G. [96b]. *Phys. Rev. E*, **54**, 6889 (1996).

NIELSEN, M., MIAO, L., IPSEN, J. H., ZUCKERMANN, M. J., AND MOURITSEN, O. G. [98]. submitted for publication in *Phys. Rev. E.*

PANAGIOTOPOULOS, A. Z. [87]. *Mol. Phys.*, **61**, 813–826 (1987).

PINK, D. A., GREEN, T. J., AND CHAPMAN, D. [80]. *Biochemistry*, **19**, 349 (1980).

PLISCHKE, M. AND BERGENSEN, B. [89]. *Equilibrium Statistical Physics.* World Scientific Publishing Co., Singapore, 1989.

PRESTI, F. T. [85]. *Membrane Fluidity in Biology*, volume 4. Academic Press, 1985.

PROST, J. AND DE GENNES, P. G. [93]. *Liquid Crystals.* Clarendon Press, Oxford, 1993.

RISBO., J. [97]. *Experimental and Theoretical methodologies to investigate Lipid bilayer phase equilibria.* Ph.D. Thesis. Department of Chemistry, The Technical University of Denmark, 1997.

ROGERS, J., LEE, A. G., AND WILTON, D. C. [79]. *Biochem. Biophys. Acta.*, **552**, 23 (1979).

SAFRAN, S. A. [94]. *Statistical Thermodynamics of Surfaces, Interfaces and Membranes.* Frontiers in Physics. Addition-Wesley Publishing Company, 1994.

SAHNI, P. S., GREST, G. S., AND ANDERSON, M. P. [83]. *Phys. Rev. Lett.*, **50**, 263 (1983).

Schlenkrich, M., Brickmann, J., Jr., A. M., and Karplus, M. [96]. *An empirical potential energy function for phospholipids: Criteria for parameter optimization and application*, pages 31–81. Biological Membranes, A Molecular Perspective from Computation and Experiments. Birkhäuser, Bosten.

SHILLCOCK, J. C. [98]. Private communication. Julian has confirmed that this indeed was how he implemented the chemical potential in his simulations.

SHILLCOCK, J. C. AND BOAL, D. H. [96]. *Biophys. J.*, **71**, 317–326 (1996).

SHILLCOCK, J. C. AND SEIFERT, U. [98]. *Biophys. J.*, **74**, 1754–1766 (1998).

SINGER, S. J. AND NICOLSEN, G. L. [72]. *Science*, **175**, 720 (1972).

STANLEY, H. E. [71]. Clarendon Press, Oxford, 1971.

STINCHCOMBE, R. B. [83]. *Phase Transitions and Critical Phenomena*, volume 7. Academic Press, 1983.

STOCKTON, B. W. AND SMITH, I. C. P. [76]. *Chem. Phys. Lipids*, **17**, 251 (1976).

STRANDBURG, K. J. [89]. *J. Chem. Phys.*, **67**, 747 E (1989).

THEWALT, J. L. [96]. Unpublished.

THEWALT, J. L. AND BLOOM, M. [92]. *Biophys. J.*, **63**, 1176–1181 (1992).

THEWALT, J. L. AND BLOOM, M. [95]. Private communication.

TIELEMAN, D. P., MARRINK, S. J., AND BERENDSEN, H. J. [97]. A computer perspective of membranes: molecular dynamics studies of lipid bilayer systems. **1331**, 235–270 (1997).

TU, K., TOBIAS, D. J., BLASIE, J. K., AND KLEIN, M. L. [96]. *Biophys. J.*, **70**, 565 (1996).

TU, K., TOBIAS, D. J., AND KLEIN, M. L. [95]. *Biophys. J.*, **69**, 2258 (1995).

VEKIĆ, M., LIU, S., AND HAMBER, H. W. [94]. *Phys. Lett. B.*, **329**, 444 (1994).

VIST, M. AND DAVIS, J. H. [90]. *Biochemistry*, **29**, 451 (1990).

WILHELM, C., WINTERHALTER, M., ZIMMERMANN, U., AND BENZ, R. [93]. *Biophys. J.*, **64**, 121–128 (1993).

Winterhalter, M. [96]. *Handbook of Nonmedical Applications of Liposomes, Liposomes in electric fields.* CRC Press, Boca Raton, FL.

WOLDE, P. R. AND FRENKEL, D. [98]. Submitted for publication.

YEAGLE, P. L. [92]. *The Structure of Biological Membranes.* CRC Press, Boca Raton, FL, 1992.

YOUNG, A. P. [79]. *ibid.*, **19**, 1855 (1979).

ZHELEV, D. V. AND NEEDHAM, D. [93]. *Biochim. Biophys. Acta.*, **1147**, 89–104 (1993).